

THESIS FOR THE DEGREE OF DOCTOR OF PHILOSOPHY

Investigation of new recycling strategies for spent Li-ion batteries
based on early Li recovery via selective leaching

Léa M.J. ROUQUETTE

Department of Chemistry and Chemical Engineering

CHALMERS UNIVERSITY OF TECHNOLOGY

Gothenburg, Sweden 2025

Investigation of new recycling strategies for spent Li-ion batteries based on early Li recovery via selective leaching

Léa M.J. Rouquette

© Léa M.J. Rouquette, 2025.

ISBN : 978-91-8103-234-5

Doktorsavhandlingar vid Chalmers Tekniska Högskola
Ny serie nr 5692
ISSN: SSN0346-718X

Nuclear Chemistry and Industrial Materials Recycling
Department of Chemistry and Chemical Engineering
Chalmers University of Technology
SE-412 96 Gothenburg
Sweden
Telephone + 46 (0)31-772-1000

Cover: Investigation of new recycling strategies for spent Li-ion batteries based on early Li recovery via selective leaching

Printed by:
Chalmers digitaldryck
Gothenburg, Sweden 2025

Investigation of new recycling strategies for spent Li-ion batteries based on early Li recovery via selective leaching

Léa M.J. ROUQUETTE

Industrial Material Recycling
Department of Chemistry and Chemical Engineering
Chalmers University of Technology

Abstract

In response to our society's environmental challenges, great efforts are being made worldwide to achieve climate neutrality: one of the actions is the electrification of transport, with significant help from rechargeable batteries mostly based on Li-ion chemistries. However, with this increasing demand for Li-ion batteries, many concerns have arisen regarding their life cycle, from raw materials supply to waste management. Recycling is necessary not only to dispose of the waste safely, but also to recover the critical metals such as Li, Co, Ni, Cu, and Mn. Hydrometallurgical techniques have been favoured in the last decades, as they enable the recovery of most elements (including Li) at a high rate and purity. This thesis investigates two new recycling strategies based on early Li recovery, which aim to increase the Li yield and allow the recovery of cathode metals together as precursors to directly re-synthesize the electrode material. The first strategy is based on the pyrolysis of the black mass, followed by water leaching. The second approach is based on using oxalic acid for the selective recovery of Li. In the first route, it was shown that during pyrolysis, the cathode material was reduced and transformed to more leachable forms: a mixture of Co, CoO, Ni, NiO, MnO, Mn₂O₃, and Li₂CO₃. Since Li₂CO₃ is sparingly soluble in water, water leaching was applied, and up to 70% of Li was recovered from the sample pyrolyzed at 600°C. Li recovery limitations could be connected to the formation of 3 distinct by-products of the pyrolysis: LiF, Li₃PO₄, and LiAlO₂. The presence of Al and fluorine in the final leachate solution was considered to be unavoidable. However, the pyrolysis positively impacted the transition metal leachability, and they could be recovered with sulfuric acid without a reducing agent. The second strategy investigated the direct use of oxalic acid without any thermal pretreatment. The best operating conditions were determined as a temperature of 60°C, a solid to liquid ratio of 50 g/L, and an acid concentration of 0.6 M, corresponding to a molar ratio of 1:2.5 (cathode material metals: acid). This leads to more than 95% recovery of Li and 100% of Al. It was determined that the Li dissolution rate is chemically controlled, and the activation energy was estimated to be 76 kJ/mol. The leaching residue comprises a mix of graphite and a disordered (Co,Ni,Mn)C₂O₄ ·2H₂O phase. This residue was then leached with sulfuric acid to dissolve the metal oxalates and separate them from the graphite. A one-stage leaching (2 M H₂SO₄, 65°C, 120 min, S/L = 20 g/L) results in more than 95% recovery of Ni, Co, and Mn and about 70% of Cu. Solvent extraction was used for Cu removal, and a 30 vol% Acorga M5640 in ESCAID was applied for 30 min at 25°C, with θ = 4 and 4 stages. The resulting recycled solution, free from Al, Li, and Cu, represents a promising feedstock for producing NMC 111 (LiNi_{1/3}Mn_{1/3}Co_{1/3}O₂).

Keywords: Lithium, recycling, hydrometallurgy, thermal treatment, organic acid.

List of Publications and Manuscripts

This thesis is based on the following paper and manuscript:

(I) **Léa M.J. Rouquette**, Nathália Vieceli, Martina Petranikova (2023). Intensification of lithium carbonation in the thermal treatment of spent EV Li-ion batteries via waste utilization and selective recovery by water leaching. *Resources, Conservation and Recycling Advances*, Vol. 17, 200125, DOI 10.1016/j.rcradv.2022.200125

Contribution: Main author and most experimental work and analysis of data.

(II) **Léa M.J. Rouquette**, Martina Petranikova, Nathália Vieceli (2023). Complete and Selective recovery of lithium from EV lithium-ion batteries: modelling and optimization using oxalic acid as a leaching agent. *Separation and Purification Technology*, Vol. 320, 124143, DOI 10.1016/j.seppur.2023.124143

Contribution: Main author and all experimental work and analysis of data.

(III) Martina Petranikova, **Léa Rouquette**, Andrea Locati and Burçak Ebin (2023). Advances in hydrometallurgical processing of black mass from EV Li-ion batteries. *14th Hydroprocess conference, Santiago 2024, peer-reviewed proceedings*

Contribution: Co-author and part of the experimental work and analysis of data.

(IV) **Léa M.J. Rouquette**, Laura Altenschmidt, Matea Culina, William R. Brant, Burçak Ebin, Martina Petranikova (2025). Kinetics study of the dissolution of black mass material using oxalic acid as a leaching agent. *Hazardous Material Advances*, Vol. 18, 100750, DOI 10.1016/j.hazadv.2025.100750

Contribution: Main author and most experimental work and analysis of data.

(V) **Léa M.J. Rouquette**, Laura Altenschmidt, Andrea Locati, Camille Travers, William R. Brant, Burçak Ebin, Martina Petranikova (2025). Towards the production of transition metal oxalate precursors from NMC111 black mass via selective leaching of Li and Al and solvent extraction of Cu. Manuscript soon submitted Power Source to Special Issue on Battery Recycling Science and Technology.

Contribution: Main author and most experimental work and analysis of data.

Related publications not included in the thesis:

Andrea Locati, Maja Mikulić, **Léa M.J. Rouquette**, Burçak Ebin, and Martina Petranikova (2024). Production of High Purity MnSO₄·H₂O from Real NMC111 Lithium-Ion Batteries Leachate Using Solvent Extraction and Evaporative Crystallization. *Solvent extraction and ion exchange*, Vol. 42, Issue 6–7, 636–657, DOI 10.1080/07366299.2024.2435272

Brenda Segura-Bailón, **Léa M.J. Rouquette**, Nathália Vieceli, Karolina Bogusz, Cécile Moreau, Martina Petranikova (2025). Recycling of Li-ion batteries: The effects of mechanical activation on valuable metals leachability from the black mass of NMC 111. Submitted to Mining, Metallurgy & Exploration (09/05/2025 – 1st round revision).

Natrawee Khetwunchai, **Léa M.J. Rouquette**, Saengchai Akeprathumchai, Martina Petranikova (2024). Leaching of valuable metals from spent batteries of electric vehicles using disodium ethylenediaminetetraacetic acid. Submitted to Journal of Environmental Management (11/06/2024 – 2nd round revision).

Léa M.J. Rouquette, Ilyes Mahti, Martina Petranikova (2024). Selective recovery of molybdenum from steel making dust leachate using Cyanex 600. Submitted to Hydrometallurgy.

Abbreviations and definitions

The following abbreviations and definitions are used throughout this thesis:

BM	Black mass	PCM	Progressive conversion model
ca.	around	PE	Polyethylene
CAM	Cathode active material	pHeq	Equilibrium pH
CMC	Carboxymethyl cellulose	PP	Polypropylene
CO ₂	Carbon dioxide	PVDF	Polyvinylidene fluoride
D	Distribution ratio	PYRO	Pyrolysis
DE2HPA	Bis(2-ethylhexyl) hydrogen phosphate	R ²	Coefficient of determination
DMF	Dimethylformamide	rpm	Rotation per minute
E	Percentage extracted (solvent extraction [%])	R _{wp}	Weight profile R-value
E _a	Energy of activation [kJ]	S/L	Solid to liquid ratio
EU	European Union	SBR	Styrene-butadiene rubber
EV	Electric vehicle	SCM	Shrinking core model
FT-IR	Fourier-Transform Infrared Spectroscopy	SEM -	Scanning electron microscopy -
		EDS	Energy dispersive X-ray spectrometry
GHG	Greenhouse gasses	SX	Solvent extraction
ICP-OES	Inductively coupled plasma – Optical emission spectrometry	t	Time [min]
IEA	International energy agency	T	Temperature [°C]
INC	Incineration	TM	Transition metal
IX	Ion exchange	TOC	Total carbon content
k	Kinetic constant [min ⁻¹]	UN	Untreated material
K _{sp}	Solubility constant	US	Ultrasound
LCA	Life cycle assessment	vol%	Volume percent
LCO	Lithium cobalt oxide	WEEE	Waste electrical and electronic equipment
LFP	Lithium iron phosphate		
LiB	Lithium-ion Battery	wt%	Weight Percentage
LMO	Lithium manganese oxide	XRD	X-Ray Diffraction
m	Avrami order	Y	Leaching yield [%]
n	Theoretical number of stages	ΔG	Free Gibbs Energy [kJ]
NCA	Lithium nickel cobalt aluminium oxide	θ	Organic to aqueous volume ratio (solvent extraction)
NMC	Lithium nickel manganese cobalt oxide	%P	Precipitation yield [%]
NMP	N-methyl pyrrolidone		
OA	Oxalic acid		

Table of Contents

1	INTRODUCTION	1
	GOAL AND DRIVING FORCE FOR THIS THESIS.....	2
2	BACKGROUND	3
2.1	LI-ION BATTERY	3
2.2	COLLECTION AND SORTING OF SPENT LI-ION BATTERY	5
2.3	RECYCLING OPTIONS FOR SPENT LI-ION BATTERY.....	5
2.3.1	<i>Pre-treatment</i>	6
2.3.2	<i>Direct recycling</i>	7
2.3.3	<i>Pyrometallurgy methods</i>	8
2.3.4	<i>Hydrometallurgy methods</i>	8
2.4	RESEARCH QUESTIONS AND SCOPE	13
2.4.1	<i>Identified recycling challenges</i>	13
2.4.2	<i>Project boundary and Research question enunciation</i>	13
3	THEORY OF EXTRACTIVE METALLURGY.....	15
3.1	CARBOREDUCTION OF METAL OXIDES	15
3.1.1	<i>Overview</i>	15
3.1.2	<i>Black Mass Carboreduction</i>	15
3.2	CHEMICAL FUNDAMENTALS OF METALLURGY	16
3.2.1	<i>Thermodynamics and equilibrium considerations</i>	16
3.2.2	<i>Metal ions in solution</i>	16
3.3	LEACHING – METAL EXTRACTION	18
3.3.1	<i>General principle</i>	18
3.3.2	<i>Kinetics & Mechanism investigation</i>	19
3.3.3	<i>Selective Li dissolution from Black mass</i>	20
3.4	METAL SEPARATION TECHNIQUES	21
3.4.1	<i>Precipitation</i>	21
3.4.2	<i>Solvent extraction</i>	21
4	MATERIALS AND METHODS	23
4.1	OVERVIEW OF THE EXPERIMENTAL WORK	23
4.2	MATERIALS	23
4.2.1	<i>Black mass</i>	23
4.2.2	<i>Chemicals</i>	24
4.3	EQUIPMENT	24
4.3.1	<i>Thermal treatment set-up</i>	24
4.3.2	<i>Leaching</i>	24

4.3.3	<i>Evaporative crystallization</i>	24
4.3.4	<i>Precipitation</i>	25
4.3.5	<i>Solvent extraction</i>	25
4.4	ANALYTICAL METHODS.....	25
4.5	THERMODYNAMICS CONSIDERATIONS	26
4.6	DESIGN OF EXPERIMENTS – STATISTICAL METHODS	27
5	RESULTS AND DISCUSSIONS.....	29
5.1	BLACK MASS CHARACTERIZATION.....	29
5.2	STRATEGY 1: BASED ON EARLY RECOVERY OF Li VIA WATER LEACHING AFTER BM THERMAL TREATMENT	30
5.2.1	<i>Water leaching after incineration and pyrolysis of battery cells' electrodes</i>	30
5.2.2	<i>Water leaching on pyrolyzed BM at the optimised conditions (Leaching 1)</i>	33
5.2.3	<i>Sulfuric acid leaching (Leaching 2)</i>	36
5.2.4	<i>Conclusions and perspectives on Strategy 1</i>	36
5.3	STRATEGY 2: BASED ON THE EARLY RECOVERY OF Li VIA OXALIC ACID LEACHING	37
5.3.1	<i>Oxalic acid leaching (Leaching 1)</i>	37
5.3.2	<i>Sulfuric acid leaching (Leaching 2)</i>	50
5.3.3	<i>Purification leaching solution 2 -Towards the production of CAM precursors</i>	56
5.3.4	<i>Conclusions and perspectives on Strategy 2</i>	60
6	CONCLUSION	61
FUTURE WORK.....		63
ACKNOWLEDGEMENTS.....		65
REFERENCES.....		67
APPENDIX		81

1 INTRODUCTION

Our modern world faces several environmental challenges, such as climate change, biodiversity destruction, deforestation, and ocean acidification, all caused by human activities, principally through greenhouse gas emissions (GHG) [1]. Many efforts are being made worldwide to achieve climate neutrality in response to these challenges. One transition path is the electrification of our societies, which, through the energy transition, offers cleaner alternatives to fossil fuels [2]. This change is concomitant with rising concerns about energy consumption, waste electrical and electronic equipment (WEEE) and the environmental impact of production and disposal. Li-ion batteries (LiBs) have become an essential part of our daily lives, as these rechargeable energy storage devices can be found in various portable electronic equipment like smartphones, tablets, and laptops [3]. Lately, thanks to performance improvements, LiBs have found large applications in the field of electric mobility and energy storage systems. The transport sector is one of the major contributors of GHG, responsible for 37% of CO₂ emissions from end-use sectors in 2021 [4], equating to approximately 15% of global GHG emissions. In 2020 alone, the use of electric vehicles (EVs) contributed to more than 50 Mt CO₂-eq of savings in GHG emissions globally [5,6]

The extensive usage of LiBs has resulted in significant pressure on the market for critical and strategic materials needed for battery production, including natural graphite, Li, Co, Cu, Mn, and Ni, classified as such by the European Commission due to their significant economic importance and elevated supply risk [3,7,8]. Moreover, the production of these raw materials from primary resources is associated with GHG, technological, and societal issues [9–12]. For example, life cycle assessment (LCA) data indicate that recycled LiOH yields a 37 or 72% reduction in GHG emissions compared to virgin LiOH production from Chilean brine and Australian ore, respectively. Similarly, the production of NMC811 cathode active material using recycled materials results in a 40-48% decrease in life cycle GHG emissions relative to virgin material production [10]. Furthermore, significant waste volumes are expected by the end of the decade [6], and its disposal will pose significant environmental challenges as it can lead to the release of hazardous compounds (metal oxide, organic solvents, fluorinated compounds, ...) [3,11,13,14]. Our modern society is concerned about the different environmental impacts of the LiBs value chain, from raw materials extraction to waste disposal. The circular economy concept dictates a paradigm shift toward the reusability of each waste component with minimal resource usage; this outlines that new raw material mining should be kept at a minimum and that recycled material should be fed into new products [14,15]. Regarding waste management strategy, the established hierarchy for waste handling prioritizes the following levels:

Prevention / Reduction > Re-use > Recycling > Recovery > Disposal

In the case of batteries, reuse accounts for only a limited share due to technical and economic challenges, with only 10% of the global storage demand being met by reuse in 2050 [3]. Recycling is an inevitable option for end-of-life management of LiBs [3]. It would have various positive impacts, such as creating a secondary source of supply that reduces the burden on the primary supply from new mines, providing enhanced security for countries and regions with clean energy technology deployment but limited mineral resource endowment, and lowering the environmental footprint of clean energy technologies [5,6]. For example, it is estimated that 250 tons of ore are processed to produce 1 ton of Li (Li carbonate equivalent - LCE), when 256 EV batteries would be needed to achieve the same production.

Worldwide, policymakers are working to establish a framework to improve the recycling of all LiBs components and enable the reuse of recycled materials in battery production. For instance, EU battery regulations (No 2023/1542) have been adopted in July 2023 [16]. It provides a legal framework for the entire battery life cycle, particularly emphasizing recycling practices. Notably, the regulation mandates that all spent LiBs collected by the end of 2030 must undergo recycling processes, achieving a minimum recycling efficiency of 70% by weight. Furthermore, it imposes minimum recovery rates of 80% for Li and 95% for Ni, Cu, and Co by the end of 2031 [16]. Moreover, the implementation of a percentage requirement for recycled material in newly produced batteries is pushing toward better recycling processes. For the same timeline, new LiBs are expected to contain a minimum of 16% recycled Co, 6% recycled Li, and Ni [16]. The regulation mandates that recyclers utilize the *so-called* Best Available Techniques to achieve the specified recovery rate targets.

Goal and driving force for this thesis

In practice, LiBs recycling poses significant challenges. Three major recycling family processes exist: direct recycling, pyrometallurgy, and hydrometallurgy. The latest option enables high recovery rates and requires lower energy consumption, but it is a complex and chemically intensive process [17]. It has been the subject of various research over the last decades [6]. Pilot and commercial systems already exist, but researchers are still pushed to develop innovative solutions that enhance the circular use of critical minerals, minimize recycling's environmental impact, and support a more sustainable and resilient supply chain [3]. As an example, the International Energy Agency (IEA) states that next generation leaching techniques should be based on a selective leaching approach with maximized recovery [3].

This thesis is part of a larger initiative to develop a more sustainable and circular process using eco-friendly chemicals such as organic acids and water. The process's key innovation is 1) the early Li recovery coupled with 2) the direct production of NMC cathode material from recycled solutions. This would significantly reduce the number of stages required for metal recycling and close the loop in the recycling process, thereby promoting and simplifying a circular value chain for materials and sustainable resource management. On that account, two approaches have been investigated, both starting with the early Li recovery: the first combines pyro- and hydrometallurgy, and the second consists of hydrometallurgy only. The synthesis of the recycled cathode material is not investigated here.

This thesis is divided into several sections. The initial section establishes the current state of LiBs hydrometallurgical recycling, leading to the research's objectives and limitations. Following this, the fundamentals aspects of each unit operations employed throughout this research are provided and explained. Subsequently, all the materials and methods used are listed. Finally, the last section analyses the key results, discusses, and offers insights into practical applications. The document finishes with a summary and conclusion of the work, outlining the remaining steps needed for industrializing the process.

2 BACKGROUND

2.1 Li-ion Battery

Over the past decades, multiple battery chemistries have been investigated and implemented for energy storage applications. So far, due to its small atomic radius and high electrochemical potential, Li is an ideal charge carrier, leading to its widespread use in batteries. However, Na-ion batteries have seen their market share increase, and research is ongoing to develop this technology [18]. Moreover, next-generation batteries, like solid-state batteries, are under development, and there could be many breakthroughs in the future.

LiBs comprise a series of cathode and anode layers wrapped multiple times, soaked in liquid electrolyte within a casing, which forms a battery cell. The casing is usually made of steel, Al, and plastic. Depending on the application, the produced battery cells are interconnected in series to form a module, and these modules are further assembled to create a battery pack. An EV battery pack can weigh around 300 to 900 kg, with a capacity ranging from 30 to 100 kWh [19]. For example, the battery system of the Audi e-tron Sportback comprises a pack of 36 modules with 12 pouch cells (providing 95 kWh with a voltage of 396 V) for a volume of 1.24 m³ and a mass of 700 kg [20]. The different components of a battery cell, with their average weight composition, detailed in Figure 1, include the following:

1. The anode electrode is composed of an active material, commonly graphite (about 10 to 20 wt% of the battery cell) [21–23]. Its specific capacity can be improved by adding silicon particles up to 5 to 10 wt% of the active electrode material, which could be problematic for recycling. The active material and conductive agent are bound to a Cu current collector using a binder; polyvinylidene difluoride (PVDF) is commonly employed. Although greener alternatives such as carboxymethyl cellulose (CMC) and styrene butadiene rubber (SBR) are increasing in popularity [21,22,24]. The Cu foil constitutes ca. 7 to 17 wt% of the cell.
2. A separator avoids electrode contact; it is commonly a porous polyolefin membrane allowing Li ions' flow, representing 3 to 12 wt% of the cell. The composition of the separator includes polyethylene (PE), polypropylene (PP), and their blend [21,23–25].
3. The liquid electrolyte (10 to 20 wt% of the battery cell) is composed of a Li salt, with LiPF₆ being the most widely used, and a solvent comprising a mixture of alkyl carbonates, among which ethylene carbonate, propylene carbonate, dimethyl carbonate, diethyl carbonate, are the most popular, but many more molecules can be identified [21–23].
4. The cathode electrode (15 to 41 wt%) is composed of an active material bound together with a conductive agent (typically acetylene black) to an Al current collector (4 to 7 wt% of the cell) with a binder (typically PVDF) [17,23,26]. The binder is present in a range of 1–4 wt% [26,27].

The cathode active material (CAM) can be a Li-transition metal oxide, giving the battery its name, i.e. lithium cobalt oxide (LiCoO₂, LCO), lithium manganese oxide (LiMn₂O₄, LMO), lithium nickel manganese cobalt oxide (LiNi_xCo_yMn_{1-x-y}O₂, NMC), and lithium nickel cobalt aluminium oxide (LiNi_xCo_yAl_{1-x-y}O₂, NCA) or phosphate based compound such as lithium iron phosphate (LiFePO₄, LFP). For NMC-type batteries, transition metal molar ratios can vary from one battery type to another, and the ratio is typically indicated in the name (NMC111, NMC811, ...). Nowadays, Ni-

rich chemistries and LFP dominate the EV market [3,28,29], Figure 1b presents the current and projected market shares for batteries. The elemental composition of the CAM varies, accounting for approximately 5 - 7 wt% Li, 5 - 15 wt% Ni, 5 - 10 wt% Mn, and 5 - 20 wt% Co, and about 15 wt% of organic matter, and about 7 wt% of plastic [27]. It is worth mentioning that the average content is much higher than the average grade of corresponding primary ores (i.e. in China average content can be the following: Li ca. 2.75 wt%, Ni ca. 0.02 wt%, Co ca. 1.5 wt%), once again showing the genuine interest of recycling the waste [23]. In fact, battery recycling could meet 20 to 30% of Li, Ni, and Co demand by 2050 [3].

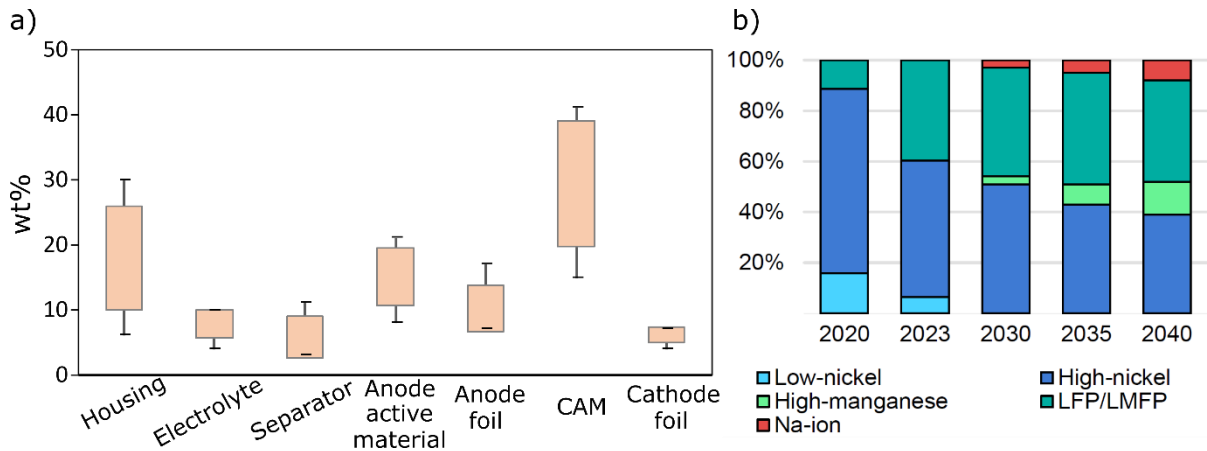


Figure 1: a) Generic composition of LiB cell in weight percentage (wt%) (mix LCO and NMC) [22,27,30,31] and b) EV battery cathode development projection – (Low-Ni chemistry includes NMC333, NMC532, while High-Ni includes NMC622, NMC721, NMC811, NCA, and LNO) [3,28,29].

There are several methods to produce the CAM, such as co-precipitation, sol-gel synthesis, or spray pyrolysis [32]. The most common is the co-precipitation of CAM precursor [32] before its roasting to transform it into the actual active material; typical CAM precursors are transition metal (TM) hydroxides. TM carbonates and oxalates are also considered effective precursors [33–35]. One standard procedure is that TM sulphates are precipitated as hydroxides under a controlled environment (pH, temperature, mixing rate, reagent concentration, drying rate, ...) to obtain uniform spherical particles with homogenized chemical distribution. The atmosphere must be inert, because elements such as Mn are prone to oxidation, which would decrease the purity of the hydroxide. A chelating agent is usually needed to control the crystallinity of the precursor and produce a single-phase structure. In the case of hydroxide, typical precipitation and chelating agents are NaOH and (NH₄)OH [36]. Then, CAM precursors are mechanically combined with a Li source such as LiOH or Li₂CO₃. Typically, LiOH is used to produce NMC cathode material. The mixture is then calcinated and sintered to obtain the CAM. This method is already applied in industry and is cost-effective. It allows efficient particle size, morphology, and tap density control [32].

In this thesis, the waste received for investigation is NMC111-based; this remains one of the most significant batteries on the market, and the waste volume is projected to reach millions of tons worldwide per year by 2030 [3,4,6]. Hence, a solution for its recycling is urgently needed to maximize metals' circularity.

2.2 Collection and Sorting of Spent Li-ion Battery

No waste management strategy can be sustainable without a proper collection system, which is often seen as the bottleneck in waste handling. Different policies have been made globally to increase collection, i.e., the extended producer responsibility in Europe involves the battery producers in end-of-life management [37]. Recycling centres are emerging worldwide and will be responsible for sorting, assessing, and storing the batteries [38,39]. The vast diversity of battery technology makes these steps challenging regarding logistics and safety. A global agreement on battery labelling would be beneficial, such as the European battery passport or QR code in China [40,41]. Moreover, researchers and companies are developing tools to screen the left battery's performance and evaluate whether it should be reused, repaired, or sent for recycling [5,41,42].

2.3 Recycling Options for Spent Li-ion Battery

The following sections will detail each recycling option's process parameters, benefits, and drawbacks. These existing primary processes for battery recycling are summarized in Figure 2, based on the literature presented below [44-95].

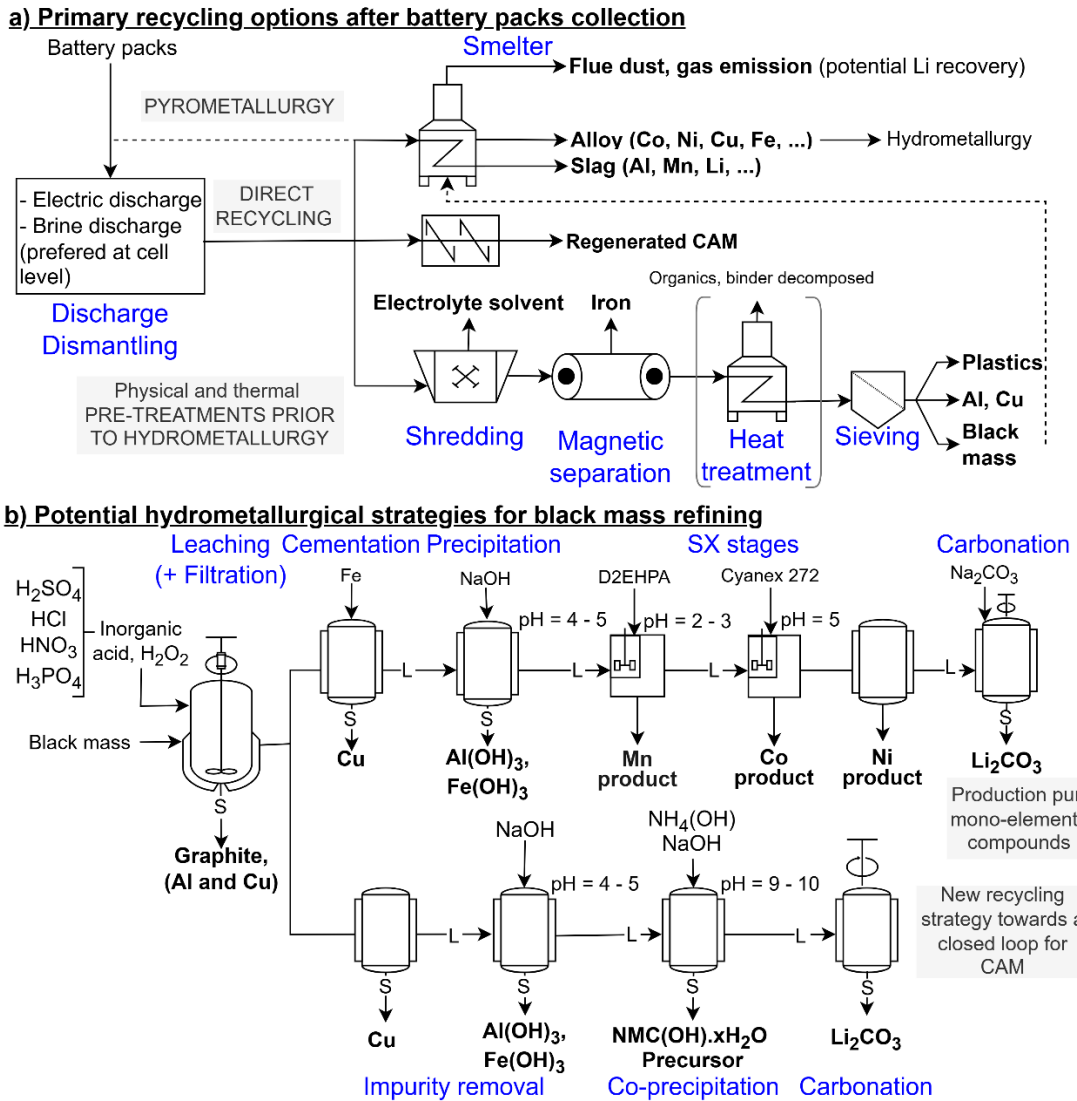


Figure 2: Summary of the significant recycling routes after collection of the batteries.

2.3.1 Pre-treatment

Discharge

Once the batteries are collected, they are discharged (forcing Li⁺ ions to transfer to the CAM structure). This is a crucial step to prevent thermal runaway and product loss through fires while opening the battery [22,43]. Three predominant methods exist on the market: salt-water baths (such as sodium chloride or sulphate), electrical discharge, and thermal treatment. Salt discharge is done more at the cell level. During LiB insertion into the solution, violent reactions might occur, and corrosion of the casing may lead to polluted brine water, which will be complex to handle. Hence, electrical discharge is usually preferred in the industrial landscape; the potential energy recovery and reuse would make the operation more economic [43].

Mechanical treatment

Discharged modules or packs are then disassembled to access the cells. This step can be done manually or automatically. So far, it is mainly done manually, as automation is very challenging due to the large variety of batteries. However, a lot of research and development is being done, as it would reduce the risk and cost of the operation [42,43]. The following steps consist of crushing and separating the battery components into different fractions, including electrolyte solvents, plastics (from separator or casing), steel casing, current collector foils (Al and Cu), and a fine fraction called black mass (BM), a blended mixture of the active materials [17]. Crushing must be carried out with strict safety procedures, as the electrolyte can react with air and risk burning due to oxidation and heat release. Hence, it is usually done under a dry, inert atmosphere. Wet crushing has also been investigated, but it is associated with large wastewater volume, and the resulting BM contains more impurities, making this option less preferred [38]. One major challenge of this step is handling electrolyte solvents. One option is to crush at a medium temperature (under 170°C) to cause the volatilization of the solvent, which can be collected after distillation. More intense heating operations can be applied (300°C max) to decompose the anode binder and organics. Following crushing, a sequence of separation steps separates the components based on their physical properties, such as particle size, density, or conductive and magnetic properties.

The BM fraction is considered to have high economic value, varying depending on the content of Li, Co, Ni, Mn, and other impurities [3,44]. The BM composition significantly influences the downstream hydrometallurgical process; rigorous specifications on its content are needed to enhance the metal recycling rate and purity later. Currently, the most significant impurities are Al, Cu, Fe, electrolytes (salt and solvent), and traces of separator.

Additional novel techniques have been investigated to enhance a higher recovery rate for the production of purer BM (i.e., supercritical fluid, graphite flotation) or to optimize the separation of the CAM from the current collector foil (i.e., binder dissolution, alkaline Al selective dissolution, ultrasonic separation), all methods are listed in Table 1, a combination of all of them could be considered if proven efficient and economically reasonable [45]. These pre-treatments would have a substantial impact on the whole recycling process. It was suggested that deep separation and recovery of Al before hydrometallurgical treatment would have a significant positive effect

on the carbon footprint of the overall recycling process [11]. A thermal treatment can also be applied as a BM pre-treatment, developed later in the text.

Table 1: Additional pre-treatment options for the electrolyte removal or the separation of the active material from the current collector foil [47-54].

Methods	How	Pros	Cons
Supercritical fluid [27,46]	Fluid under controlled P and T, mainly CO ₂ (with potential co-solvents), with a gas trap at the exit.	Remove and recover the electrolyte solvent or binder.	Solubility limit might necessitate the use of co-solvents. Research level only.
Graphite flotation [47]	Water (with potential frothers or collector agents) in a flotation column.	85% of the graphite recovered in the overflow product: potential regeneration or downcycling, i.e., to graphene.	Significant losses of CAM.
Binder dissolution [45,48]	N-methyl pyrrolidone(NMP) or Dimethylformamide (DMF) dissolution.	Weakens the adhesion of the binder with CAM, facilitating its removal from Al foil.	Solvents' high cost and toxicity present significant environmental and health concerns.
Al dissolution [49,50]	Alkaline leaching, mainly with NaOH.	Al leaching yield can reach over 90%.	Li losses, and the alkali wastewater containing Al is complex to purify.
Ultrasounds [51]	Cavitation effect (probe or bath in lab scale).	Efficient separation of CAM from Al.	Hard industrialization and high energy costs.
Mechano-chemical methods [52,53]	High power milling (ball or disk mill).	Structural and physicochemical properties of BM change, facilitating leaching.	High energy cost.

2.3.2 Direct recycling

Direct recycling is part of a holistic paradigm change for recycling, where waste is treated for its direct reusability with minimal resource inputs in terms of time, energy, chemicals, and costs [19]. During its usage, the CAM loses performance due to different degradation phenomena (crystal defects, Li atom losses, ...). Still, its crystal structure remains relatively stable, and there are potential solutions to correct structural defects and re-lithiate the structure to regain its original performance. CAM regeneration can be performed via hydrothermal, solid state, electrochemistry, ionothermal re-lithiation, or molten salt solution treatment [19,54,55]. These challenging operations require stringent CAM pre-treatment; the electrolyte must be removed efficiently, and the CAM must be delaminated from the current collector foil. One can add that direct recycling is a specifically favoured route for the scrap production of LFP CAM, which, as they contain less valuable material, will not be as interesting for the recycling market. Graphite and electrolytes recovery are also under investigation, but fewer options exist, and there is less economic incentive to recycle these fractions so far. One big market challenge for direct recycling is the constant evolution of battery chemistry. Indeed, LiBs with obsolete battery chemistries cannot be short-loop recycled but must be chemically processed into a more relevant cell chemistry [42].

2.3.3 Pyrometallurgy methods

Smelting (above 1000°C)

In this operation, LiBs are smelted at a high temperature (1000-1200°C), allowing the production of an alloy containing Co, Ni, Cu, and Fe since those elements have a low oxygen affinity. This alloy must be further processed using hydrometallurgical techniques to separate the metals. Two major by-products can be recovered: the slag mate and flue dust. The slag comprises high oxygen affinity elements such as Li (and all alkaline metals), Al, and Mn [56,57]. Besides the slag, some Li may be present in the flue dust stream due to the low vapor pressure of Li compounds, such as Li metal, fluoride, or carbonate, and some other volatile elements and fluorinated compounds. All carbon and organic compounds are burnt and leave the furnace as off-gases (CO and CO₂) [7]. The pyrometallurgy process is a mature technology; commercial processes already exist. For example, Umicore (Belgium) is currently recycling batteries using a pyrometallurgical treatment called ultra-high temperature (UHT), and recovering Ni, Co, and Cu from the alloy using a hydrometallurgical process after smelting [56]. The predominant advantages are handling large volumes of battery waste and the high flexibility regarding the input material, since there is no need to sort collected batteries based on their chemistry. Moreover, no prior discharge or mechanical treatment is needed. However, the need for energy in such a process is concerning, and various gases are emitted. Lastly, Li is distributed among the flue dust and slag, making it hard to recover [7].

Heat pre-treatment (above 500°C)

Pyrometallurgy techniques can also be used to pre-treat waste. Here, the temperature applied will be lower than in the smelting process; typically, it is between 500°C and 900°C under a controlled atmosphere (Air, O₂, H₂, N₂, Ar, etc.). The sole BM processing can already have a substantial effect, as the carbon in the waste can trigger the carboreduction of the CAM (forming Li carbonate and reduced TM, more details are given in the next section) [58–61]. Additionally, some reagents can be added to the BM to assist the roasting operation. These agents are selected to help transform Li metal oxide into more soluble substances such as sulphate, chloride, or nitrate [58,60,62]. This strategy has some advantages; again, the batteries can be inserted without preliminary discharge, and it would reduce waste volume, facilitating transport [63]. Moreover, the binder will decompose, allowing easy separation of the active material from the current foils [17]. This benefits the hydrometallurgical processes, concentrating the BM and increasing the contact surface between the valuable elements and the leaching agent. Lastly, the Li metal oxides from the cathode material can be transformed into more leachable species and offer the possibility for selective Li recovery, as explained later in the thesis.

2.3.4 Hydrometallurgy methods

Compared to the pyrometallurgy route, hydrometallurgy methods enable higher recovery rates, along with lower hazardous gas emissions, and require less energy [38,64]. They have high potential for industrial realization. However, they are a more complex and chemically intensive process involving metal leaching, followed by separation and purification through chemical precipitation, solvent extraction, or electrochemistry techniques such as cementation.

Black mass leaching

The valuable metals in the BM (Li, Co, Ni, Mn, Al, Cu, Fe) are first dissolved in the leaching medium. At the same time, insoluble components, such as graphite or plastic fragments, are recovered in the solid leaching residue. The commonly used acids are mainly inorganic, such as HCl, H₂SO₄, and HNO₃ [65–68]. Usually, adding a reducing agent is needed to reduce the element into a more leachable oxidation state, i.e., from Co(III) to Co(II) or Mn(IV) to Mn(II). In fact, the NMC dissolution mechanism with mineral acid has been investigated [65]. With sulfuric acid (which has a low reducing power), the mechanism is shown to be in two steps: first, the structure is delithiated, which, by charge compensation, initiates the dissolution of TM [69]. Then, the mechanism is chemically controlled by the solution pH, and the dissolved TM can act as a reducing agent, enhancing the TM recovery. Some authors showed that Al, Cu, or Fe from the BM could take part in the dissolution mechanism, acting as reducing agents, but their low content implies using an external reducing agent [67,68]. The most common acids and reducing agents used are sulfuric acid and hydrogen peroxide [22]. The leaching conditions vary depending on the chosen process, operation parameters can be acid concentration from 1 to 5 M, H₂O₂ addition from 3 to 10 vol%, temperature from 50 to 90°C, time from 1h to 6h, and a solid-to-liquid ratio (S/L) from 20 to 200 g/L [17,21,24,70].

Using these inorganic acids is associated with various gaseous emissions such as SO_x, Cl₂, or NO_x, depending on the acid used, and the formation of waste streams and wastewater [28,30,64,71]. Therefore, some research is ongoing to replace inorganic acid with organic acid (citric, malic, or oxalic acid) to avoid gaseous emissions. They are usually considered more environmentally friendly than classic inorganic agents [30,64,72]. The composition of the leaching solution will depend on the feed material, the impurity content, and the wrong sorting of battery type, which can lead to a higher content of certain elements. For example, some authors tested the leaching of a mixture of synthetic NMC material and LFP to assess the impact of higher Fe content on the sulfuric acid leaching. It was shown that by adding LFP, the transition metal extraction increased (as the presence of Fe(II) lowered the redox potential), as well as the acid consumption. Additionally, H₂O₂ was decomposed by the high concentrations of Fe(II) and Mn(II), reducing its total efficiency.

Towards mono-elemental compounds production

Leached metals can be recovered and purified using different techniques, such as solvent extraction (SX), ion exchange (IX), precipitation, or crystallization; wherein, selectivity is a very important factor in minimizing valuable metal losses and enhancing battery recycling costs.

Impurities such as Al, Cu, and Fe can be eliminated through precipitation [73,74]. Typically, NaOH is used as a precipitating agent; the equilibrium pH to remove Al and Fe is ca. 4-5. However, co-precipitation of Mn, Ni, Co, or Li can occur at different levels, up to 21%, depending on the amount of Al to be removed [49,75]. Temperature is known to decrease pH_{eq} but to increase co-precipitation, thus, it must be controlled carefully [76]. Researchers explore other reagents or methods to mitigate the losses, like IX or SX [22]. For example, LiOH or Na₂PO₄ can be used as precipitating agents. The first one can reduce valuable metal losses by 50% and avoid Na⁺ ion addition [75]. Meanwhile, precipitation with phosphate reduces losses and increases the

filterability of the Al-Fe cake by avoiding the formation of Al(OH)_3 particle gel-like colloids [76,77]. Although Cu could be precipitated, it usually involves higher Ni losses. Hence, other separation techniques, such as cementation before Al and Fe removal or SX (Acorga M5640 or LIX extractant can be applied), are typically used.

Downstream, Ni, Co, and Mn separation is typically executed through SX, IX, or precipitation methods. Although precipitation with LiOH, NaOH, or Na_2CO_3 is efficient and viable, pH control complexities may lead to the co-precipitation of other elements [17,27,64,78]. For instance, Li losses can be up to 25% in total when using NaOH [22]. Solvent extraction techniques can mitigate these losses and recover highly pure compounds. It separates the metal ions using organic extractants such as D2EHPA (Bis(2-ethylhexyl) hydrogen phosphate), Cyanex 272 (bis(2,4,4-trimethylpentyl) phosphinic acid), PC-88A (2-ethylhexyl 2-ethylhexylphosphonic acid), or TODGA (tetra-octyldiglycolamide) [70]. Many flowsheets have been developed at different scales. One possible process is the use of D2EHPA to recover Mn from the leachate (at a pH of 2–2.5) [17]. Cyanex 272, an organophosphorus acid extractant, is frequently used in the mineral industry to separate Co from Ni in sulphate solutions. Co is extracted at a pH of about 5, while Ni is efficiently recovered at a pH of about 6.5 [17]. Their main disadvantage is the complexity of such a method, with multiple extraction stages, and the high cost of solvent, which in many cases is toxic [22].

Finally, Li is recovered using Na_2CO_3 as a precipitating agent [78,79]. A significant amount of Na_2SO_4 is generated (about 2 kg for every 1 kg of Li_2CO_3 produced) as a secondary waste stream, currently unused and disposed of. Since Li is obtained at the end of the recycling flowsheet, different extraction steps lead to Li losses, resulting in lower Li recovery. The exact loss percentage is hard to obtain, but an estimation of around 20% is very probable. For example, some authors evaluated the presence of Li in large quantities in the waste process water (from 1 to 5 g/L [80]). Thus, more research has been performed to increase the overall Li recovery from process water or end stream solutions via direct Li extraction. For example, precipitation with sodium and choline alkanoate soaps was proven efficient to reduce the Li concentration to the ppm level (less than 100) [80]. In the same way, cationic resins or Mn and Al-based adsorbents can be employed to remove Li, but they have low selectivity towards other alkaline cations (Na, Mg, etc.) [81,82]. Finally, some SX systems were investigated [83,84]. These techniques are still at the laboratory level and require some optimization to be industrialized for the recycling of LiBs.

Towards the direct reproduction of CAM

Due to the similarity of TM ions like Co, Ni, and Mn in solution, their separation is challenging. To simplify the recycling process and reduce costs, a precursor material can be directly prepared by adjusting the leaching solution's composition, followed by the cathode material's regeneration through co-precipitation or sol–gel methods. This approach has started to be widely investigated in recent years [85–90]. For example, Sa et al. [86] demonstrated the feasibility of synthesizing the precursor $\text{Ni}_{1/3}\text{Mn}_{1/3}\text{Co}_{1/3}(\text{OH})_2$ from the leachate of mixed LiBs using co-precipitation with carefully controlled reaction parameters, thereby reducing the complexity of separating these metals.

Factors such as pH, temperature, and metals' concentration must be optimized to maximize the CAM production. One challenging aspect of this method is impurity management. The primary

contaminant in the TM-loaded solution, regarding its potential for CAM precursor, is Cu [91–93]. Metallic Cu is known to have a negative effect on the electrochemical performance of the regenerated NMC materials. A moderate amount of Cu ions could promote particle nucleation, enhance primary particle growth, and reduce cation mixing in the NMC cathode. However, an excess of Cu would degrade electrochemical performance [92,93]. It is worth noting that Li in very low quantities will not affect the NMC synthesis [94,95]. On the contrary, it could participate depending on the synthesis process chosen in the end.

State of the art of selective lithium dissolution

As stated above, the hydrometallurgy process can suffer from significant Li losses. Different methods can be considered for its removal before the co-precipitation of TM. This early recovery would have two major advantages: it would increase the recovery rate and reduce the concern about impurity for CAM re-synthesis. The current state of the art for an early recovery of Li is presented here (2 major strategies), which has been the starting point of this research project, helping to identify the best operating conditions and strongly assess the process's limitations.

1. Combination of pyro and hydrometallurgy

The first method combines pyrometallurgy and hydrometallurgy techniques. Here, one potential pre-treatment of the BM is evaluated to enhance Li dissolution, and the other metals later: the BM is thermally reduced, followed by water leaching. Li carbonate, produced during metal oxide reduction, is dissolved selectively in water while the remaining valuable metals remain in the solid phase. Li carbonate crystals can then be obtained after evaporative crystallization at 95°C. Some authors have investigated this technique, and the parameters corresponding to the optimal leaching yield of Li are summarized in Table 2. This technique already shows high recovery rates (between 60 and 95%), which makes it very promising. Previous research has been using synthetic material mimicking industrial BM.

*Table 2: Summary of conditions for Li dissolution after thermal pre-treatment and water leaching reported in the literature (commercial cathode material *, INC: Incineration, and PYRO: pyrolysis).*

Material		Initial composition wt% (%)	Thermal treatment				Leaching		Li Yield (%)	Ref.
Active material	Reducing agent		Type	T (°C)	t (min)	S/L (g/L)	T (°C)	t (min)		
LiMnO ₂	Anode material	4.8% Li, 0.1% Ni, 51% Mn	INC	650	60	40	Amb.	20	83	[96]
LiMn ₂ O ₄	Anode material	-	Vac. PYRO	700	45	40	Amb.	30	82	[97]
LiCoO ₂	10% Coke	7.2% Li, 20.0% Ni, 20.5% Co, 19.4% Mn	PYRO	650	30	34	25	60	83	[61]
NMC										
*NMC 111	20% activated carbon	6.5% Li, 1.6% Ni, 40.6% Co, 1.6% Mn, 7.8% Al	PYRO	700	30	-	0	60	94	[98]
LCO										
NMC	Anode + 10% of graphite	2.2% Li, 6.2% Al	PYRO	700	60	50	80	180	60	[99]

2. The use of oxalic acid as a leaching agent

The second method is only hydrometallurgical-based, saving the use of the thermal treatment method and avoiding inorganic acid. Oxalic acid is a good candidate as a leaching agent as it forms strong chelating complexes, which makes the dissolution mechanism based on protonation and complexation. Li reacts with oxalate ion to form a simple soluble oxalate, while Cu, Co, Mn, and Ni are reported to form insoluble compounds [100]. Some authors have already investigated this technique, and the parameters corresponding to the optimal leaching yield of Li are summarized in Table 3.

Table 3: Summary of conditions for Li extraction using oxalic acid (OA) as a leaching agent reported in the literature.

	Preparation of the feed material	[OA] (M)	S/L (g/L)	T (°C)	t (min)	Stirring (rpm)	Leaching yield (%)				Ref.
							Li	Co	Ni	Mn	
LCO	LCO powder from cathode and anode after crushing and magnetic separation (18mesh)	3	50	80	90	300	99	0.4	-	-	[101]
LCO	Discharged, crushed by shear crusher, and sieved (size < 1.43mm)	1	15	95	150	400	98	< 3	-	-	[102]
NMC	Dismantling and manual separation of the anode and cathode. Cathode foil treated with NMP to recover active material. Pyrolysis at 700°C.	0.6	20	70	120	-	81	< 1.5	< 1.5	< 1.5	[103]
NMC	Commercial NMC (111, 532, 811)	1	10	95	12h	-	96	< 0.5	< 0.5	22	[104]

2.4 Research Questions and Scope

2.4.1 Identified recycling challenges

Based on this state-of-the-art recycling for LiBs, a few challenges can be defined:

1. Long and complex processes may result in Li loss during precipitation or SX, diminishing economic benefits and elevating pollution levels. The sequential TM separation adds further operational costs, including chemicals and energy. This emphasizes the necessity for optimized recycling technologies to reduce metal loss and enhance sustainability [105].
2. Leaching with inorganic acids for LiBs recycling presents environmental challenges due to wastewater and gas emissions (i.e., CO₂, Cl₂, SO₂). This process contributes to equipment corrosion and generates secondary waste over the long term [80,81]. Disposal of wastewater containing acid, hazardous fumes, and acidic leachates is a significant issue leading to economic and energy losses. The resulting low pH leaching solution complicates direct metal extraction, further exacerbating the financial and energy losses associated with hazardous fumes and acidic waste disposal [106].
3. Leaching mechanisms (with inorganic and organic acids) require further investigation. Considerable effort must still be exerted to direct the selection of leaching reagents and operating conditions. For instance, more research is needed to determine the alterations in the crystal structure during the leaching process. This will offer valuable insights into the reaction mechanism occurring during leaching. Additionally, the influence of different feed material compositions should be analysed and considered, as a very diverse battery type can lead to specific impurities (Fe, Cd, F, ...).
4. The rapid evolution of batteries can slow down the development of recycling processes; the approaches developed must be versatile and very cost-efficient to achieve industrialization. The incentive to recycle one day can be absent in a few years; a strong example can be given with reducing the Co proportion in NMC material, which can lower economic motivation.

2.4.2 Project boundary and Research question enunciation

The project aims for a greener and circular LiBs recycling and production process, tackling the abovementioned challenges. First, a selective and efficient recovery of Li will be investigated, followed by testing the dissolution of the remaining valuable TM using environmentally friendly chemicals or aiming at acid regeneration. Finally, after impurity removal, the solution (containing Ni, Mn, and Co) will be used as feed for the CAM precursor, striving to close the loop of battery production. The initial idea of the process is presented in Figure 3. Foremost, two strategies for this early and selective recovery of Li were assessed as presented above. The thesis does not include the investigation of the CAM re-synthesis, only the production of the so-called recycled leaching solution.

The primary focus of the research is optimizing selected methods and improving our understanding of their mechanisms, complemented by evaluating their feasibility.

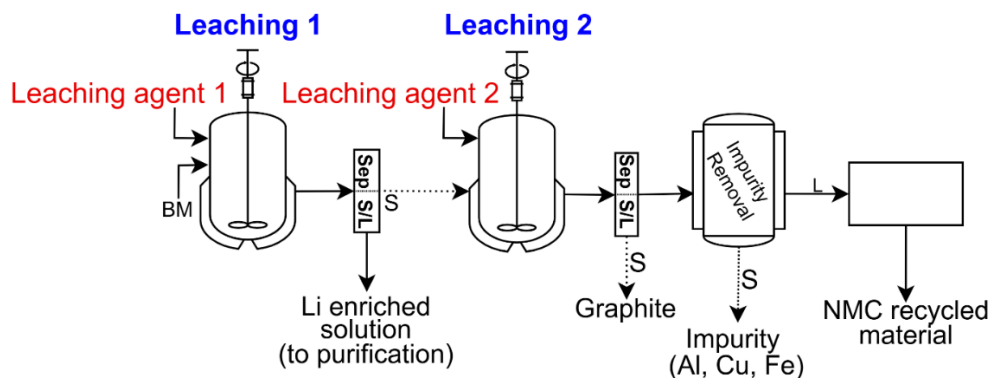


Figure 3: Proposed recycling flowsheet in the research project based on early Li recovery – NMC re-synthesis is not investigated here.

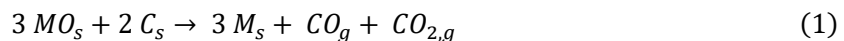
3 THEORY of EXTRACTIVE METALLURGY

The following section provides the fundamental aspects of extractive metallurgy, focusing on concepts necessary to understand the research performed in this thesis.

3.1 Carboreduction of Metal Oxides

3.1.1 Overview

Solid-state carbothermic reduction is described as reducing metal oxides (written as MO in the equation) to a lower oxidation stage using carbon as a reductant. The main reaction products are reduced metals, CO , and CO_2 . This phenomenon is happening above $500^\circ C$ [107,108], and likely occurs through two mechanisms [108]. The first one is a direct reduction between the two solid species in contact with each other (Equation 1), and the second one is an indirect reduction, which occurs through the gaseous intermediate products and the metal oxides (Equation 2). The produced CO_2 can react again with carbon, regenerating CO (Boudouard reaction). This can be performed under an inert atmosphere, the operation is called pyrolysis, or in the presence of oxygen, it is called incineration.



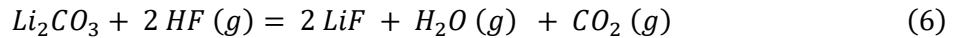
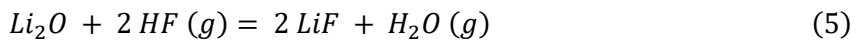
3.1.2 Black Mass Carboreduction

Carbothermal reduction is one of the most important methods of recovering CAM in pyrometallurgy. The reducing agent plays a pivotal role in facilitating the degradation of oxygen octahedra within Li-oxygen batteries, catalysing the progression of the reaction [58]. BM can contain ca. 10 to 45 wt% of carbon, present as graphite (20 – 45 wt%), separator (mainly PP or PE, 3 – 10 wt%), residual active carbon, or electrolyte solvent [22]. Graphite is a known reducible source. Beyond $500^\circ C$, PP and PE also completely decompose, forming CO , CO_2 , and H_2O , which can participate in the reduction.

The $LiNi_{1/3}Mn_{1/3}Co_{1/3}O_2$ structure is reduced, forming different phases: Ni, NiO , Mn_3O_4 , MnO_2 , MnO , Co, CoO , and Li_2O [28,63,109–111]. While Co and Ni can be reduced entirely after optimal pyrolysis, Mn keeps an oxidation state higher than 0 (at +2). Their different phase ratio differs depending on the thermal treatment conditions and how effective the reduction could be. Li_2O reacts with CO_2 to form the Li_2CO_3 compound [112]. Less CO_2 is emitted during pyrolysis, which is more sustainable than incineration [34]. These reactions were considered when analysing the results of Papers I and III. The reduced oxides will be more easily leached, which decreases the consumption of expensive reductants [113].

PVDF decomposition occurs when subjected to temperature; it starts at $450^\circ C$ under nitrogen, while oxygen concentration decreases the initial decomposition temperature to $320^\circ C$ [114]. The primary decomposition product is gaseous HF and other fluorinated compounds; generating such hazardous gaseous substances requires stringent off-gas cleaning, typically done by a water trap at lab scale. Another source of HF is electrolyte salt decomposition, $LiPF_6$, at a temperature higher than $200^\circ C$ in the presence of water [57], presented in Equations 3 and 4. POF_3 generated can

continue reacting, generating more HF. Moreover, the gaseous HF formed can react with Li₂O or Li₂CO₃ to form LiF (Equations 5 and 6). At 600°C, those reactions are spontaneous with a Free Gibbs Energy change (ΔG) of -224.2 kJ and -135.0 kJ, respectively.



Finally, Al melts at 660°C. The thermal treatment should aim to be under this limit, as melted Al can prevent carbo reduction and coat the product, limiting the downstream leaching. Al is most likely to form the stable oxide Al₂O₃ in the presence of oxygen.

3.2 Chemical Fundamentals of Metallurgy

3.2.1 Thermodynamics and equilibrium considerations

Metals or minerals interact with chemicals through different reactions. Thermodynamics can be used to determine if a considered reaction is likely to occur under specific conditions (temperature, pressure, ...) [115,116]. The Gibbs free energy change of a reaction at a specific temperature, T, is described by Equation 7. Q is the ratio of products' activities over reactants' activities in nonstandard conditions (molar concentrations can be used if ideal solution assumptions are made), when ΔH_R and ΔS_R are the enthalpy and entropy change of the reaction, respectively.

$$\Delta G_R(T) = \Delta G_R^0(T) + RT \ln Q = \Delta H_R(R) - T \Delta S_R(T) \quad (7)$$

At equilibrium, $\Delta G_R(T) = 0$, meaning that the system has no free energy to gain or lose and no driving force to induce any modification. In that case, the standard free energy of a reaction may be calculated from Equation 8 and a negative value will describe a spontaneous reaction. Q becomes K_R , the equilibrium constant. If a system at equilibrium is subjected to any variation (i.e., temperature, addition of reactants, ...), the system adjusts to reestablish equilibrium, a principle known as *Le Chatelier's Principle* [115–117].

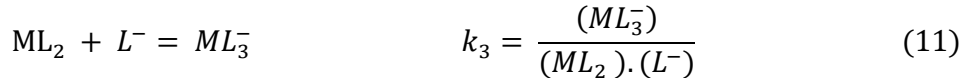
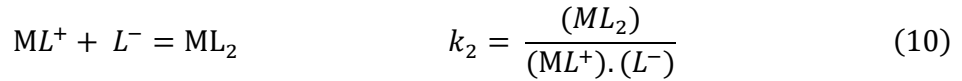
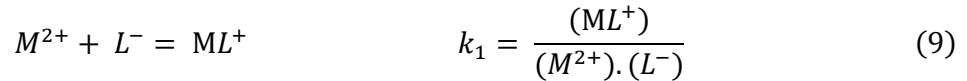
$$\Delta G_R^0(T) = -RT \ln K_R = \Delta H_R^0(T) - T \Delta S_R^0(T) \quad (8)$$

3.2.2 Metal ions in solution

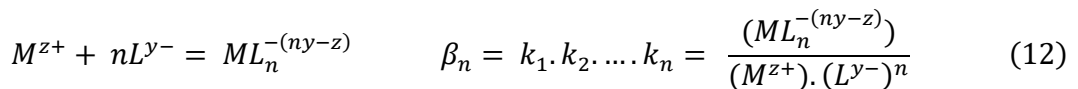
Basics of coordination chemistry

In a water solution, a metal ion is typically associated with water molecules; we speak of coordination chemistry when ligands replace these water molecules in the inner coordination sphere. A ligand is a compound that can coordinate to the metal ion via a donor atom to form a complex (Lewis acid-base association); it can be anionic, neutral, or even cationic [116]. Some ligands, known as polydentate, present more than one donor atom (coordination sites) and produce chelate complexes. Such complexes generally have additional stability due to the chelate effect [118].

Complex formation is a step mechanism where one ligand is coordinated to the metal or metal complex at a time. Equation 9, 10, 11 present these first steps in the case of a metal ion (M , charged 2+, omitting its hydration sphere) with a ligand (L , charged negatively). Each step, n , can be defined by the stability constant, k_n .



Consequently, the general expression of complex formation for a generic metal, M , and ligand, L , is expressed in the Equation 12. Here, β_n is the cumulative stability constant. In general, the greater the value of β_n , the greater is the complex stability. The (...) denotes the compound's concentration, generally mol/L.



Basics of solubility

As described above, different ionic species can combine in solution; precipitation occurs when the product of reactant activities exceeds the solubility constant (K_{sp}), which is only valid at equilibrium [115,116]. Conversely, the precipitate would re-dissolve if the solubility product is not exceeded. The constant is written for the dissociation reaction as described in Equation 13. K_{sp} is typically lower than 1 for an insoluble product; the more negative the log K_{sp} , the less soluble the compound. This concept is essential for all research (Papers I, II, IV, and V).



Speciation and phase diagram

Speciation diagrams help determine the effects of conditions (pH, ligand concentration, potential, ...) on species distribution. They can provide a visual and quantitative representation of species availability at equilibrium. For example, Figure 4 provides the speciation of oxalic acid in water under standard conditions. Metal speciation in different systems can also be provided. It is worth mentioning that at low pH values, protons can compete with the metal ions for the ligand, and the extent of complex formation will, therefore, depend on the pH in the case of many ligands.

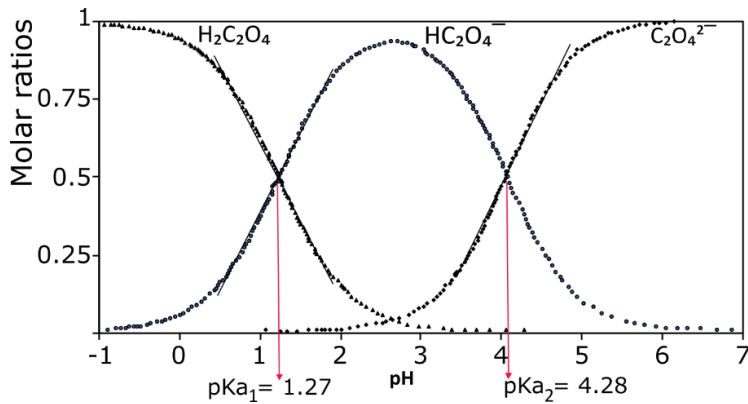


Figure 4: Predominance diagram of oxalic acid at 25°C [119].

3.3 Leaching – Metal Extraction

3.3.1 General principle

Leaching aims to dissolve desired elements from a solid phase into a liquid medium called the leaching solution or leachate. Typically, leaching involves a heterogeneous reaction between a target compound in the solid and the liquid leaching reagent. Such a reaction results from multiple phenomena that operate in series; the particle morphology will strongly influence the mechanism. For a dense spherical particle, the dissolution will likely follow these steps [117,120–122]:

1. Reactant mass transfer from the bulk to the outer surface of the solid particle.
2. Diffusion of the reactant in the solid-liquid interface.
3. Interface reaction. The interface reaction mechanism of oxide dissolution usually comprises different reaction steps, starting with protonation, then complexation and/or reduction. The latest can be combined, one promoting the other. In general, the protonation mechanism is the slowest. To study these intrinsic reactions and not bother with mass transport, it is necessary to work with a stirring factor that makes the liquid composition on the surface equal to the bulk [121]. At a fixed stirring speed, it can be possible to identify which of the diffusion or intrinsic reactions is rate-controlling.
4. Diffusion of the product in the interface.
5. Product mass transfer to the bulk.

Overall, several factors influence the operation, including process conditions (such as temperature, stirring speed, S/L ratio, or time), solid characteristics (such as composition, size, or surface area), and leaching reagent characteristics (such as concentration, pH, or redox potential). The leaching yield or conversion (Y) for each element corresponds to the ratio of this element, which has transferred from the solid to the solution; it can be calculated following Equation 14.

$$Y_i (\%) = \frac{C_i \times V}{m_0 \times w_i} \times 100 \quad (14)$$

Where C_i is the concentration of the element, i , in the final solution (mg/L), V is the volume of leaching solution (L), m_0 is the initial weight of the sample (mg), and w_i is the elemental weight percentage in the sample (%).

3.3.2 Kinetics & Mechanism investigation

While thermodynamics provide insights into how a system can evolve by considering only the initial and final states of the reaction, kinetics offer information about the timing of various phenomena. By investigating chemical reaction rates, it is possible to understand the chemical mechanism behind an operation, thereby helping in engineering design [120,121]. Different models have been developed focusing mainly on the physical properties of the particle; the progressive conversion model (PCM) and shrinking core model (SCM) are the two most applied models [121]. SCM considers that the reaction starts from the particle surface and continues until the particle centre is reached. Different scenarios can be considered, i.e., the particle size remains constant or decreases during the reaction.

Through experimentation, an empirical rate expression can be derived for one target leaching agent. The reaction rate generally depends on the temperature and concentration of different species (S/L ratios and reagent concentration). Other factors can be considered, such as pressure, chemical composition, and/or distribution of the compounds of interest in the solid.

This can then be juxtaposed with a rate expression derived from a theoretical sequence of intermediate reactions, essentially an assumed reaction mechanism. This comparative analysis allows for the elimination of mechanisms that do not align with the observed expression. However, it's essential to note that multiple mechanisms can yield the same expression rate. Consequently, relying on experimentation may not always determine which mechanism is truly at play [120]. A complete reaction rate calculation is complicated if all steps have a rate constant of similar magnitude. Usually, the rate constant for one of the above steps is significantly smaller, and this step is rate-controlling, whereas other steps are close to equilibrium [120]. Several different models describe the dissolution rate, the most relevant are presented in Table 4. Where the leaching conversion or yield is noted Y , k is the reaction rate constant (min^{-1}), and m is a constant proper to the used model. The significance of each model evaluated will be discussed in the results section.

Table 4: Models for the dissolution rate – Equation and physical background associated.

Physical background	Equations	
1D Diffusion	$Y^2 = k \cdot t$	(15)
2D Diffusion	$(1 - Y) \ln(1 - Y) + Y = k \cdot t$	(16)
3D Diffusion	$\left[1 - \left(1 - Y^{\frac{2}{3}}\right)\right]^2 = k \cdot t$	(17)
3D Diffusion	$\left(1 - \frac{2}{3}Y\right) - (1 - Y)^{\frac{2}{3}} = k \cdot t$	(18)
First order	$-\ln(1 - Y) = k \cdot t$	(19)
Second order	$\frac{1}{(1 - Y)} - 1 = k \cdot t$	(20)
Third order	$\frac{1}{2} [(1 - Y)^{-2} - 1] = k \cdot t$	(21)
Shrinking disk	$1 - (1 - Y)^{\frac{1}{2}} = k \cdot t$	(22)
Contracting sphere	$1 - (1 - Y)^{\frac{1}{3}} = k \cdot t$	(23)
Avrami order, m	$-\ln(1 - Y) = k \cdot t^m$	(24)
	$\ln(-\ln(1 - Y)) = m \ln(k) + m \ln(t)$	(25)

The effect of temperature on reaction rate is described by the Arrhenius law as described in Equation 26.

$$k = k_0 e^{\frac{-E_a}{RT}} \quad (26)$$

With E_a , the energy of activation in kJ, R the gas constant of $8.314 \text{ J.mol}^{-1}\text{K}^{-1}$, and T the temperature in K. E_a can be determined by plotting $\log(k)$ as a function of $1/T$. Chemically controlled reactions are more sensitive to temperature, as the energy of activation of a reaction is usually higher than the activation energy for diffusion during a leaching operation. However, at high temperatures, the diffusion can become the rate-controlling step [121]. A value higher than 40 kJ/mol emphasizes the chemically controlled nature of the dissolution [117,121]. It is essential to remember that a sequence of consecutive reactions involves steps with specific activation energies; an increase in temperature can lead to the step with the lowest activation energy becoming the rate-determining step [120].

3.3.3 Selective Li dissolution from Black mass

Water leaching of thermally treated Black mass

The water leaching mainly relies on the solubility of Li compounds in water. The solubilities of all Li compounds expected in the thermally treated BM (Li_2CO_3 and LiF) are given in Table 5. Another compound formed during the thermal treatment is Li_2O , which spontaneously reacts with water to form Li hydroxide (Equation 27 - $\Delta G^\circ = -105.7 \text{ kJ}$ at 25°C).



Table 5: Solubility of Li compounds in aqueous solution [123,124].

	Li_2CO_3	LiOH	LiF
Solubility (g/L) at 20°C	13.3	110	1.2
$\log(K_{sp})$	-3.1	8.4	-2.7
Solubility (g/L) at 100°C	7.2	161	1.3

Oxalic acid leaching of Black mass

Oxalic acid is an acid with complexing and reducing properties (making the mechanism of dissolution acid/complex based). Hence, BM oxalic acid leaching is a reactive leaching, where Li reacts with oxalate ions to form a simple oxalate, while Cu, Co, Mn, and Ni form simple and complex oxalates [100]. A simple oxalate complex is a complex in which a single oxalate ligand coordinates to a single metal cation. The main dissolution reactions identified for the leaching of LCO cells are seen in Equations 28 and 29 [102,125]. Verma et al. evaluated the energy of activation of the LCO dissolution at $61.0 \pm 2.5 \text{ kJ/mol}$ [71]. The leaching selectivity lies in the low solubility of Mn, Ni, and Co oxalate formed, as seen in Table 6, additionally, the complex formation stability constants for most metals in LiBs are given in Table 7. This is the base of paper II.



Table 6: Solubility and K_{sp} of oxalate compounds [124].

	LiC_2O_4	CuC_2O_4	MnC_2O_4	CoC_2O_4	NiC_2O_4
Solubility (g/L) at 18°C	6.6	-	-	0.035	0.003
$\log(K_{sp})$	-	-9.4	-6.8	-7.2	-9.4

Table 7: Cumulative formation constant, K , of metal oxalate compounds [124].

$\text{M}(\text{C}_2\text{O}_4)_n$ - Metals	Mn (II)	Co (II)	Ni (II)	Al (III)	Cu (II)	Fe (III)
$n = 1$ - $\log(K_1)$	4.0	4.8	5.3	7.26	6.16	9.4
$n = 2$ - $\log(K_2)$	5.8	6.7	7.6	13.0	8.5	16.2
$n = 3$ - $\log(K_3)$		9.7		16.3		20.2

3.4 Metal Separation Techniques

After the leaching operation, the resulting solution must be subjected to one or more chemical operation steps to remove the impurities and/or concentrate the solution to recover the desired metal in a pure form. These processes can involve precipitation, SX, IX, adsorption, cementation, or crystallization. The first two are utilized in this research and are developed in this section.

3.4.1 Precipitation

The separation of impurities by precipitation is commonly used. This operation is carried out by adding reagents that precipitate insoluble hydroxides or salts. The solubility of many metals in aqueous media is pH-related; metals tend to form hydroxides at specific pH levels, as seen in Figure 5. As mentioned in the background section, some metals will precipitate at the same pH level (i.e., Cu and Ni around a pH of 7). Several factors, such as temperature, stirring speed, time, and precipitation reagent characteristics, influence the operation. To evaluate performance, the precipitation yield can be given as presented in the Equation 30. This method is used in Paper V.

$$\%P_i = \frac{C_i \times V_{solution,t}}{C_i \times V_{solution,0}} \times 100 \quad (30)$$

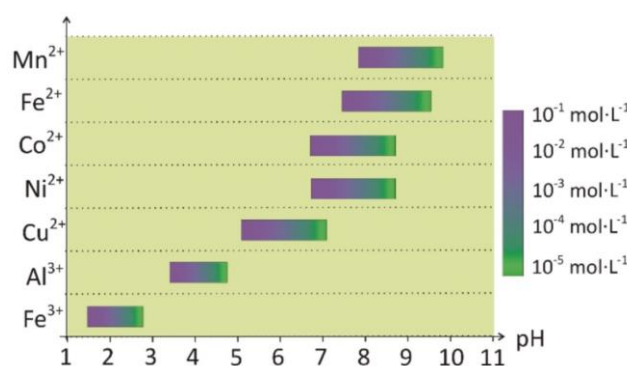


Figure 5: Hydroxide precipitation pH range for Cu^{2+} , Al^{3+} , Fe^{3+} , Ni^{2+} , Co^{2+} ions from 0.1 M to 10^{-5} M [95].

3.4.2 Solvent extraction

Solvent extraction or liquid-liquid extraction is a widespread unit operation in hydrometallurgy. It is based on the distribution of the solute, typically a metal, between two immiscible liquid phases: an organic phase (composed of an extractant in a diluent) and an aqueous phase (usually the leaching solution).

The solvent extraction process comprises three steps [126]:

1. Extraction of the solute from the solution (Loading).

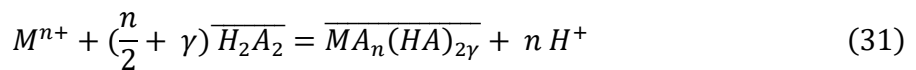
The extraction rate depends on fundamental parameters such as the extractant type and concentration, the diluent, the phase volume ratio between the organic and the aqueous phase, θ , the contacting time, the temperature, the pH of the aqueous solution, etc.

2. Scrubbing: co-extracted impurities are removed.

3. Stripping (unloading) of the solute via another aqueous phase. The depleted solvent can be recirculated in the first step.

Finally, the metal compounds are produced using a chemical reagent (to extract it by precipitation or complexation) or by evaporation (crystallization).

In LiB recycling, acidic extractants are mainly used [127,128]. The general mechanism for such an extractant is described in Equation 31, where $\overline{H_2A_2}$ is the dimeric protonated form of the extractant in the organic phase (indicated by the above bar) and $\overline{MA_n(HA)_{2\gamma}}$ is the neutral complex formed and extracted in the organic phase. Protons are released in the reaction; the pH_{eq} strongly influences the reaction's completion as it governs the dissociation of the extractant in the aqueous phase.



The distribution ratio, marked D, describes the metal partition between the two phases. It is computed, using Equation 32, as the total metal concentration ratio between the organic ($\overline{[M]_{tot}}$) and aqueous phases ($[M]_{tot}$), usually measured at equilibrium. The extraction percentage can also be calculated using the Equation 33 to evaluate the performance of the extractant, it relies on the elemental mass balance of the operation. It quantifies the transfer of the metal, M, initially present in the aqueous phase ($[M]_0$) into the organic phase ($\overline{[M]_t}$) after a specific time, t, and θ is the volume ratio between the organic phase (V_{org}) and the aqueous phase (V_{aq}).

$$D = \frac{\overline{[M]_{tot}}}{[M]_{tot}} \quad (32)$$

$$E = \frac{\overline{[M]_t}}{[M]_0} = \frac{[M]_0 - [M]_t}{[M]_0} = \frac{100 \cdot D}{D + 1/\theta} \quad (33)$$

Finally, to develop a solvent extraction process, knowing how many stages are required to achieve the expected purity and extraction rate is essential. Equation 34 presents a simplified expression of the extraction percentage in the case of crosscurrent extraction. While Equation 35 is the expression of the percentage extracted for counter-current extraction, also known as the Kremser equation [126]. They can both be used to determine the theoretical number of stages (n) needed.

$$E = 1 - \frac{1}{(1 + D \cdot \theta)^n} \quad (34)$$

$$E = 1 - \frac{D \cdot \theta - 1}{D \cdot \theta^{n+1} - 1} \quad (35)$$

4 MATERIALS and METHODS

4.1 Overview of the Experimental Work

The experimental work performed is presented in Figure 6, it is based on the five papers and manuscripts attached to this thesis. In red, the limit of this research. The following section presents all materials, instruments, or equipment used and the methodology applied to perform the research.

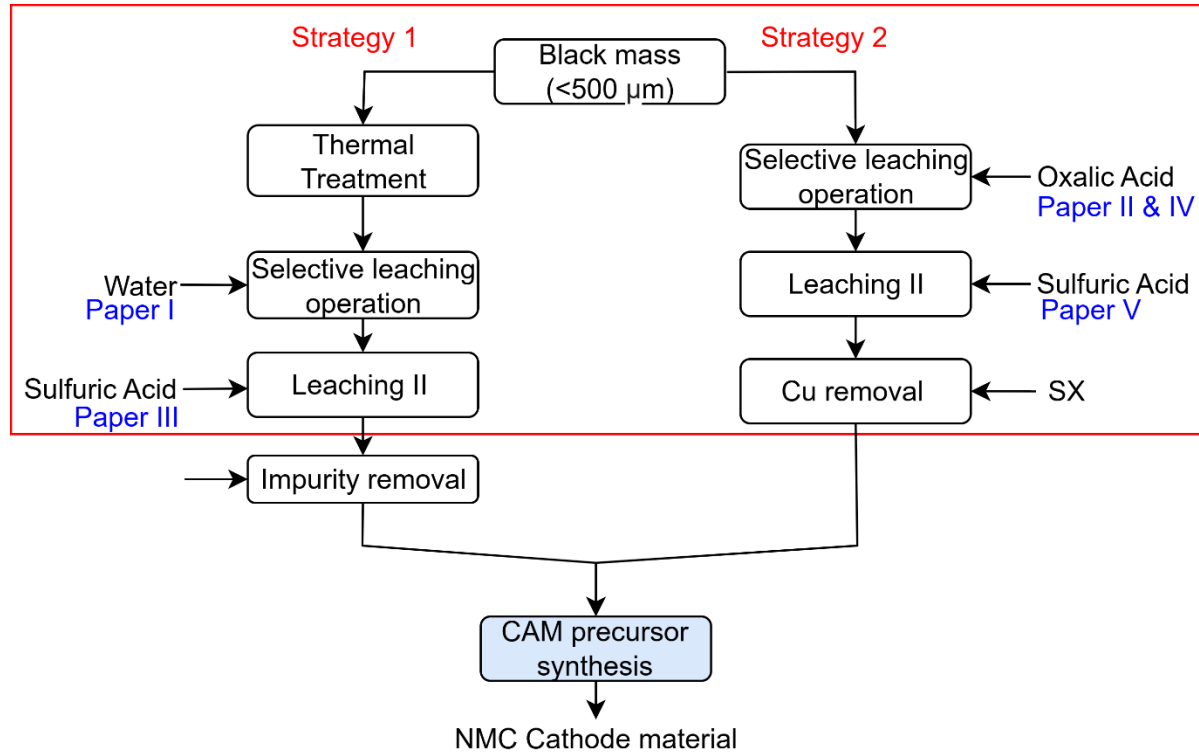


Figure 6: Overview of the experimental work done in this thesis. CAM precursor synthesis was considered but not investigated in the work.

4.2 Materials

4.2.1 Black mass

The industrial BM was obtained from dismantling 150 kg of EV spent LiBs provided by Volvo Cars AB (Sweden). First, Volvo Cars AB discharged the battery packs, and Stena Recycling AB (Sweden) dismantled them to the cell level. The cells (120 kg) were then processed through three steps: crushing, mechanical sieving, and magnetic separation by Akkuser Oy (Finland). The processing temperature stayed below 50°C. The fine fraction obtained represents 58.5% of the initial weight and comprises the active materials from the cathode and anode, along with traces of the current foils and separator. The fine fraction was further sieved under 500 µm at Chalmers University of Technology to obtain a homogeneous BM powder, more representative of the industrial standard. The sieving was performed with a sieve shaker (Retsch) for 5 min at an amplitude of 1.2 mm in interval mode and a sieve aperture of 500 µm. The obtained BM is NMC-111 based.

4.2.2 Chemicals

The chemicals used in this work are listed below (Milli-Q water ($18.2\text{ M}\Omega\text{-cm}$) was used to prepare all solutions):

- HCl, Merk Millipore, Chloric acid 37% w/w, used for solid digestion.
- HNO_3 , Merk Millipore Nitric acid 65% w/w, used for solid digestion.
- HNO_3 , Merk Suprapure Nitric acid 69% w/w, diluted at 0.5 M for ICP dilution.
- Metal nitrate standard solution (1000 mg/L) for ICP standard preparation.
- Oxalic acid was prepared by dissolving solid oxalic acid dihydrate (Sigma Aldrich, $\geq 99\%$).
- Diluted solution of H_2SO_4 , Sigma Aldrich, ACS Reagent, 95-98% w/w used for leaching.
- NaOH solution at 10 M (pellets, Sigma Aldrich, $> 95\%$).

4.3 Equipment

4.3.1 Thermal treatment set-up

Thermal treatments were performed in a horizontal tube (high purity alumina tube 65 cm, alumina tube, Degussit AL23, Aliaxis) furnace (Nabertherm GmbH Universal Tube furnace RT 50-250/13). The samples were held in an alumina crucible. Two different types of thermal treatment were performed: active pyrolysis under a constant pure nitrogen flow of 340 mL/min and incineration under 340 mL/min of air. The exhaust gases were washed with a water bathing system (plastic-sealed bottles) [31]. Upscaled pyrolysis was performed in a muffle furnace at IME RWTH Aachen University (Germany).

4.3.2 Leaching

Three types of leaching reactors were used for this work. The first consists of small glass vials with caps and magnetic stirrers (300 rpm) of 20 mL, used for preliminary experiments. The temperature was monitored and sustained via a heating plate, coupled with a thermocouple, and associated with an aluminium block in which glass vials were inserted. The second option was 100 mL PVDF-closed double-jacketed reactors equipped with inner baffles and a specific agitator design with a headed electric stirrer. Lastly, a 2 L double-jacketed glass reactor with a mechanical overhead stirrer and heating bath was used for upscale experiments. Solid samples were introduced into the reactors when the leaching media had reached the defined temperature. The solid sampling was performed using the coning and quartering technique to reduce the uncertainty associated with grabbing a sample from a container [129]. During the operation, samples were taken at different time intervals and filtered, so the concentration and pH of the leachate were measured to follow the metals' behaviour. Finally, the obtained slurry was filtered using a filter (VWR 516 0811 11 μm particle size retention). The solid residues were dried in an oven ($T = 60^\circ\text{C}$) and collected for analysis. All experiments were carried out in triplicate.

4.3.3 Evaporative crystallization

Evaporative crystallization was conducted utilizing a heating plate associated with magnetic stirring. Temperature $90 \pm 5^\circ\text{C}$ and low agitation (100 rpm) were maintained to facilitate evaporation and crystal growth. Upon reaching the desired degree of supersaturation

(percentage of evaporation), the resulting crystals were separated by vacuum filtration, washed with water or ethanol, and dried at 50°C in an oven before further analysis.

4.3.4 Precipitation

Precipitation was performed by adding a controlled amount of the precipitating agent (NaOH 10 M) to reach the target solution pH, in our case at room temperature under constant stirring (300 rpm). The addition rate was not controlled but can be a determining factor for the quality of precipitates (i.e., amorphous content, crystal size, co-precipitation, ...). Samples were taken to follow the reaction's advancement until the metal concentration was stable. The precipitate was then separated by vacuum filtration and dried at 50°C.

4.3.5 Solvent extraction

Batch experiments for solvent extraction were carried out in 3.5 mL glass vials; they were shaken at 1000 rpm for 15 minutes under constant temperature ($25^{\circ}\text{C} \pm 1^{\circ}\text{C}$) using a shaking machine (VXR basic Vibrax®). The organic phase was prepared with Acorga M5640 and ESCAID 100 as diluent. All experiments were triplicated. Sampling was performed after satisfactory phase separation was visually observed. The parameters allowing maximal loading, such as the extractant concentration, contacting time, and temperature, were investigated.

4.4 Analytical Methods

All analytical instruments used in the research are presented in the following tables.

Table 8: Analytical instruments used for liquid sample characterization (Instrument name, target analytes, and applied method).

Techniques	Analytes	Equipment	Method applied
ICP-OES	Li, Al, Cu, Ni, Co, Mn, P, Na, Si, Fe, Zn	Thermo Fisher Scientific, Model iCAP™ 6000 Series.	Sample dilution in 0.5 M HNO ₃ with internal standard (1 ppm Y). Calibration ranges from 0.3125 to 20 mg/L. The limit of detection is ca. 0.1 mg/L.
Ion-selective electrode	F	Fluoride-selective electrode + reference electrode Ag/AgCl ₃ (Metrohm) with a double junction system.	Sample dilution with TISAB IV solution (volume ratio 1:1) for pH and ionic strength control. TISAB also binds with interfering cations and releases any complex fluoride. Additional needed dilution with MQ-water. Calibration ranges from 10 to 100 mg/L.
pH meter	pH	Electrode Metrohm 6.0258.600.	Calibration with pH 2, 4, and 7 buffer solutions (T = $22^{\circ}\text{C} \pm 1^{\circ}\text{C}$). Connection to Tiamo software.
Redox Electrode	E	Electrode Metrohm 6.0451.100.	Connection to Tiamo software.
Titration	Oxalate	Colorimetry.	Redox titration using KMnO ₄ solution in the presence of concentrated H ₂ SO ₄ (2 M) at 50°C. Change of colour when an excess of MnO ₄ ⁻ no oxalic acid is left to be oxidized into carbon dioxide.

Table 9: Analytical instruments used for solid phase characterization (Instrument name, role, and applied method).

Techniques	Role	Equipment	Method applied
Acid digestion + ICP-OES	Elemental analysis	Thermo Fisher Scientific, Model iCAP™ 6000 Series.	Sample digestion via aqua regia (HCl/HNO ₃ : 3/1 volume ratios) leaching at 80°C for 4 h (S/L ratio 7g/L). Slurry filtration (filter VWR 516-0811 11 µm). ICP-OES analysis of diluted sample.
X-ray diffraction (XRD)	Structural analysis	Bruker D8 Twin-Twin diffractometer.	Cu ($\lambda = 1.54184 \text{ \AA}$) radiation source in a 2θ range of 10°–80° with a rotational speed of 15 rpm. Operating current 40 mA and voltage 40 kV. EVA software and the JCPDS database. Pawley fittings were done by Dr. Laura Altenschmidt and discussed as a team.
Carbon analysis (TOC)	C	LECO CS744.	Approximately 20 mg of the sample was weighed in an alumina vial and introduced into the machine to be oxidized to CO ₂ , which was then measured by an infrared detector.
Fourier-transformed infrared spectroscopy (FT-IR)	Functional group	Perkin Elmer Spectrum Two UATR.	450 to 4000 cm ⁻¹ range with a resolution of 2 cm ⁻¹ and 16 scans.
Laser diffraction size analyser	Particle size	MasterSizer 300 (Malvern Instrument – ms2000, UK).	About 10 mg of solids were dispersed in water with ultrasound to degrade the potential aggregation.
Scanning electron microscopy (SEM) and energy dispersive X-ray spectroscopy (EDS)	Morphology + Elemental analysis	Phenom Pro X microscope (Thermo Fisher Scientific, USA).	BSD FULL 263 mode at an accelerating voltage of 15 kV.

4.5 Thermodynamics Considerations

The HSC Chemistry 10 software was used to calculate standard enthalpy, entropy, and Gibbs free energy change for some expected reactions (papers I, IV, and V). Additionally, predominance and species distribution diagrams for metal-oxalate systems, used to determine which oxalate species can co-exist in aqueous solution (paper IV), were generated using the HYDRA (Hydrochemical Equilibrium- Constant Database) and MEDUSA (Make Equilibrium Diagrams Using Sophisticated Algorithms) programs [130].

4.6 Design of Experiments – Statistical Methods

The factorial design of experiments is an efficient tool to investigate and optimize a chemical operation while minimizing experimental efforts. The main objectives are to assess the main factors, their sole influence or interaction, and obtain a model of the process response. The response surface methodology and contour plots can assist in visually interpreting the modelled responses [131]. Each factor (x) comprises two levels (min and max), and the process response (Y) was defined as the leaching yield of each metal (%). To apply this method, the factors must be fixed beforehand (usually through a literature review or preliminary experiments); factors with less influence should be kept constant and out of investigations.

In this research, a cubic face-centered design is selected as shown in Figure 7. Axial points are performed (2k axial points – Red points) at a distance of $\alpha = 1$ from the central point to estimate the second term and curvature. The test order must be randomized. The design was replicated four times at the central level (black point) to assess the experimental error. The coefficients of a linear second-order regression model representing the process response were fitted using the linear least squares method (second-order regression models with two- and three-way interactions), which was solved using Excel's regression analysis tool. Only statistically significant variables were included in the models (p -value < 0.05), and the significance of the models was assessed using ANalysis Of VAriance (ANOVA). The existence of pure curvature was evaluated by hypothesis testing, and the variance of the response accounted for by the models was assessed using the coefficient of determination (R^2).

This method was used in Paper II, and the factors and respective levels used can be observed in Figure 7. The design factors are oxalic acid concentration, leaching time, and temperature. They were chosen based on the range of conditions from the state-of-the-art presented on page 11. Setting a representative working range of conditions is essential when using such an approach, as the model obtained is only valid within the experimental limits. The S/L ratio was fixed at 50 g/L to have sufficient dispersion of the slurry and efficient mixing.

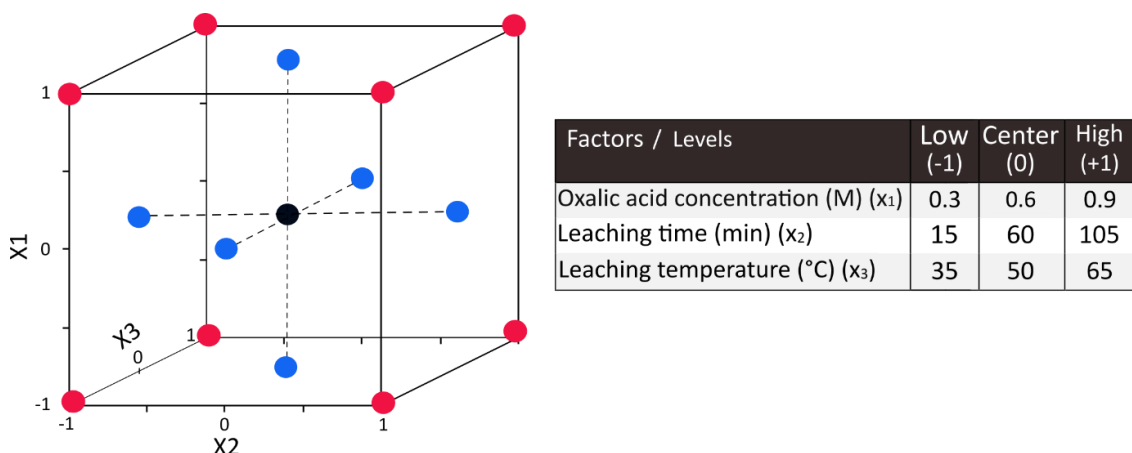


Figure 7: Face-centred cubic factorial design matrix and factor levels applied (Paper II).

5 RESULTS and DISCUSSIONS

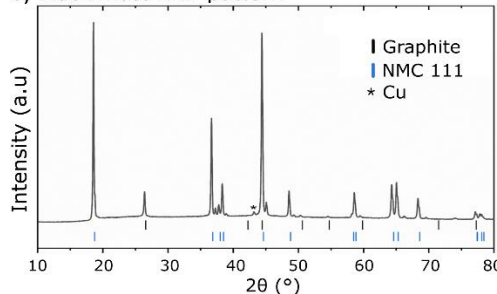
5.1 Black Mass Characterization

The BM powder elemental composition (fraction under 500 µm) is given in Figure 8a, and its XRD pattern is depicted in Figure 8b. It shows that the BM primarily consists of NMC 111, graphite, and Cu. The particle size distribution, presented in Figure 8c highlights the existence of three groups of particles: the first one ca. 5 to 30 µm, then from ca. 30 to 110 µm, and finally from ca. 110 to 140 µm. Associated with the SEM images and EDS analysis (seen in Figure 8d), each group can be associated with the different components of the BM: the smaller particles correspond to graphite particles from the anode, the second group consists of active cathode material, and the largest group comprises the remaining current collector foils, Al, Cu, and separator. Moreover, the round morphology of the cathode material particle is seen with a smooth and flat surface; particles seem closely bound together with the binder. The EDS analysis shows the even distribution of all transition elements through the CAM (right image). The mapping (left image) reveals the presence of fluorine in the sample, homogeneously distributed, which can be seen as the binder footprint or electrolyte salt [13,132].

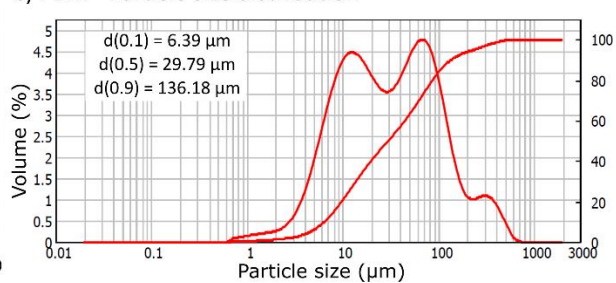
a) Elemental composition of the BM powder (STD given out of triplicate measurement)

	wt% (%)	Ni	Mn	Co	Li	Al	Cu	P	Fe	Si	C	Tot
Akkuser Fine fraction	8.2	7.5	10.5	3.4	3.5	7.8		0.2				100
± STD (%)	± 0.2	± 0.1	± 0.3	± 0.1	± 0.1	± 0.1		± 0.1				
Fraction > 500 µm	4.6	4.3	5.3	1.8	8.5	19		0.1				31
± STD (%)	± 0.1	± 0.1	± 0.2	± 0.1	± 0.9	± 2		± 0.1				
BM < 500 µm	8.7	7.5	11.6	3.4	0.8	2.4	0.4	0.1	0.2	32.0	69	
± STD (%)	± 0.2	± 0.2	± 0.2	± 0.1	± 0.1	± 0.1	± 0.0	± 0.1	± 0.0	± 0.2	± 0.2	

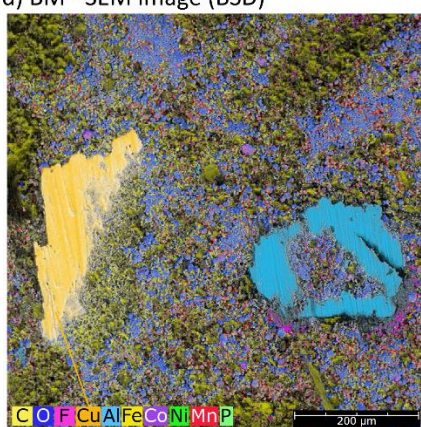
b) Black mass XRD pattern



c) PBM - Particle size distribution



d) BM - SEM image (BSD)



Elemental composition (EDS data)

Element	Atomic Conc. (%)	Weight Conc. (%)
C	52.63	41.33
O	33.65	19.84
Co	5.05	14.56
Ni	4.63	13.40
Mn	4.03	10.87

Element	Atomic Conc. (%)	Weight Conc. (%)
C	61.45	44.45
O	22.50	21.68
F	6.79	7.78
Cu	1.64	6.29
Al	3.33	5.41
Fe	1.14	3.82
Co	1.04	3.69
Ni	0.96	3.38
Mn	0.94	3.10

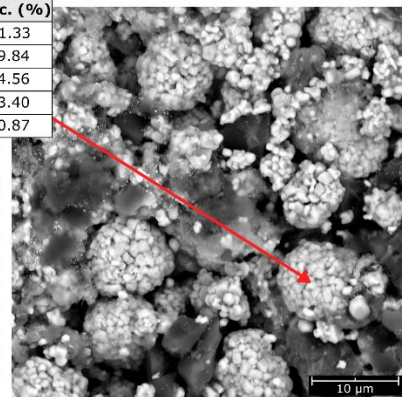


Figure 8: BM characterization a) elemental composition, b) XRD pattern (Graphite: PDF 00-056-0159, NMC 111: PDF 04-013-4379, Cu: PDF 01-091-1717), c) Particle size distribution, and d) SEM image and element composition from EDS data (Paper IV).

5.2 Strategy 1: Based on Early Recovery of Li via Water Leaching after BM Thermal Treatment

5.2.1 Water leaching after incineration and pyrolysis of battery cells' electrodes

The results presented here are based on Paper I [133] and III [134].

For this first part of the study, another feed material was used for thermal treatment: the anode, cathode, and separator foils were directly cut from a Volvo battery pouch cell into small flake pieces (after letting the electrolyte evaporate). The battery cell provided is *NMC111-based*. The feed material consists of the three foils in equal proportion. The positive influence of the separator during the thermal treatment was demonstrated for Li recovery (see Paper I [133]), only this data is presented here. The elemental composition of the material is presented in Table 10.

Table 10: Metal and carbon composition of the untreated feed material [3]

wt% (%)	Li	Al	Cu	Ni	Co	Mn	C
Feed material	2.2 ± 0.2	6.2 ± 0.3	15.0 ± 0.4	4.3 ± 0.4	4.3 ± 0.4	9.5 ± 0.8	40.8 ± 2.8

After both thermal treatments, a 5 to 20% weight loss was measured, associated with organic losses and graphite transformation [31,107,111]. The relative metal content (wt%) increases after thermal treatment due to this material loss (exact values in Paper 1 [133]), highlighting the treatment's concentration effect. Additionally, the binder has been decomposed, releasing the active material from the foil in many places. A sieving stage would effectively separate the BM (CAM and graphite) from the Al and Cu.

The XRD pattern for the untreated (UN) and pyrolyzed feed material at different temperatures is presented in Figure 9. The untreated feed material pattern presents the diffraction peaks characteristic of the NMC111 material, graphite, and metallic Al and Cu. This confirms the chemistry of the battery cell studied. At 400°C, the diffraction pattern is unchanged, while above 500°C, the peaks of NMC material decrease, and the peaks of reduced metal or oxide phases (Ni, NiO, MnO, Mn₃O₄, Co, and CoO) appear. Thus, the carbothermic reduction of the oxide happens above 500°C. The higher the temperature, the more efficient the reduction is. Over 700°C, the NMC 111 peaks disappear entirely, and the

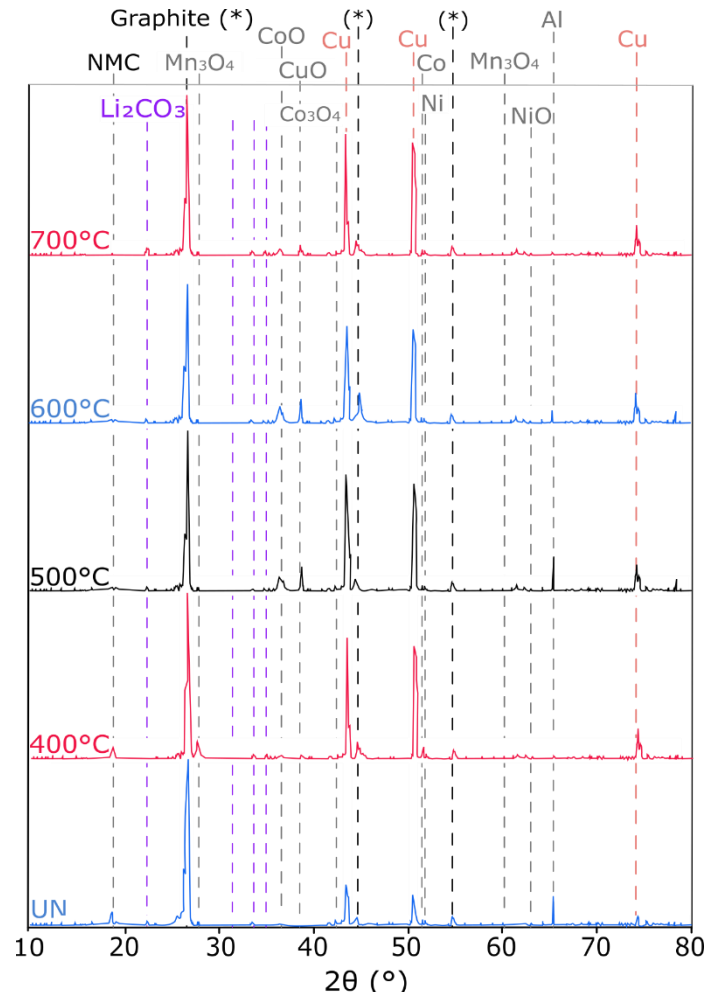


Figure 9: XRD pattern of the untreated feed material and pyrolyzed at different temperatures (60 min) [31].

presence of Li_2CO_3 is more evident. Al does not show structural changes as it remains a metallic element; Al_2O_3 could be expected, but is not visible on the pattern. Cu is oxidized despite the inert atmosphere and is present as Cu and CuO . This is consistent with reported literature [61,123,135]. Due to the instrument's detection limit, no other degradation products could be identified.

The Li leaching yields for every feed material (untreated, incinerated, or pyrolyzed) are presented in Figure 10a, b, c, along with the concentration of Li and Al in the final leaching solution (after thermal treatment time of 60 min), as visible in Figure 10d. Results are given after 60 min of leaching, but the kinetics test shows that the dissolution reaches a plateau after 20 min (Paper I [133]). Only Al is co-dissolved; the concentration of other valuable elements is under the ICP limit of detection. The water leaching of the untreated material yields a 7% recovery of Li; this is associated with the electrolyte salt dissolution, typically LiPF_6 in water, which will easily ionize or dissociate, forming LiF and PF_5 as seen in Equation 3.

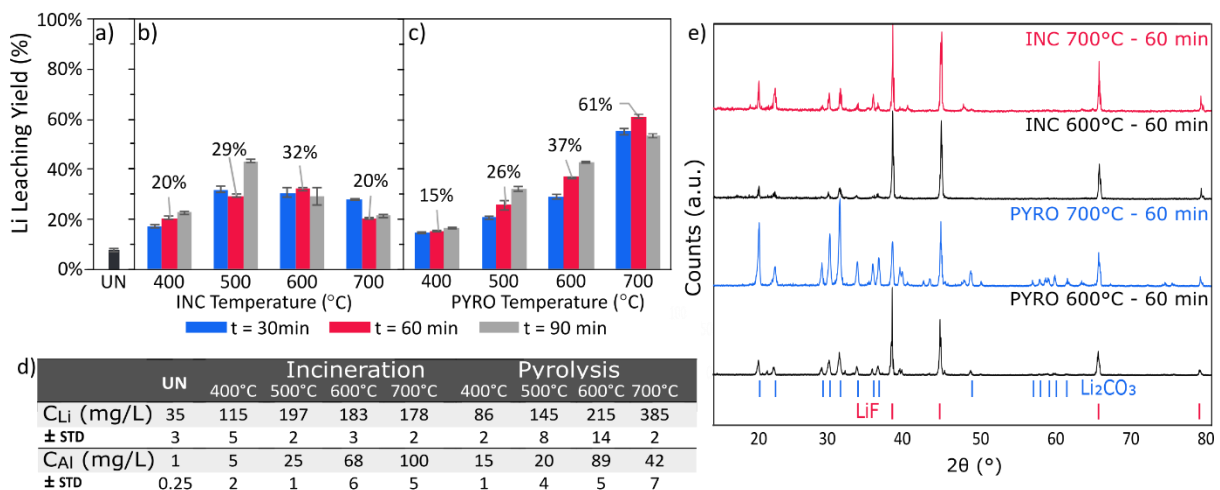


Figure 10: Water leaching yield ($S/L = 20 \text{ g/L}, 25^\circ\text{C}, 1 \text{ h}, 300 \text{ rpm}$) on a) the untreated feed material (UN), b) incinerated and c) pyrolyzed feed at different temperatures (400 - 700 °C) and treatment time (30 - 90 min), error bar represented standard deviation from triplicates, d) Li and Al concentration in leaching solution 1 and e) XRD pattern of residue obtained after evaporative crystallization of the leaching solution 1 (Li_2CO_3 PDF 00-022-1141; LiF PDF 01-071-3743).

Water leaching on incinerated sample - Effect on Li recovery

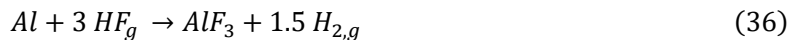
After 400°C incineration and water leaching, a 20% Li leaching yield is observed, with only a 10% improvement over the untreated material. Thermal treatment time has a negligible impact on Li recovery, suggesting shorter processing times should be applied to save energy cost. A notable decrease in recovery occurs at 700°C. This can be attributed to Al melting above 660°C, which coats particles and impedes carboreduction. Furthermore, water leaching demonstrates limited selectivity for Li; the higher the thermal treatment temperature, the more Al leaches into the water, suggesting that temperature influences the formation of a water-soluble species.

Optimal results were obtained by incineration at 500°C in 90 min, achieving 43% Li recovery and 90% solution purity. The respective Li and Al leaching solution concentrations are 215 mg/L and ca. 25 mg/L.

Water leaching on pyrolyzed sample - Effect on Li recovery

Conversely, pyrolysis is undoubtedly more efficient in terms of Li recovery. The optimal thermal treatment conditions are a treatment time of 1 h at 700°C, which resulted in Li recovery of 61% and a purity of 92%. Again, a portion of Al is dissolved, but slightly less than after incineration. Under these conditions, the Li and Al concentrations in the leachate were 385 mg/L and ca. 42 mg/L, respectively.

At 400°C, Li recovery does not surpass recovery of Li after incineration at the same temperature, remaining relatively low at 15%. This observation reinforces that the reducing conditions are not established below 500°C, as illustrated by the persistence of the NMC structure in the XRD pattern in Figure 9. Furthermore, given that PVDF decomposition initiates at 450°C under nitrogen, its potential partial presence at 400°C may impede particle-leaching media contact. The pyrolysis temperature positively and gradually influences the Li leaching yield, and the processing time does not show a significant impact. Notably, Al co-leaching occurs again, decreasing the leachate purity with increasing treatment time and temperature. This unexpected Al dissolution, not previously documented, necessitates further investigation to identify the water-soluble Al species formed during either thermal treatment, aiming to mitigate their generation. Its dissolution decreases at 700°C, indicating a change in the thermal treatment mechanism above this limit. The first hypothesis is that Al melting can hinder other surface reactions. XRD analysis could not identify any other Al phase explaining this dissolution. After evaluating the potential transformation reactions, one is more probable: the metallic Al could have reacted with gaseous HF at its surface, forming AlF₃, as presented in the Equation 36. This reaction is spontaneous at high temperatures, with a ΔG of -446.4 kJ at 600°C, and AlF₃ is a relatively water-soluble compound (solubility at 25 °C, ca. 0.559g/100 mL water [136]).



Despite the demonstrated total reduction of all metal oxides at temperatures exceeding 600°C (Figure 9), the incomplete Li recovery suggests the presence of Li in non-aqueous-soluble forms. It is worth mentioning that some authors have shown that a temperature of ca. 800°C is required for a complete reduction of the CAM [137]. On that account, the presence of residual NMC material cannot be entirely discarded in our sample; even if the characteristic peaks are missing on the XRD pattern, it could be left in a very low amount, undetectable by the instrument.

The Li concentration in the leaching solution is very low and under the Li₂CO₃ solubility limit; thus, the solution is not saturated, showing that up to 40% of Li is in another speciation. LiF is a great potential candidate, as shown in section 3.1 (Page 15), it is a decomposition product of the electrolyte salt and can also be formed from the reaction of Li₂O and HF gas. It is rather insoluble in water, and other authors have highlighted its presence. For example, Safoura et al. indicate that during pyrolysis, LiF will form regardless of the temperature applied [138]. Below 600 °C, the predominant phases of Li are Li₂O and Li₂CO₃. Above that temperature, an additional phase can be formed: LiAlO₂, a product of the Li metal oxides' reduction with Al, a stable oxide known for its insolubility in water [139]. The Equation 37 describes the potential for Al to act as a reductant at elevated temperatures, it is supported by a significant negative Gibbs free energy (ΔG = -511.8 kJ at 600°C), indicating a spontaneous exothermic reaction. The higher the temperature, the more

likely this reaction is to occur. This suggests that LiAlO_2 formation is thermodynamically favourable and likely contributes to the observed incomplete Li recovery.



Moreover, Safoura et al. also mentioned the potential formation of a LiAlF_4 product. The same authors studied the fluorine behaviour during the thermal treatment, and they found that ca. 90% of the initial fluorine content remains in the pyrolyzed sample [140]. This is of great importance in understanding the mechanism, as only a small portion of fluorine is leaving the system. It reacts with its environment, forming undesirable by-products. However, these by-products can be hard to identify and characterize in the sample.

Evaporative crystallization of Leaching solution - Lithium compounds production

The XRD patterns of the Li crystals obtained after evaporative crystallization of the leaching solution are presented in Figure 10e. The final product is a mixture of LiF and Li_2CO_3 . The presence of Al was not detected using the XRD, which can be explained by the minimal amount of Al in the product (< 2.5 wt%). After pyrolysis at 700°C for 60 min, the product has a Li purity of 92%. The formation of LiF could be explained by the presence of F^- in the leachate solution, which would react with Li^+ coming from the dissolution of Li_2CO_3 . The fluoride content is ca. 1 mmol of F^- per gram of solid, representing 2.3% of LiF against 97.7% of Li_2CO_3 . Thus, to produce battery-grade lithium material, more purification will be needed to remove free fluorine and increase the recovery yield.

This first investigation identified the best thermal treatment, a pyrolysis at above 600°C is recommended. Already, some Li recovery limitations were observed, and the potential reasons for such limitations were listed, including the LiF presence or the formation of LiAlO_2 . To continue in the research and to be able to compare both recycling strategies, the process was applied on the provided BM powder (its characterization is presented in Figure 8 – Page 29).

5.2.2 Water leaching on pyrolyzed BM at the optimised conditions (Leaching 1)

The pyrolysis temperature was fixed at 600°C, and treatment was performed for 2 h in a large muffle furnace (performed at IME RTWH Aachen University). It was decided to proceed with the pyrolysis using larger-scale equipment to be closer to an industrial setup for the pyrolysis and to focus the research on the following hydrometallurgy process.

There are several differences between the sample used in the section 5.2.1 and the BM provided, starting with the sample's morphology: the BM powder offers a higher surface area compared to the foil flakes. Then, the composition is different, the BM production process has concentrated the valuable elements (Li, Ni, Mn, and Co) while removing impurities; there is a lower presence of separator foil, Al (ca. 1 wt% instead of 6.2 wt%), and Cu (ca. 2.4 wt% instead of 15 wt%). Moreover, most of the electrolyte solvents should have been more efficiently removed from the waste, which could decrease the presence of some decomposition products in the pyrolyzed BM. Additionally, the lower presence of Al should reduce the formation of LiAlO_2 at 600°C [140].

Pyrolyzed Black mass characterization

The composition and speciation of the obtained pyrolyzed BM are presented in Figure 11. Again, the concentration effect of the pyrolysis is underlined with higher metallic content. Despite the absence of separator foils, the carbo-reduction occurred as anticipated. Compared to Figure 8b, the XRD pattern lacks the characteristic peaks for the NMC material (18.4, 36.9, 38.5, and 44.6° 2θ), indicating its complete reduction. However, once again, due to detection limitations, the presence of trace NMC material cannot be entirely excluded. The reduced phases are visible and can be identified as Co, CoO, Ni, MnO, and MnO₂.

This time, it is possible to identify more than one lithium compound in the pyrolyzed BM, first and in a more significant proportion: the Li₂CO₃, with strong and visible peaks at 21.3, 30.6, 31.7, and 34.1° 2θ. Additionally, LiF can be evidenced despite its close structural similarities with Al, with peaks at 38.6, 44.9, and 65.3° 2θ. Furthermore, LiAlO₂ and Li₃PO₄ can be identified in very little proportions as their characteristic peaks are very small. Li₃PO₄ has its more intense peaks at 22.3, 23.1° 2θ; its presence has not been reported till now. A side reaction during the pyrolysis treatment can explain its presence. Indeed, the POF₃ produced during the LiPF₆ decomposition (see Equation 4) can react with Li₂O, forming Li₃PO₄ and LiF, as presented in Equation 38. The reaction is spontaneous and has a ΔG° of -311.4 kJ at 600°C. Li₃PO₄ has a very low solubility limit (log K_{sp} = - 8.5); its presence can explain the limitation in Li recovery.

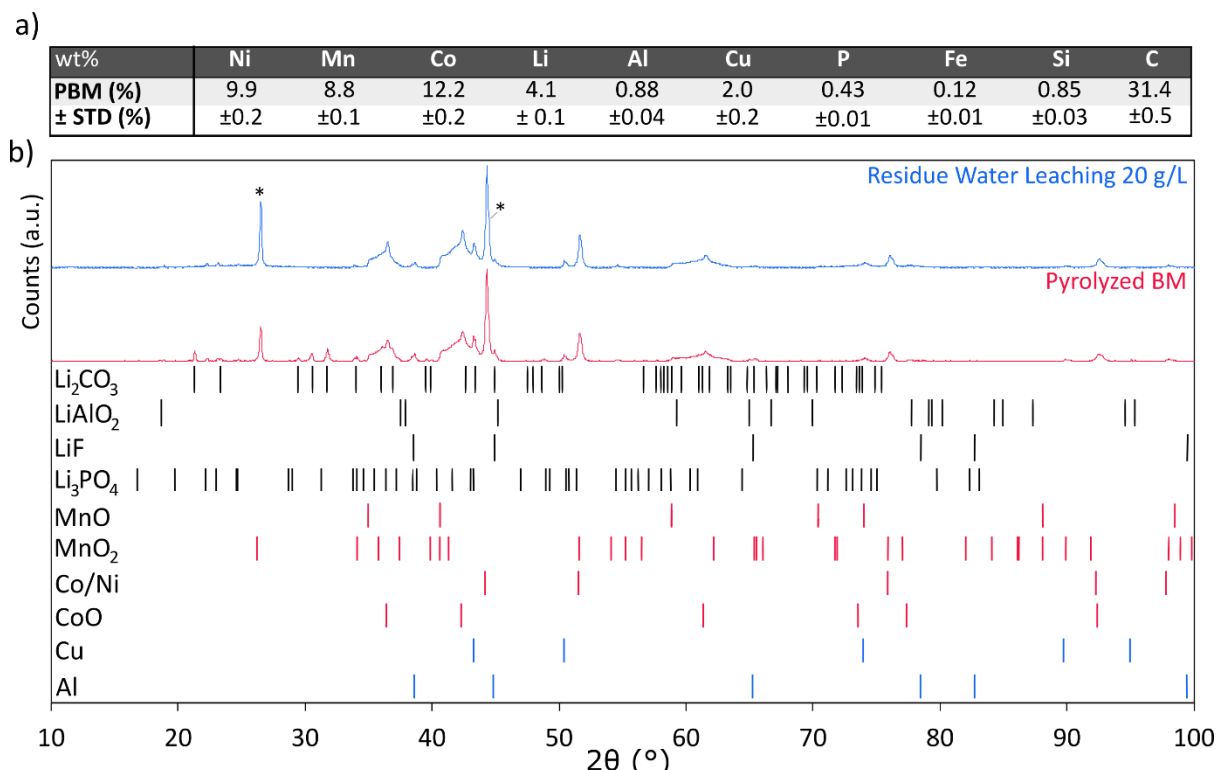


Figure 11: Scale-up pyrolysis. a) composition of the pyrolyzed BM after pyrolysis at 600°C for 2 h, b) XRD pattern of the same BM and the residue after water leaching (25°C, S/L = 20 g/L, 300 rpm) – (XRD id: Li₂CO₃ PDF 00-022-1141, LiAlO₂ PDF 04-002-8213, LiF PDF 01-071-3743, Li₃PO₄ COD 9011924, MnO PDF 04-013-0265, MnO₂ COD 9011409, Co PDF 04-014-0167, Ni PDF 04-011-8029, CoO PDF 04-002-2692, Cu PDF 01-091-1717, Al PDF 04-010-6160).

The Li recovery rate, after leaching the untreated and pyrolyzed BM, is presented Figure 12a. Some tests were performed to enhance the Li dissolution from the pyrolyzed BM (Temperature and Ultrasound to overcome some kinetic limitations or mass transfer). Moreover, Figure 12b provides the pH and concentration in Li and Al of the resulting leaching solution.

Water leaching on untreated Black mass

The untreated BM was leached with water to assess its behaviour; 5.5% ($\pm 0.1\%$) of the Li could be dissolved already, which is essentially attributed to the electrolyte salt dissolution. The equivalent Li concentration is at c.a. 50 mg/L (see Figure 12), which is below the solubility of LiF; thus, we can account for ca. 6% of the initial Li from the BM that will be transformed into LiF compounds during pyrolysis.

Water leaching on pyrolyzed Black mass

The pyrolyzed BM's water leaching results in higher Li recovery rate than observed in our preliminary tests, as presented in Figure 12. Indeed, the recovery for the same leaching conditions for 60 min (22°C and 20 g/L) leads to 56% Li recovery with a concentration of 0.5 \pm 0.1 g/L of Li in solution, which is 20% higher than previously observed. In fact, under this condition, the XRD pattern reveals that most Li₂CO₃ is dissolved as its characteristic peaks disappear (Figure 11b). This time, several S/L ratios were tested to see how the operation can be optimized. Not surprisingly, the higher the S/L ratios, the lower the recovery rate, but associated with more significant Li concentrations in the solution. With a S/L ratio of 60 g/L, 43% of the Li is recovered with a concentration of 1.4 g/L. From 100 g/L, we enter the metastable zone for Li₂CO₃ crystal, the solution becomes more saturated (ca. 2 g/L of Li), and Li₂CO₃ cannot be solubilized, explaining the lower recovery rate. Additional research was performed to increase the recovery rate, at a temperature of 70°C and with ultrasonic (US) assistance. The objective was to see if diffusion or mass transfer was limiting this operation, so that such techniques could be used to decrease it. In both cases with a leaching at 20 g/L, Li recovery increased by 10%, as 69% is recovered (0.7 \pm 0.1 g/L of Li in solution). Al is again partially co-dissolved. An interesting new aspect is the final pH of the solution, which is ca. 11-12 by the end of the leaching due to the carbonate dissolution. Al could be hydrolysed at this pH level, forming the soluble compound Al(OH)₄⁻.

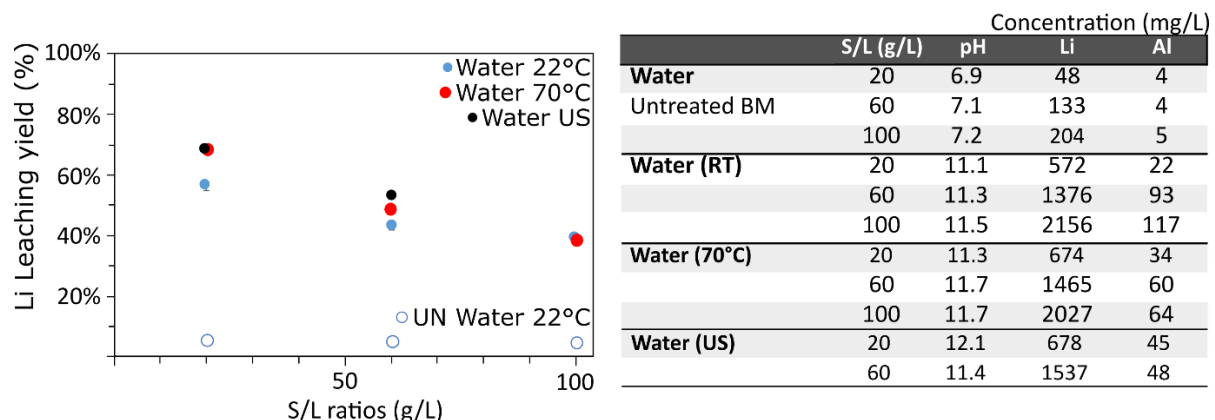


Figure 12: a) Lithium leaching yield after water leaching on the untreated (UN) BM and pyrolyzed BM. Leaching conditions: Varying the S/L ratio, at 22°C \pm 2°C, 70°C \pm 2°C, or with ultrasonic (US) assistance, associated with the final pH and concentration of Li and Al in the solution.

5.2.3 Sulfuric acid leaching (Leaching 2)

After Li removal (with water leaching at 20 g/L, 70°C for 2 hours), the residue is submitted to acidic leaching to recover the remaining valuable elements. The leaching conditions (2M H₂SO₄, 3 h, and 400 rpm) were selected based on paper III [113,134], no additional reducing agent was employed. The S/L ratios and temperature influence are investigated for the leaching of the untreated BM and the residue (after pyrolysis and water leaching). The leaching yield for all valuable elements is presented in Figure 13.

On the untreated BM sample, about 50% of the TM from the CAM are dissolved with about 80% of Li, with a low influence of the conditions chosen. The faster dissolution of Li highlights the leaching mechanism, with first the delithiation of the NMC structure in the acidic solution [69]. Al is also readily dissolved in the acid, with a positive temperature impact. On the other hand, Cu is more affected by the explored leaching condition, with a high positive temperature impact.

Pyrolysis has a significant positive influence on the leaching of valuable metals. When the leaching is performed at 50°C, more than 98% of Li, Ni, Co, and Mn are dissolved. However, pyrolysis did not affect Cu recovery due to the reductive conditions. Cu stayed in the metallic form (Figure 11) and since it requires oxidative conditions for the leaching, it was not recovered. In the same way, the pyrolysis influence on the Al is not proven, as the same amount of Al is recovered (ca. 80%).

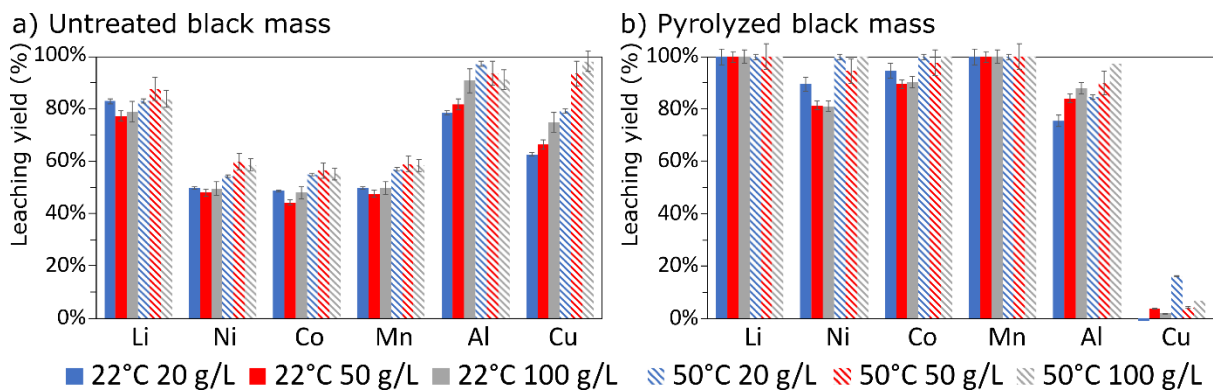


Figure 13: Leaching yield of the main valuable element (Li, Ni, Co, Mn, Al, Cu) after a H₂SO₄ leaching (2 M, 3 h, 400 rpm) at different S/L ratio (20, 50, and 100 g/L), different temperature (22 and 50°C) applied on the untreated BM and pyrolyzed.

5.2.4 Conclusions and perspectives on Strategy 1

This first strategy is promising, with a high recovery of all metals observed. Many recyclers commonly apply pyrolysis as it simplifies the handling of spent LIBs. Thus, investigating the pyrolysis effect is very important, and understanding how this pre-treatment could improve metal recovery is essential. A large part of the Li can be recovered (up to 70% under the appropriate conditions). The Li recovery limitation could be thoroughly attributed to the formation of 3 distinct by-products of the pyrolysis: LiF, Li₃PO₄, and LiAlO₂. Their dissolution typically requires acidic media; thus, to recover 100% of Li, a second-stage leaching with low acidic concentration could be proposed. However, acid might also affect the transition metals' dissolution. Additionally, it might not be profitable for larger-scale applications of the process to have more

leaching steps (challenging slurry management and filtration) without sharp selectivity. Moreover, the presence of Al and fluorine in the final leachate solution seems unavoidable; a purification process would be needed to produce battery-grade material. This work has not yet investigated this issue. For fluorine management, some authors propose the usage of CaOH, which could precipitate as CaF. It has also been suggested that the same compound be inserted in the pyrolysis feed material to mitigate the formation of by-products at their sources.

The pyrolysis positively impacted the TM's leachability, and they could be recovered without the usage of a reducing agent. A preliminary flowsheet process is proposed based on this research in Figure 14. The rest of the recycling process would rely on well-known chemical operations presented in the background.

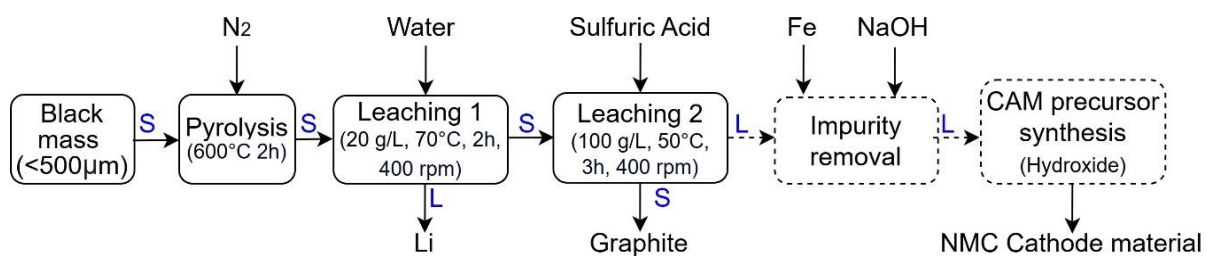


Figure 14: Summary of the developed route with combined approach with identified optimal conditions: 1) BM pyrolysis; 2) water leaching 1; 3) H_2SO_4 leaching 2 for the TM.

Considering the limits of combined method, this thesis investigates another option for selective Li recovery using only a hydrometallurgical route.

5.3 Strategy 2: Based on the Early Recovery of Li via Oxalic Acid Leaching

5.3.1 Oxalic acid leaching (Leaching 1)

Factorial design of experiments, regression models, and contour plots

The results presented here are based on Paper II.

As enunciated in section 0, oxalic acid was selected as a leaching agent because of its remarkable reducing and complexing properties, making a selective Li recovery possible. As a start, a design of experiments was performed to assess the feasibility of the operation, examine the main influencing parameters, and observe the behaviour of all metals during the dissolution. The tested parameters were an oxalic acid concentration between 0.3 and 0.9 M, a leaching time between 15 and 105 min, and a temperature range from 35 to 65°C, as seen in Figure 7.

The fitted regression models for each metal and the coefficients of determination (R^2) are found in Table 11 (Equations 39 – 44). The results for the analysis of the variance of the fitted model for all metals are given in the Appendix 1 & 2. It is essential to highlight that the models are valid only within the range set in the experimental design. The experimental error was calculated based on the replicate performed for the central point of the design, and a very low error was calculated for all metals (except Al, which, due to its complete dissolution, made it impossible to determine). Then, the lack of Fit can be computed from this value to assess the model adequacy. In the case of Li, it is a complex parameter to judge as the value obtained is slightly below the significant level

(0.0441), which could be a negative sign. Still, as the experimental error is so low, it is acceptable, and the model is considered adequate. One significant parameter is the coefficient of determination R^2 ; here, it is very high for all metals (close to 1), thus the fitted model can describe the variability in the experimental data well.

In the model, only statistically significant variables are included (p -value < 0.05), which can be visible when looking at the Pareto chart given in the Appendix 3 (the highest value indicates the most substantial influence on the dissolution). In the case of Li dissolution, time and temperature are the variables that have the most significant effect on the dissolution. The reduced regression model included no three-way interaction ($x_1x_2x_3$) or any second-order acid concentration terms (x_1x_2 and x_1x_3). The general observation that can be made from the analysis is that Li and Al are almost completely leached in certain conditions, whereas the leaching yield for the rest of the TMs remain under 5%.

Table 11: Regression models for the leaching yield of each element with their respective R^2 . (Factor x_1 : Oxalic acid concentration, x_2 : time and x_3 : temperature)

Equations	R ²
Li (%) = 92.09 + 6.76x₁ + 10.68x₂ + 12.61x₃ - 8.40x₂x₃ - 6.33x₁² - 5.85x₂² - 6.50x₃²	(39) 0.99
Al (%) = 94.43 + 16.24x₂ + 13.58x₃ - 8.60x₂x₃	(40) 0.92
Mn (%) = 2.64 - 0.55x₂ + 1.22x₁²	(41) 0.88
Cu (%) = 1.32 - 1.66x₁ + 2.28x₁²	(42) 0.85
Co (%) = 0.48 - 0.48x₁ - 0.29x₁x₃ + 0.16x₁x₂x₃ + 0.63x₁²	(43) 0.96
Ni (%) = 0.40 - 1.01x₁ - 0.70x₂ - 0.41x₃ - 0.37x₁x₃ + 0.52x₁x₂x₃ + 1.41x₁²	(44) 0.96

The response surfaces and contour plots for each element were plotted using Equations 39 – 44, which helps to highlight the relations between the different variables of the operation and determine the optimal condition range. The contour plots display a two-dimensional view of the response surface, where all points with the same response are connected to produce contour lines of constant responses. Whereas the response surface is viewed as a three-dimensional surface in a surface plot.

The surface plots of Li leaching yield are shown in Figure 15, including yields between 50 and 100%. It is important to stress that its dissolution has a positive correlation with all the factors investigated in this study: oxalic acid concentration, time, and temperature. At the low level of each parameter, the yield is only around 50%, reaching more than 90% at the central level of the design. Under 0.45 M of oxalic acid, less than 90% of Li is dissolved, this concentration corresponds to a molar ratio of CAM metals to oxalic acid of 1:2. Considering the goal of reaching the complete dissolution of Li with milder conditions, it is already possible to target a different set of parameters that will allow an extraction over 95% (dark red colour on the surface plots). Those parameters are oxalic acid concentrations of 0.6 M at 55°C for 60 min or 0.6 M at 40°C for 105 min (here 1:2.5 molar ratio); it is interesting to see how correlated time and temperature are. It will be the basis of the next part of the study to get more insights into the leaching mechanism and driving force.

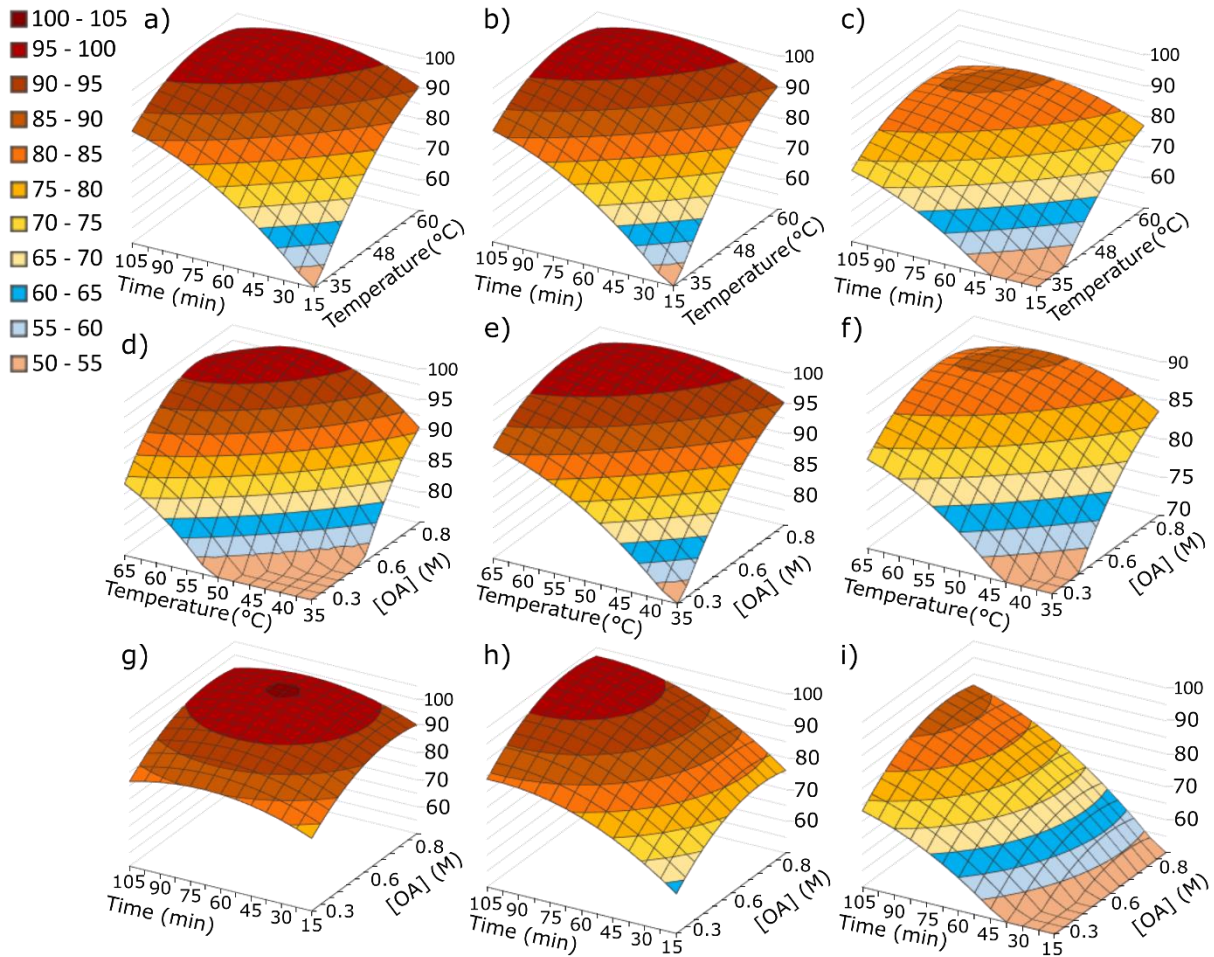


Figure 15: Li leaching yield (in %) - Surface plots a) 0.9 M of oxalic acid, b) 0.6 M, c) 0.3 M, d) 105 min, e) 60 min, f) 15 min, g) 65°C, h) 50°C, and i) 35°C [141].

The Al dissolution is not influenced by the oxalic acid concentration as seen in Equation 40; thus, one contour plot is relevant to observe the factors affecting the dissolution as seen in Figure 16. It is shown that the dissolution increases with the temperature and time, from 50% dissolution in the smaller range of time and temperature (15 min and 35°C) to over 100% extraction when the temperature goes over 60°C and a long leaching time. Complete dissolution of Al was not expected or reported by previous authors.

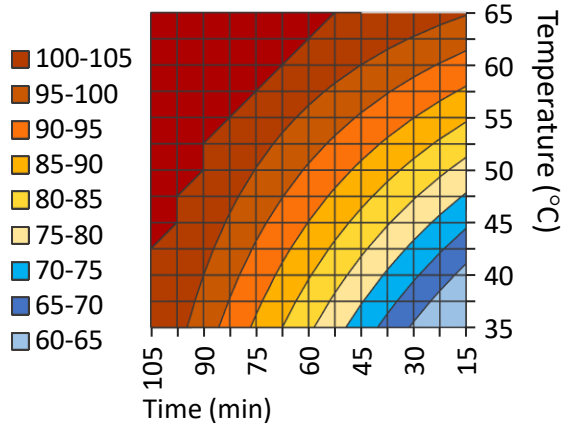


Figure 16: Al leaching yield contour plots [141].

The behaviour of the other elements was also tracked, and it is presented in Figure 17. All CAM metals are negatively influenced by time, highlighting the two-step mechanism of the leaching, with first a dissolution followed by precipitation as oxalate. Moreover, their dissolution is globally positively influenced by the oxalic acid concentration; residual oxalic acid can continue to bind with the metals, forming soluble charged oxalate complexes. As predicted by Ka Ming et al. [104],

Mn is the most dissolved element by the acid due to the higher solubility of Mn oxalate (see Table 6). In this study, 2.4% of Mn was leached at the central point, which is lower than the dissolution previously observed by Ka Ming et al. [104] (around 20%). That can be explained by the dissolution time applied in their work, which was 12 hours. When looking at the other transition metals, Ni and Co dissolution remains lower than 1%, decreasing when the temperature increases. Finally, the Cu dissolution is influenced only by the oxalic acid concentration.

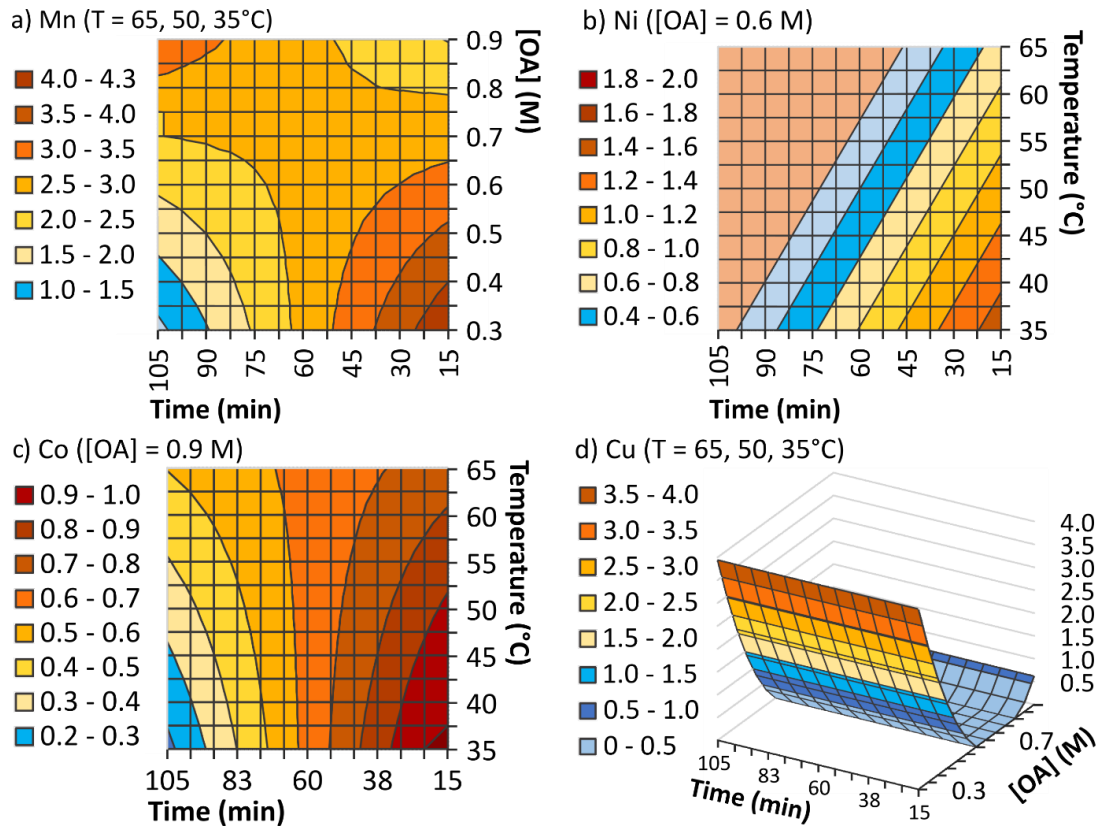


Figure 17: Contour and surface plots representing the modelled leaching yield for Mn (a), Ni (b), Co (c), and Cu (d) [141].

Upscaling and kinetics analysis

To achieve high and selective Li leaching with minimal transition metal dissolution, a temperature of 60°C, a residence time of 60 min, and an oxalic acid concentration of 0.6 M (NMC:OA 1:2.5) at a S/L ratio of 50 g/L are chosen. Under these conditions, complete Al dissolution is achieved while minimizing the dissolution of Ni, Mn, and Co. In the next part of the study, up-scaled experiments are run to validate the regression models obtained, and to understand the dissolution mechanism more deeply via kinetics calculations, identifying the controlling steps. Moreover, more thorough characterization is pursued to support the research.

The results presented here are based on Paper IV.

In this set of experiments, the leaching operations were conducted across a temperature range of 30°C to 80°C, with durations extending up to 7 hours. The leaching yield variation of all significant components in the system is illustrated in Figure 18. During the dissolution, the pH evolves, rising from 0.8 to 2 across all temperatures. The final solution potential is measured at

300 mV for every solution (see Appendix 3). Having a pH value that is not too low is already interesting, as lower pH values would increase the need for a neutralizing agent in the case of precipitation and might also increase the corrosion linked to the inorganic acid. The temperature directly influences proton consumption rates, with stabilization observed after 60 minutes above 50°C, suggesting a shift from protonation to complexation reactions. In contrast, the consumption rate of oxalate is slower, and the concentration keeps evolving after 60 min. This correlates with the previous statement and highlights the ongoing reactions between simple oxalate complexes (dissolved or solid) and oxalate ions. Around 0.3 M of oxalic acid is left, ca. half of the initial amount. This is very important for the later development of the process, and acid regeneration will need to be investigated for its economic and sustainability potential. This analysis highlights the interplay between pH and oxalate dynamics in CAM dissolution.

As the model predicted, the higher the temperature, the faster Li dissolves. At 80°C, only 30 min is needed to reach a plateau of dissolution (Li concentration of 2.5 g/L in the final leachate). While more than 6 h are required when the leaching is performed at 30°C, with a final Li concentration corresponding to 1.8 g/L. This correlates with the regression model obtained above. However, for all temperatures (except 30°C), the maximum recovery of Li is 90%, which is lower than the projected recovery rate. Hence, a limitation in the dissolution is observed for this small up-scaled set of experiments. Different phenomena could induce this limitation. The produced oxalates could coat the unreacted NMC particle, blocking the leaching reagent access, hence limiting Li dissolution. On the other hand, dissolved Li could get trapped in the crystal structure formed during the oxalate precipitation.

For Al, a total dissolution is observed after 60 min for most studied temperatures (except 30°C), corresponding to a final concentration of ca. 0.5 g/L in the leachate. No deviation from the modelled response is visible. While Al shows very fast dissolution, Cu behaves differently in the oxalic acid solution, as illustrated in Figure 18c. This set of experiments gives more insight regarding its dissolution. Here, the temperature positively affects the dissolution rate; after 7 h, only 5% of the Cu is dissolved at 30°C (final concentration of approximately 50 mg/L). In contrast, 15% or 25% are dissolved at 50°C or 80°C, with ca. 570 mg/L of Cu in the leaching solution after the leaching at 80°C. In addition, for all observed temperatures, the operation can be divided into three steps, raising questions regarding the reaction of Cu with oxalic acid. Cu can be initially dissolved as Cu(II), up to ca. 10-15% of dissolution in the first minutes, which is higher than the other TM. In a second step, Cu precipitated as simple CuC₂O₄ (negative slope), with the latter continuing to react with oxalic acid to form a soluble oxalate complex (again positive slope).

Regarding the transition metals from the CAM (Co, Ni, and Mn), they present the same dissolution behaviour globally, as visible in Figure 18d-e-f. The two-step mechanism is evident at lower temperatures (30 and 40°C) in the time observed. As seen in the inset, in the very first minutes, their dissolution can be observed (positive slope) followed by a negative slope indicating precipitation of some kind. This highlights that the release of metals into solution is initially faster than complexation, but complexation seems to take over the reaction rate, becoming the limiting factor of the operation. The final recovery is equivalent for all the temperatures investigated; less than 0.5% for Co and Ni and 2% for Mn (for a respective concentration of 15, 5, and 100 mg/L).

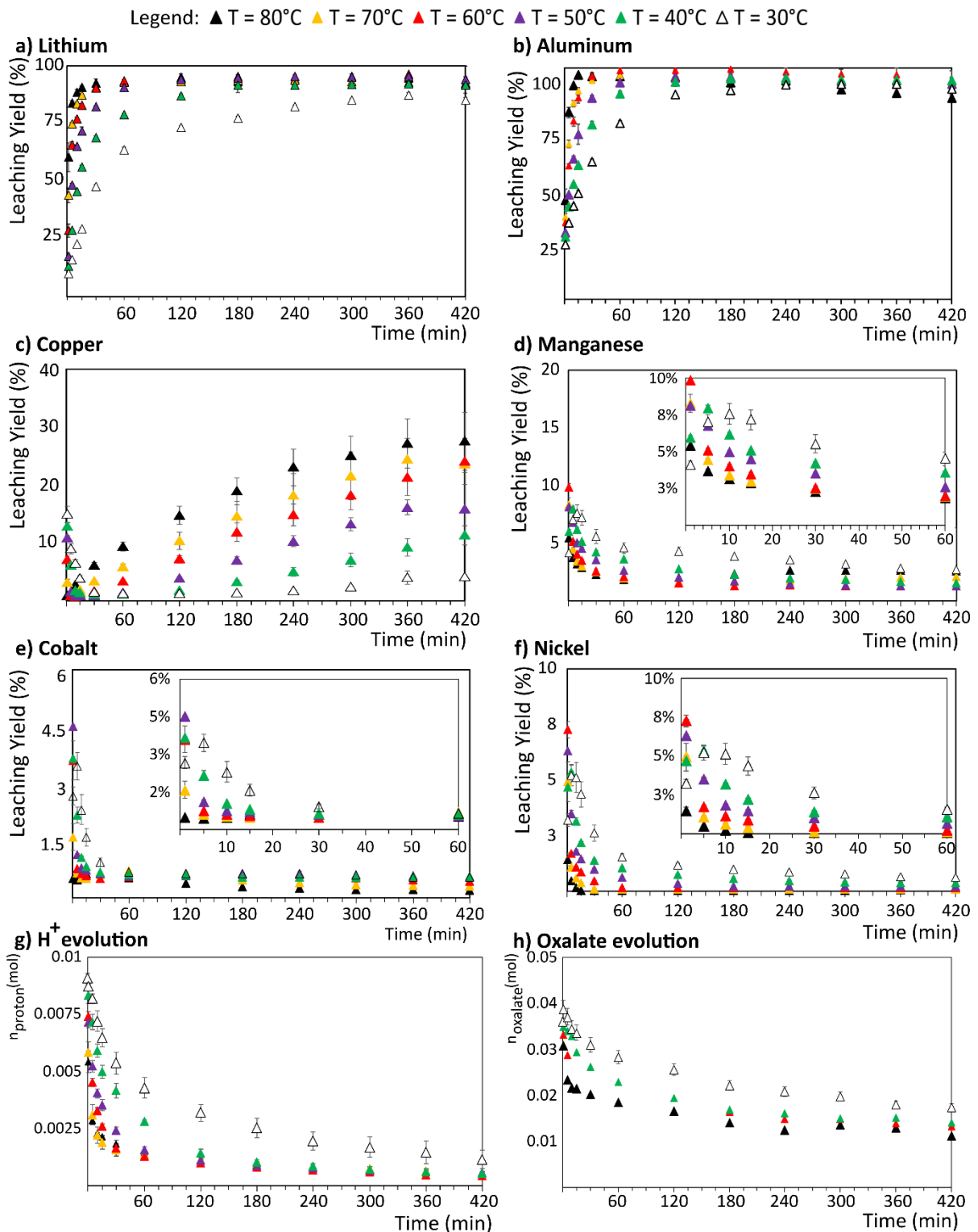


Figure 18: Evolution of the leaching yield ($S/L = 50 \text{ g/L}$) of all battery elements: Li a), Al b), Cu c), Mn d), Co e), Ni f), plus the proton consumption g) and oxalate evolution h) throughout the leaching operation. Error bars represent the standard deviation of the triplicate.

To complement the discussion on the dissolution behaviour of different metals in oxalic acid, predominance and species distribution diagrams were generated using Medusa, the resulting plots are shown in Figure 19 (the final molar concentrations are aligned with those observed in the leachate). At about pH 2, two anionic complexes coexist $\text{Al}(\text{C}_2\text{O}_4)_2^-$ and $\text{Al}(\text{C}_2\text{O}_4)_3^{3-}$. This

diverges from data reported in the literature; for instance, Zeng et al. [102] suggest that at a molar ratio OA:LCO of 1:2.5, a mixture of $\text{Al}(\text{HC}_2\text{O}_4)_3$ and $\text{Al}_2(\text{C}_2\text{O}_4)_3$ is formed, although the latter is reported to be insoluble. The Cu concentration is higher than the solubility of simple Cu oxalate, meaning that Cu is also present as another complex: the solution's most probable is the $\text{Cu}(\text{C}_2\text{O}_4)_2^{2-}$. More oxidative conditions could be needed to achieve higher dissolution of metallic Cu; this partial dissolution is not appreciated in the selective process in development [134,142]. Regarding the NMC metals, it is worth highlighting that Ni and Co concentrations are lower than the solubility limit of their simple oxalates; it could be considered that they are found in solution as such. While Mn's concentration exceeds the solubility limit, suggesting that the neutral simple oxalate and the anionic species, $\text{Mn}(\text{C}_2\text{O}_4)_2^{2-}$, co-exist in the solution. Additionally, the model indicates the presence of Mn(II) in the solution. Mainly anionic oxalate complexes, $\text{M}(\text{C}_2\text{O}_4)_2^{2-}$, can be formed in the solution. That knowledge is essential when developing a purification method for the solution. Traditional alkaline precipitation methods do not seem recommended as they would require substantial neutralization (up to pH 8), and the concentrations are low. In the objective of process development, ion exchange would be recommended as a fast and selective method for removing these impurities.

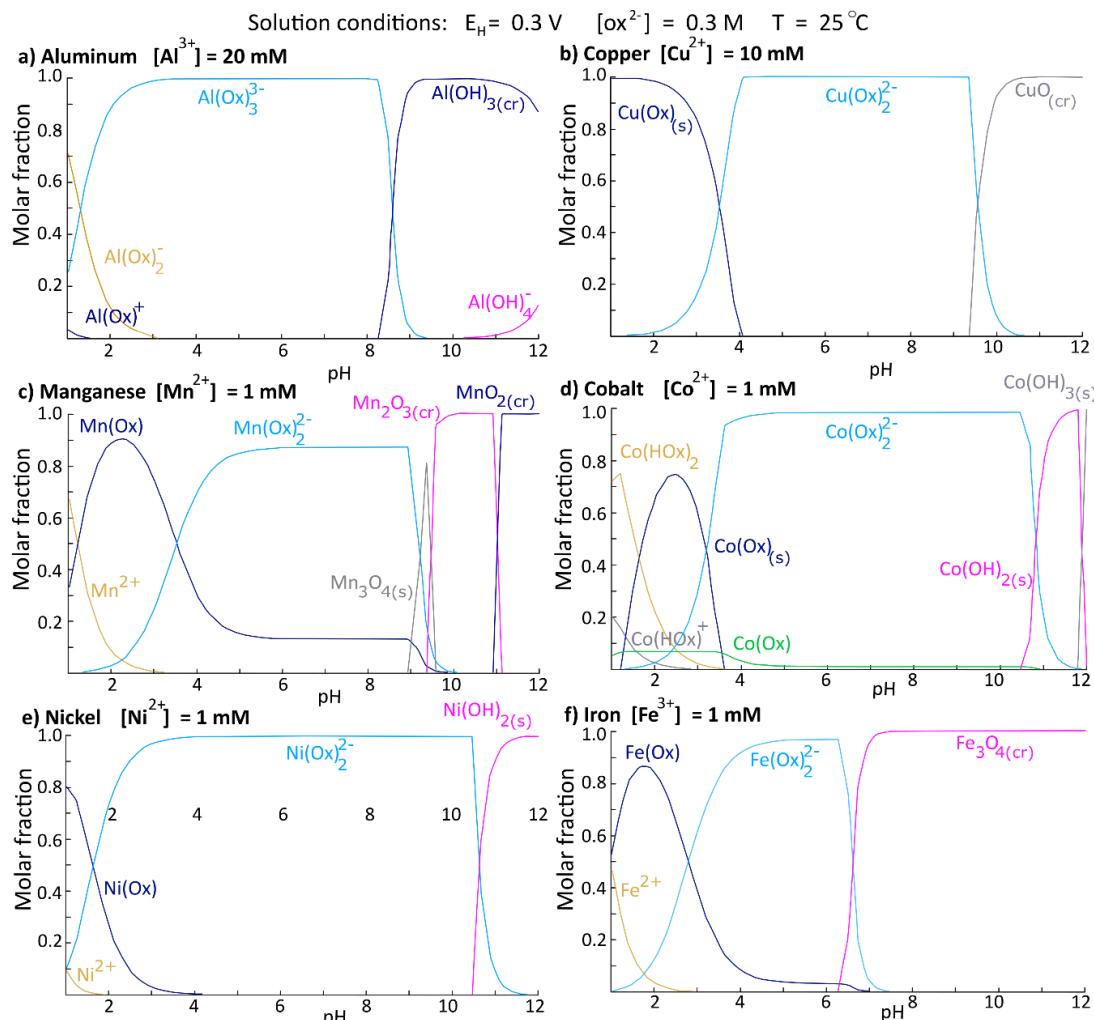


Figure 19: Species distribution diagram based on thermodynamic modelling with Medusa software for a) Al (20 mM), b) Cu (10 mM), c) Mn (1 mM), d) Co (1 mM), e) Ni (1 mM), and f) Fe (1 mM) with oxalate concentration of 0.3 M and potential of 300 mV.

To gain a deeper understanding of the leaching mechanism, various kinetic models have been applied to the Li dissolution (Equations 15 to 24 – Page 19). These models are deliberately used for this element, as Li behaviour best represents the CAM's dissolution. Figure 20 illustrates the computed experimental data points with the fitted models (dashed lines) at 30 and 60°C, along with the calculated kinetic constants for all models (k in min^{-1}) up to 360 min. The coefficient of determination (R^2) is also provided, indicating the linear model's goodness of fit. A value close to 1 reveals that the model fits the experimental data points well.

The best R^2 values are obtained for Equations 20, 21, and the Avrami model. With higher fit at low temperature with an R^2 of about 0.98 – 0.99 in the 3 cases, while at 60°C, an R^2 of 0.96 is obtained for Equation 21 and ca. 0.90 for Equation 20 and the Avrami model. The equations 20 and 21 are models describing homogeneous or pseudo-homogeneous reactions, respectively, 2nd and 3rd order reactions. The particles are considered to be uniformly distributed in the leaching solution, and the slurry can be seen as a liquid. The order typically determines how the reactant concentration affects the leaching rate. This highlights that the BM dissolution is chemically controlled, the interface's reaction rate controls the operation's speed, and it does not show any dissolution resistance due to a product layer around the unreacted lithium metal oxide particle. However, it is worth highlighting the lower fit of this operation at higher temperatures. This is not surprising, as with higher temperatures the reaction rate is faster (see later the Arrhenius law), as well as the diffusion rate; thus, there could be a transition from chemically controlled to diffusion-controlled. Additionally, products form faster at higher temperatures, and side-reactions can also occur, which could hinder the operation by coating the particle's surface (passivation layer or product layer).

One interesting aspect is that Equations 15 to 18, related to diffusion controlling, also have a reasonably good fit at 30°C. That could indicate that diffusion can also limit the reaction rate at lower temperatures, and both controlled mechanisms could be considered in this case.

The Avrami model, while exhibiting a satisfactory fit to the experimental leaching conversion data, offers a simplified representation of the process as a direct solid-to-liquid transformation, inherently neglecting the complexities of interface reactions. Despite this simplification, certain empirical observations for the Avrami model indicate the nature of the leaching. Notably, the Avrami order (m) reveals a value of 0.5 at 30°C, which decreases with increasing temperature. Conventionally, an Avrami order below 0.5 indicates a leaching mechanism governed by diffusion through a product layer. This interpretation, however, appears to contradict earlier assessments of the rate-controlling step under these conditions, necessitating a more nuanced analysis of the underlying mechanisms and the applicability of the Avrami model across the investigated temperature range.

The solid analysis characterization will aim at solving which mechanism is preponderant and characterize whether the product is formed in bulk or around unreacted particles.

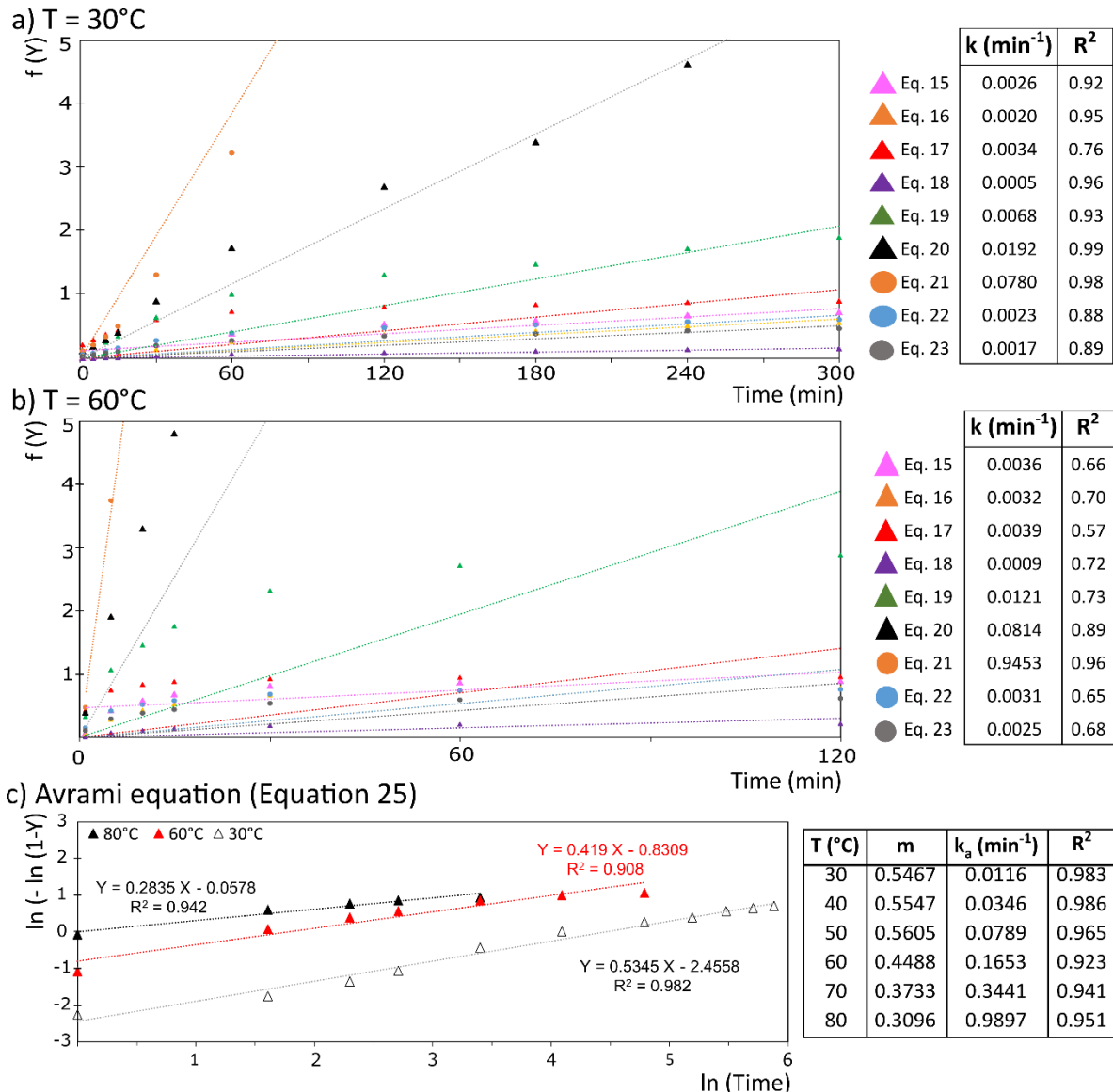


Figure 20: Fitting models (Equation 15 - 23) to the experimental data at a) $T = 30^\circ\text{C}$, b) $T = 60^\circ\text{C}$, and c) the fitting for the Avrami equation (Equation 25) with their rate constant associated and R^2 .

Based on the kinetic rate constant obtained at each temperature for the best-fitted models, the linearized Arrhenius law ($\log(k)$ as a function of $1/T$) is plotted in Figure 21 for the three best model; the energy of activation (E_a) is calculated from the slope value (Equation 26). This parameter is essential for understanding and optimizing the process toward its industrialization.

The highest R^2 (0.995) is obtained for the Avrami model, giving an energy of activation of 76 ± 3 kJ/mol. While 55 ± 4 kJ/mol and 63 ± 10 kJ/mol are determined with the 2nd and 3rd order kinetics models, with an R^2 of 0.98 and 0.91, respectively. These values are concordant with the ones obtained by Verna et al. when they leached LCO with oxalic acid [71]. It is essential to highlight that the values obtained (between 55 and 76 kJ/mol) are relatively high compared to processes using inorganic acids [49,74]. This is not abnormal for organic acids, as they typically require more energy for reaction completion and have a lower reaction rate [68,143]. Additionally, it emphasizes again the chemically controlled nature of the dissolution, as the value is higher than 40 kJ/mol [117,121]. Chemically controlled reactions are more sensitive to temperature, as the

energy of activation of a reaction is usually higher than the diffusion during a leaching operation. Hence, tight temperature control will be needed, which may lead to higher operational costs and energy. It is important to remember that at high temperatures, diffusion can become the rate-controlling step [121].

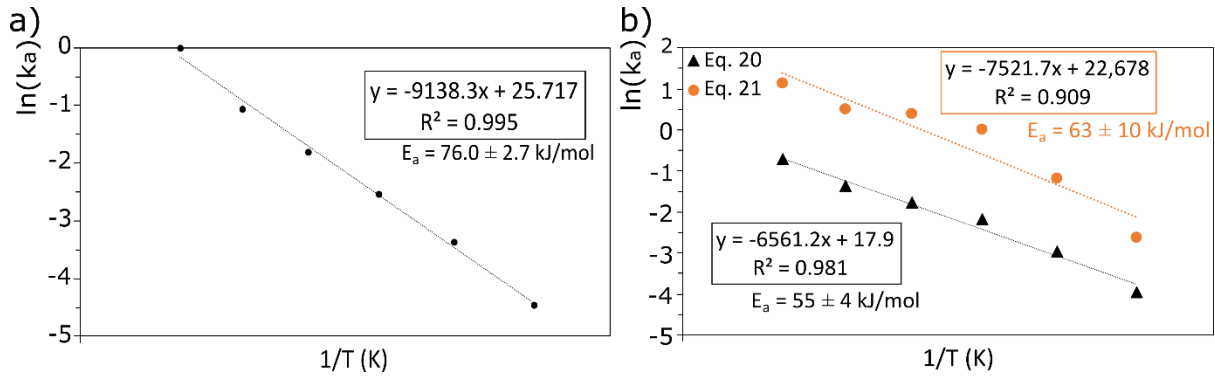


Figure 21: Arrhenius plot from a) Avrami model data and b) from data of the second and third order reaction (Equation 20 and 21).

Leaching 1 residue characterization

The results presented here are based on Paper IV.

The different morphological characterizations (SEM-EDS and particle size) of the residue are depicted in Figure 22, which is essential for the definition of the dissolution mechanism of the BM. First, a simple observation can be made regarding the size distribution of the particles in the sample, as visible in Figure 22b. The overall particle size has decreased compared to the initial sample (see Figure 8 - Page 29), with the d50 dropping from 29.8 μm to 17.5 μm . A new particle size group of around 1 μm can be observed on the size distribution graph, while the peak of the 2nd group of particles (defined previously from 30 to 110 μm) has decreased. This primary observation could support the hypothesis that the NMC particle size decreases with the leaching and that the precipitation of the metal oxalates occurs in the bulk. However, as some particles are still visible around 100 μm , some NMC unreacted particles may still be trapped inside the structure. It is also worth mentioning that the group of particles around 10 μm seems untouched by the operation, which supports the hypothesis that it is the group of graphite particles.

Secondly, SEM is used to observe the morphology of each particle after leaching at 60°C as seen in Figure 22a. The rounded particles of NMC are less prominent and are replaced by smaller agglomerates of cubic particles. This differs from the observation made by He et al., who leached NMC532 cathode material with 0.6M oxalic acid at a S/L of 20 g/L at 70°C for 30 min. The resulting residue exhibits particles of irregular shapes with very rough surfaces and an increased size [144]. Moreover, EDS analysis indicates the composition of the different particles. The small cubic particles comprise Ni, Mn, and Co associated with C and O; this elemental distribution supports the attribution to the metal oxalate precipitate. No Al foil could be found in the studied samples, which supports ICP results regarding its complete dissolution. The fluorine content has drastically decreased, indicating the dissolution of the electrolyte salt in the aqueous solution. Cu remains in the sample and can be found in a similar foil shape as previously, primarily as metallic Cu and possibly CuO.

a) SEM Image and EDS results (Leaching residue at 60°C)

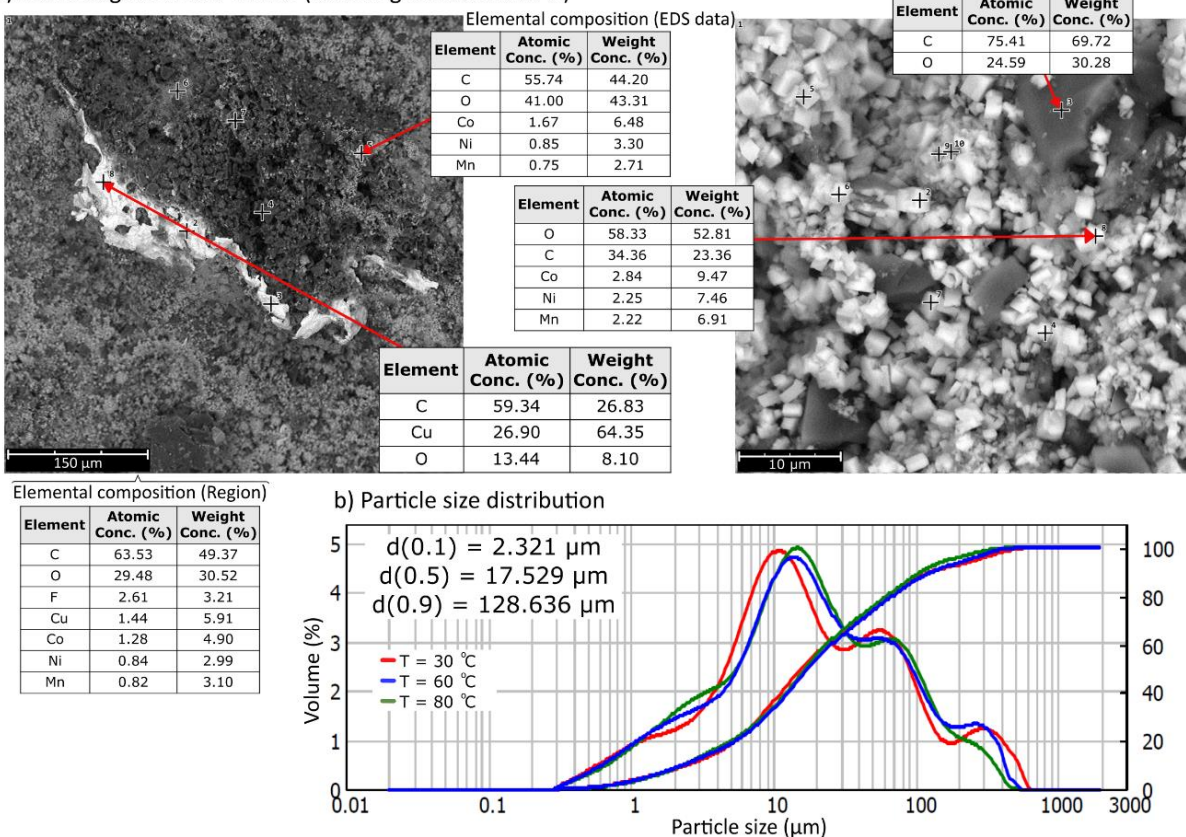


Figure 22: a) SEM image and EDS report for the residue obtained after leaching at 60°C and b) the particle size distribution for the residues obtained after leaching at 30, 60, and 80°C (d values given for the residue $T = 60^\circ\text{C}$).

In addition to morphological characterization, structural characterization is performed. The XRD patterns of the residue obtained after leaching at 30, 60, and 80°C are shown in Figure 23a, and the exact composition of the residue is given in the Appendix 5. The patterns reveal comparable diffraction peaks across all leaching temperatures, indicating the consistent presence of crystalline phases within the leaching residue. Notably, a distinct diffraction peak at $42.2^\circ 2\theta$, marked by an arrow, was observed exclusively in the leachate obtained at 30°C and was absent at higher temperatures. This peak, also present in the initial BM as depicted in Figure 8, is attributed to unidentified impurities that exhibit temperature-dependent leaching behaviour. Given their apparent solubility in aqueous media, these impurities may originate from fluorine-containing species derived from the electrolyte salt or represent decomposition products that dissolve preferentially at elevated temperatures.

The diffraction peaks at 26.6 , and $44.6^\circ 2\theta$ (marked with *) reveal the presence of a graphite phase (PDF 04-016-6937) remaining in the residue from the BM. The other peaks in the diffraction pattern can be assigned to a transition metal oxalate phase, particularly the $\text{Co}(\text{C}_2\text{O}_4) \cdot 2 \text{H}_2\text{O}$ (PDF 04-016-6937). The main question regarding the formed oxalate phase is whether a common oxalate phase containing the different transition metal precipitates or a phase separation occurs. In a study by Wang et al. [145], a Co-Ni mixed oxalate was prepared. They show that the solid solution formation between the Co and Ni oxalate phases leads to a single diffraction peak at $35.1^\circ 2\theta$, whereas peak splitting would indicate the formation of a hybrid phase. No peak splitting can be observed for our leaching residues, suggesting that a single oxalate phase containing Co,

Ni, and Mn must be formed. Hence, Mn and Ni seem to act as dopants and occupy the same crystallographic site as Co ions in the oxalate framework. Nonetheless, when comparing the expected diffraction lines of $\text{Co}(\text{C}_2\text{O}_4) \cdot 2 \text{H}_2\text{O}$ with the observed pattern, it is visible that some diffraction lines are missing, i.e. the ones corresponding to the (11 \bar{l}) lattice planes (21.2, 24.7, 29.1, 33.6, and 38.8° 2θ).

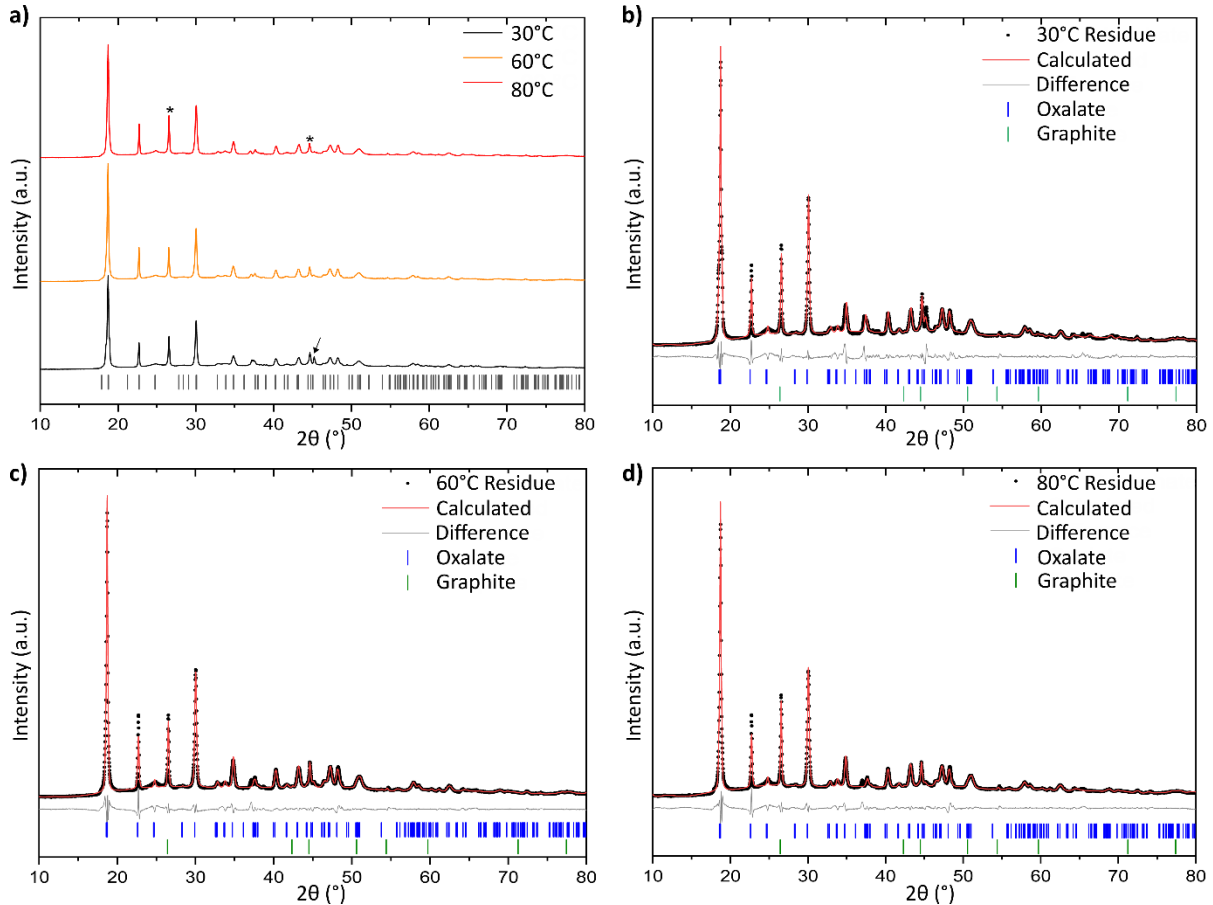


Figure 23: a) X-ray diffraction pattern of the sample residues obtained after the leaching at 30, 60, and 80°C with the expected diffraction lines for the $\text{Co}(\text{C}_2\text{O}_4) \cdot 2\text{H}_2\text{O}$ phase (PDF 04-016-6937). The asterisk indicates the peaks corresponding to the graphite phase (PDF 04-016-6937), b) Pawley fitting $T = 30^\circ\text{C}$, c) Pawley fitting $T = 60^\circ\text{C}$, d) Pawley fitting $T = 80^\circ\text{C}$. Pawley fitting was realized in collaboration with Dr. Laura Altenschmidt.

Previous reports on the structure of transition metal oxalates containing Ni or Mn showed that oxalates are prone to the formation of disordered structures, which is accompanied by the extinction of certain diffraction peaks [146,147]. This disorder is caused by a displacement of the one-dimensional oxalate chains with respect to one another. To further characterize the formed leaching residues, the unit cell parameters and the space groups are determined using a Pawley fit; the refinement results are reported in Table 12. As the starting point, the oxalate phase is based on the reported structure by Puzan et al. for the disordered nickel oxalate [147]. Figure 19 b-d shows that a description with the disordered oxalate structure and a graphite contribution allows the observed diffraction patterns to be reproduced. Even though the model fits the data well, it must be mentioned that it also accounts for more amorphous contributions around 24.7 and 33.8° 2θ , which can be indexed and correspond to the (11 \bar{l}) and (11 l) lattice planes. With increasing temperature, these broad diffraction peaks become more pronounced, suggesting a

disorder-order transition of the oxalate phase. The lattice parameters within the temperature series are close to the reported parameters for the single-phase α' -Mn, Co, or Ni oxalates [146]. The obtained values can be seen as the mean of the different lattice parameters of the individual oxalate phases. This confirms that Co, Ni, and Mn coprecipitate and form a solid solution.

Table 12: Pawley fitting results. The angles α and γ were fixed to 90°, and only β was refined. Pawley fitting was realized in collaboration with Dr. Laura Altenschmidt.

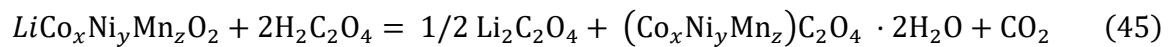
Sample Residue	Lattice parameters					Space group	R_{wp}
	a (Å)	b (Å)	c (Å)	$\alpha = \gamma$ (°)	β (°)		
30°C	11.956(1)	5.460(1)	9.860(1)	90	126.89(1)	C12/c1	5.08
60°C	11.939(1)	5.466(1)	9.843(1)	90	126.98(1)	C12/c1	4.93
80°C	11.938(1)	5.464(1)	9.838(1)	90	126.94(1)	C12/c1	4.87

Hence, the XRD analysis reveals that the leaching residue mainly comprises a solid solution consisting of a disordered $(\text{Co},\text{Ni},\text{Mn})\text{C}_2\text{O}_4 \cdot 2 \text{H}_2\text{O}$ phase and graphite. It is worth mentioning that this phase has physical properties different from those of single metal oxalate complexes. Hence, the solubility mentioned earlier (Table 6 – Page 21) has to be adapted, and it is a probable linear combination of the single oxalates. Additionally, some residual impurities of unidentified BM components are present. No residual NMC111 can be evidenced (all intense peaks are gone). If any, only very little of the NMC could be left, up to a maximum of 1% corresponding to the LOD of the machine in the case of highly crystalline materials. This indicates that the reaction is going toward a complete conversion.

Conclusion on Leaching 1 of the recycling process

This second strategy, based on the use of oxalic acid, is promising. The first leaching operation is proven to be very selective towards Li and completely removes Al. The removal of Li is not as complete (90%) as expected in preliminary tries conducted at a small scale, and the kinetics investigation and residue analysis points towards a chemical-controlled operation with a transition towards diffusion-limited at higher temperatures.

Equation 45 proposes the main reaction for the dissolution of CAM with oxalic acid, where Li remains in solution principally as $\text{Li}_2\text{C}_2\text{O}_4$, and the TM are in a solid solution structure, which is hardly soluble in aqueous media. Again, the importance of oxalic acid concentration is highlighted because, if present in excess, it can continue to react with the TM simple oxalate to form anionic oxalate complexes soluble in the solution.



5.3.2 Sulfuric acid leaching (Leaching 2)

The results presented here are based on Manuscript V.

For the next part of the investigation, another scale-up operation was done: the BM was leached in a 2 L reactor at 60°C for 120 minutes with an oxalic acid solution at 0.6 M at an initial fixed S/L ratio of 50 g/L, respecting a molar ratio NMC:OA of 1:2.5 (detailed in Manuscript V). The residue has the same composition: a mix of a disordered $(\text{Co}, \text{Ni}, \text{Mn})\text{C}_2\text{O}_4 \cdot 2\text{H}_2\text{O}$ phase and graphite.

Thermodynamics consideration and sulfuric acid leaching yields

The second leaching is performed with H_2SO_4 to leach the metal oxalates and separate them from the graphite. Despite their insolubility in water due to the formation of strong complexes, metal oxalates ($\text{MC}_2\text{O}_4 \cdot x\text{H}_2\text{O}$) can be effectively dissolved by employing strong acidic solutions, a condition known to disrupt their stable structure and enhance solubility [100]. First, some thermodynamic predictions were computed to help discuss the leaching operation, as seen in Table 13. Only the Ni and Co solid simple oxalate are present in the database, while Mn and Cu soluble simple oxalate can be found. The monometallic oxalate complexes can help us understand the dissolution mechanism, as the residue comprises a solid solution. Different reactions were considered: the dissolution of the solid complexes in water (Equations 47 and 50), in H_2SO_4 (Equations 48 and 51), and the reaction of the oxalate complexes (solid or not) with the H_2SO_4 , forming sulphate in solution (Equations 46, 49, 52, 53). Apart from these potential reactions, it is essential to mention that some side reactions are possible, like the degradation of oxalic acid molecules with concentrated H_2SO_4 , which results in the formation of CO gas, or the presence of fluorine, which could interfere and create other species with the elements. The reaction between the solid oxalate complex and H_2SO_4 , forming the sulphate-associated species, is spontaneous. On the other hand, the dissolution of the solid complexes in acid or water, forming the oxalate-associated species, is not spontaneous; this is predictable as they are known to be insoluble in aqueous solutions. It highlights that the dissolution probably holds in the amount of acid provided to solubilize the oxalate, which then forms the metal sulphate in the solution. The transformation from oxalate to sulphate seems to be the driving force of the dissolution. Also, note that the reaction between the soluble oxalate compound and H_2SO_4 is spontaneous.

Table 13: Thermodynamic consideration – computed with HSC Chemistry 10.

Reaction Equations		$\Delta G(65^\circ\text{C})$ (kJ/mol)
$\text{CoC}_2\text{O}_4 \cdot 2\text{H}_2\text{O} + \text{H}_2\text{SO}_4 = \text{CoSO}_{4(a)} + \text{H}_2\text{C}_2\text{O}_4 + 2\text{H}_2\text{O}$	(46)	-41.1
$\text{CoC}_2\text{O}_4 \cdot 2\text{H}_2\text{O} + \text{H}_2\text{O} = \text{CoC}_2\text{O}_{4(a)} + 3\text{H}_2\text{O}$	(47)	27.1
$\text{CoC}_2\text{O}_4 \cdot 2\text{H}_2\text{O} + \text{H}_2\text{SO}_4 = \text{CoC}_2\text{O}_{4(a)} + \text{H}_2\text{SO}_4 + 2\text{H}_2\text{O}$	(48)	27.2
$\text{NiC}_2\text{O}_4 \cdot 2\text{H}_2\text{O} + \text{H}_2\text{SO}_4 = \text{NiSO}_{4(a)} + \text{H}_2\text{C}_2\text{O}_4 + 2\text{H}_2\text{O}$	(49)	-31.3
$\text{NiC}_2\text{O}_4 \cdot 2\text{H}_2\text{O} + \text{H}_2\text{O} = \text{NiC}_2\text{O}_{4(a)} + 3\text{H}_2\text{O}$	(50)	27.2
$\text{NiC}_2\text{O}_4 \cdot 2\text{H}_2\text{O} + \text{H}_2\text{SO}_4 = \text{NiC}_2\text{O}_{4(a)} + \text{H}_2\text{SO}_4 + 2\text{H}_2\text{O}$	(51)	27.4
$\text{MnC}_2\text{O}_{4(a)} + \text{H}_2\text{SO}_4 = \text{MnSO}_{4(a)} + \text{H}_2\text{C}_2\text{O}_4$	(52)	-62.1
$\text{CuC}_2\text{O}_{4(a)} + \text{H}_2\text{SO}_4 = \text{CuSO}_{4(a)} + \text{H}_2\text{C}_2\text{O}_4$	(53)	-33.2
$\text{Cu}_{(s)} + 2\text{H}_2\text{SO}_{4(a)} = \text{CuSO}_{4(aq)} + \text{SO}_{2(g)} + 2\text{H}_2\text{O}_{(aq)}$	(54)	-62.7
$3\text{H}_2\text{C}_2\text{O}_4 + \text{H}_2\text{O}_2 = 6\text{CO}_{2(g)} + 2\text{H}_{2(g)} + 2\text{H}_2\text{O}$	(55)	-658.8

From the preliminary test described in paper V, the agitation (300 rpm), temperature (65°C), and molarity (2 M) are fixed as they are shown to provide enough energy and acidity to enhance the reaction. The operation was scaled up to a reactor volume of 1 L for 2 h. The S/L ratios were varied to observe the behaviour of all metals and to identify the driving force for the dissolution. The leaching yield and concentration in the solution are depicted in Figure 24.

The general observation is that the higher the S/L ratios, which can be directly correlated with a lower molar ratio, the lower the dissolution yield. Li is almost fully recovered regardless of the applied conditions. More than 90% of the Co, Ni, and Mn are dissolved for a molar ratio higher than 20, except for Cu, which is dissolved at about 70% under the same conditions. Cu is known to require oxidative conditions for its dissolution; although the reaction is thermodynamically spontaneous, it usually needs the addition of an oxidative agent to facilitate its recovery. However, using any oxidative source should be avoided here as it would enhance $H_2C_2O_4$ degradation, as seen in Equation 55. When the molar ratio is at 5 (S/L ratios of 80 g/L), Co or Mn recovery decreases by about 30%, which is somewhat proportional to the reduction of the molar ratio. Moreover, their concentration in the leachate increases promptly, 4.5 and 3.4 g/L, respectively, against 1.8 and 1.2 g/L after leaching at 20 g/L.

On the other hand, Ni dissolution behaviour does not follow the same trend as Mn and Co; its recovery and concentration are distinct when the molar ratio is lower than 20. In fact, Ni concentration reaches a plateau at about 1.5 g/L under most studied conditions in 60 min (Figure 24b) but before that, its concentration goes higher than this value for a short period (at ca. 2 g/L) as visible on the Appendix 6. It could be interpreted that Ni reaches a solubility limit. However, when looking at the solubility data, $NiSO_4$ compound is highly soluble in water (solubility of 40 g/100g H_2O at 20°C [124]). This would suggest that Ni exists as oxalate in the solution and has a solubility of about 1 g/L (in a solution at 2M H_2SO_4 at 65°C). This contradicts the thermodynamics data discussed above (Table 13), which states that sulphates are formed in the bulk.

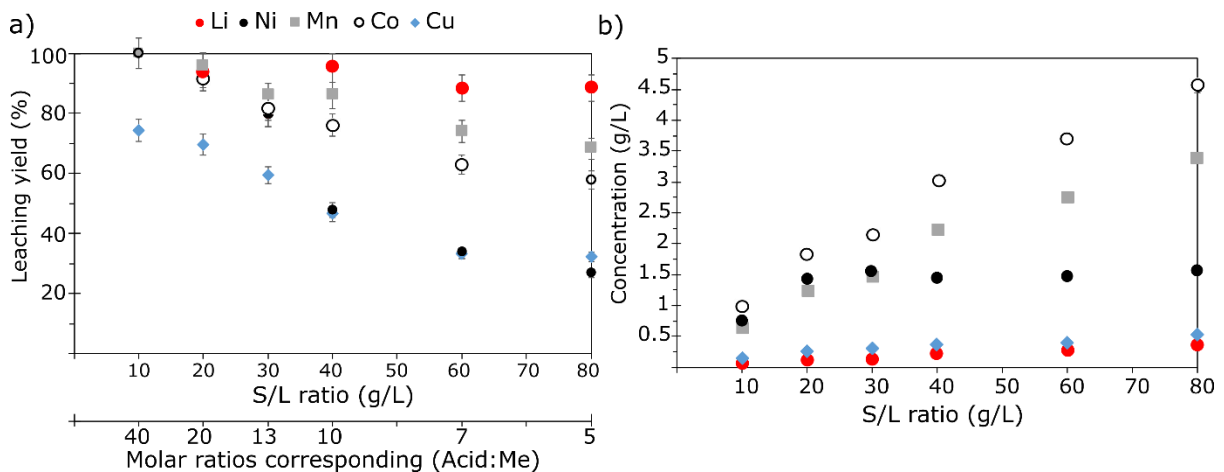


Figure 24: a) Leaching yield, b) metal concentration after leaching ($T = 65^\circ C$, $[H_2SO_4] = 2 M$, $t = 60 \text{ min}$, 300 rpm agitation) at different S/L ratios.

Leaching 2 solution characterization

FT-IR and UV-Vis analysis were performed to understand better in which speciation Ni is present in the solution; the spectra are visible in Figure 25. On the FT-IR spectra, the bands at 1182, 1106, 1050, and 884 cm^{-1} can be assigned to the S=O and S-O vibrations [148], revealing the presence of sulphate group. It can be due to the H_2SO_4 or metal sulphate compounds present in the solution. Additionally, the oxalic acid spectrum (blue spectra) shows two peaks at 1627, 2112, and 3326 cm^{-1} , which are assigned to the C-O and C=O vibrations in the oxalate structure [149]. The same bands can be observed on the spectra of the leachate solution. These data validate the presence of sulphate and oxalate in the solution, but it is hard to conclude regarding the transformation of the metal oxalate into sulphate as presented in Table 13.

Hence, a UV-Vis analysis were performed to assess which metal form is in the solution (Figure 25b and c). First, standard solutions (Figure 25c) were prepared by dissolving the respective sulphate salt in water to obtain a metal concentration corresponding to the one measured in the leachate solution at 80 g/L by the ICP (i.e., $[\text{Co}] = 3.58\text{ g/L}$, $[\text{Ni}] = 0.72\text{ g/L}$, $[\text{Mn}] = 2.99\text{ g/L}$, and $[\text{Cu}] = 0.26\text{ g/L}$). The spectra show that NiSO_4 absorbs at about 400 nm and 650 nm, CoSO_4 at 520 nm, and CuSO_4 has a prominent peak in the region of 800 nm, while no absorbance band can be seen for the MnSO_4 . The leaching solutions (Figure 25b) present absorption peaks in the same range as the standard sulphate solution, highlighting the presence of Co and Ni sulphate. For the Ni, there is a maximum absorbance for all solutions at around 0.2, which is coherent with ICP measurement and validates the limit of dissolution. It can be confirmed that Ni exists primarily as sulphate in the solution, and its recovery limitation could be in the solubility limit of an intermediate product instead of the final one. The reaction presented in Equation 49 is not complete, even if thermodynamics considers it spontaneous. More than the solubility argument, some limitations could stand in the amount of acid provided or the kinetics. Lastly, the large absorbance band from 350 nm present in all leaching solutions matches the absorbance band observed in the oxalic acid, which would indicate the presence of oxalic acid in the solution, hence, corroborating the transformation in sulphate associated with the production of oxalic acid.

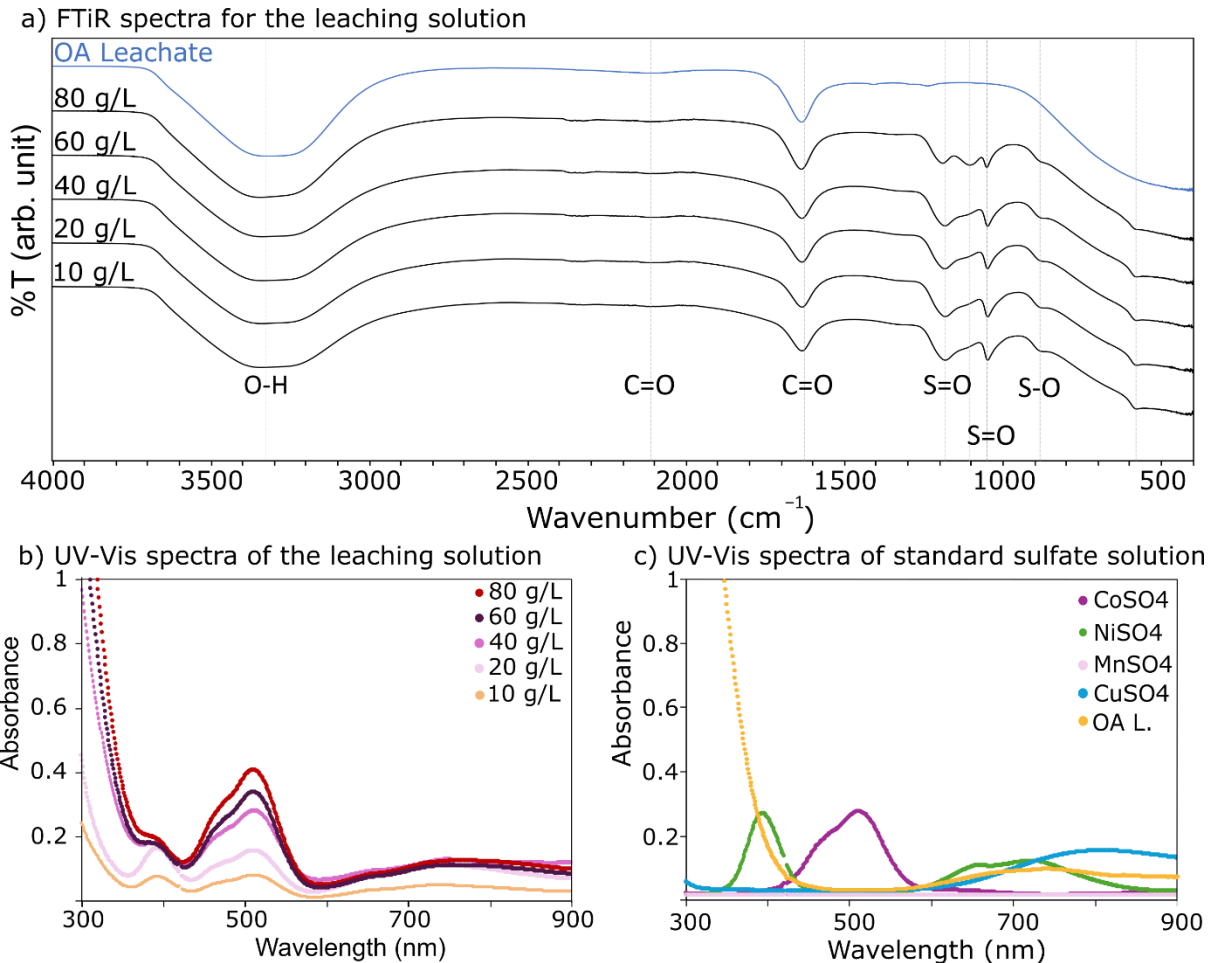


Figure 25: a) FT-IR spectra and b) UV-Vis spectra of the leaching solutions ($T = 65^\circ\text{C}$, $[\text{H}_2\text{SO}_4] = 2 \text{ M}$, $t = 120 \text{ min}$, 300 rpm agitation) at different S/L ratios, with the c) UV-Vis spectra of standard solutions of metal sulphate.

Leaching residue characterization

The leaching residues were analysed by ICP and XRD, as seen in Figure 26a-b. The metal composition of each leaching residue obtained (Figure 26a) aligns with the measured concentration in the solution; at low S/L ratios, most metals are leached, and the resulting composition in the residue is very low. On the other hand, from 40 g/L, the presence of Ni is relatively increasing compared to the other TM (ca. 8 wt%, against ca. 4 wt% for Co and 1 wt% for Mn). And the higher the S/L ratio, the less the solid solution phase is leached, and the more TMs are left in the residue (ca. 8 wt%, ca. 5.5 wt% for Co and 2 wt% for Mn).

The FT-IR spectra of the residues are provided in Appendix 7. It can be seen that the spectra for the 10 g/L and 20 g/L residues do not show any peaks or only weak ones. For higher S/L ratios, the appearance of bands at 1315 cm^{-1} , 1358 cm^{-1} , and in the $1610\text{-}1630 \text{ cm}^{-1}$ range can be observed. These peaks are assigned to the C-O vibrations of the oxalate group [149]. This implies that the solid residue (above a S/L ratio of 40 g/L) is composed of oxalate. This suggests that (above that S/L ratio) the oxalate from leaching 1 either did not fully react or re-precipitated.

The XRD patterns provide valuable insights into the underlying leaching mechanism, enabling the identification of phase transitions and structural changes during the process. For instance, after leaching at 20 g/L, graphite is detected as the main phase remaining in the solid (main diffraction peaks at 26.6 and 44.6° 2θ). Additional peaks, which fit NMC cathode material, CoO, NiO, and Cu, can be observed. Their presence, till now undetected, is made visible as the rest of the material has been leached out. We can conclude that the undissolved Li in the residue after oxalic acid (Leaching 1 – see Page 41) was in the unreacted NMC material, the produced oxalate were coating the core and the oxalic acid could not reach the centre of the particle.

On the other hand, after leaching at 40 g/L and 80 g/L, the residues consist of a mixture of graphite and oxalate phases. Unlike the oxalic acid leaching residue, which consists of a single solid solution of $(\text{Co}, \text{Ni}, \text{Mn})\text{C}_2\text{O}_4 \cdot 2\text{H}_2\text{O}$, here a phase separation is observed: identified with the peak splitting at 35.1° 2θ. The first phase is a solid solution similar to the previous one (named Mixed Oxalate in Figure 26), and the other is a structure mainly composed of Ni oxalate. With high S/L ratio, the pic relative to the mixed oxalate phase is more intense (see inset in Figure 26b). This is not surprising, the higher the S/L ratio, the lower the $(\text{Co}, \text{Ni}, \text{Mn})\text{C}_2\text{O}_4 \cdot 2\text{H}_2\text{O}$ phase leaching, which leads to its increased presence in the residue.

a) Residue elemental composition in wt% (%)

S/L (g/L)	Co	Ni	Mn	Li	Cu
10	0.87	< LOD	< LOD	< LOD	0.76
20	0.27	0.16	< LOD		0.39
40	3.99	8.17	1.00		1.83
60	4.53	7.27	1.05		1.41
80	5.53	8.1	2.11		1.62

b) XRD pattern

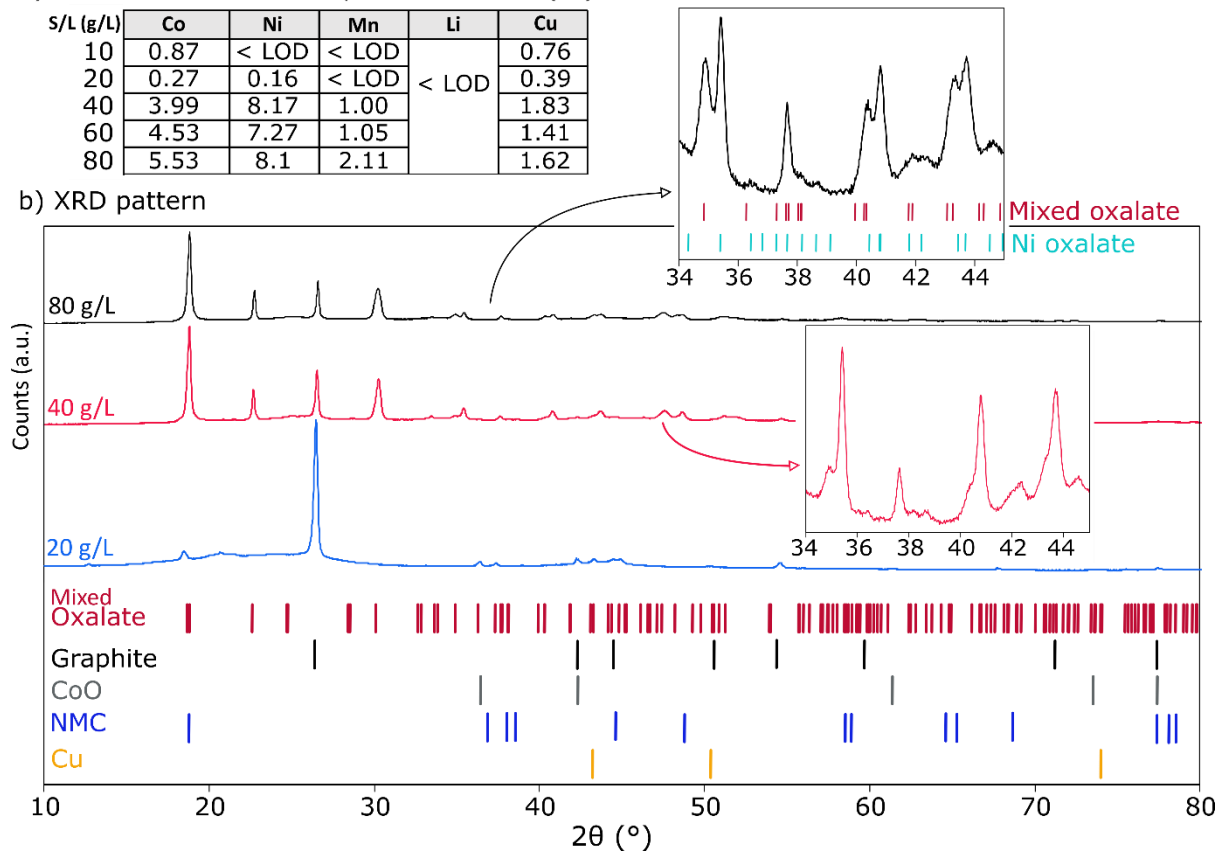
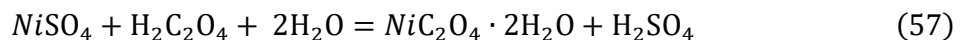
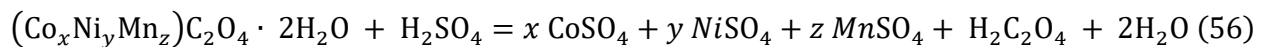


Figure 26: a) Residue metal composition (wt%), and b) XRD pattern of the solid residue after leaching ($T = 65^\circ\text{C}$, $[\text{H}_2\text{SO}_4] = 2 \text{ M}$, $t = 120 \text{ min}$, 300 rpm agitation) at different S/L ratios - (Graphite: PDF 04-016-693; CoO: PDF 04-002-2692; NMC 111: PDF 04-013-4379; Cu PDF 01-091-1717).

Conclusion on Leaching 2 of the recycling process

Simple oxalate complexes need a strong acidic solution to be leached; Ni oxalate stands out from the other TM with lower solubility under the conditions provided. The Equation 56 and 57 express the leaching reaction mechanism ($x + y + z = 1$); a significant excess of acid is required to complete the reaction. The unique solid solution of the oxalate splits into two phases, revealing the mechanism. On one side, the structure is depleted of the three elements more or less simultaneously, leading to the production of metal sulphate in the solution. On the other side, a new oxalate phase composed mainly of Ni is formed, highlighting the maximum dissolution of the element under the studied conditions (Equation 57).



Now, if we focus more on the process, it is clear that some limitations are observed, and that low S/L will be needed to recover the most significant part of the valuable elements. This is not favoured by the industry, which prefers large S/L. Two main flowcharts can be proposed at this point of the study, presented in Figure 27. The first (up) is a one-stage leaching with an S/L ratio of 20 g/L. Another path could be to apply a two-stage leaching, which will enhance the same recovery rate but then produce two leaching solutions with the potential to produce different NMC materials. This option was applied, and the data provided in Figure 27, are experimental based.

The first option would remain the preferred one as it is more straightforward, but no option should be discarded at this point.

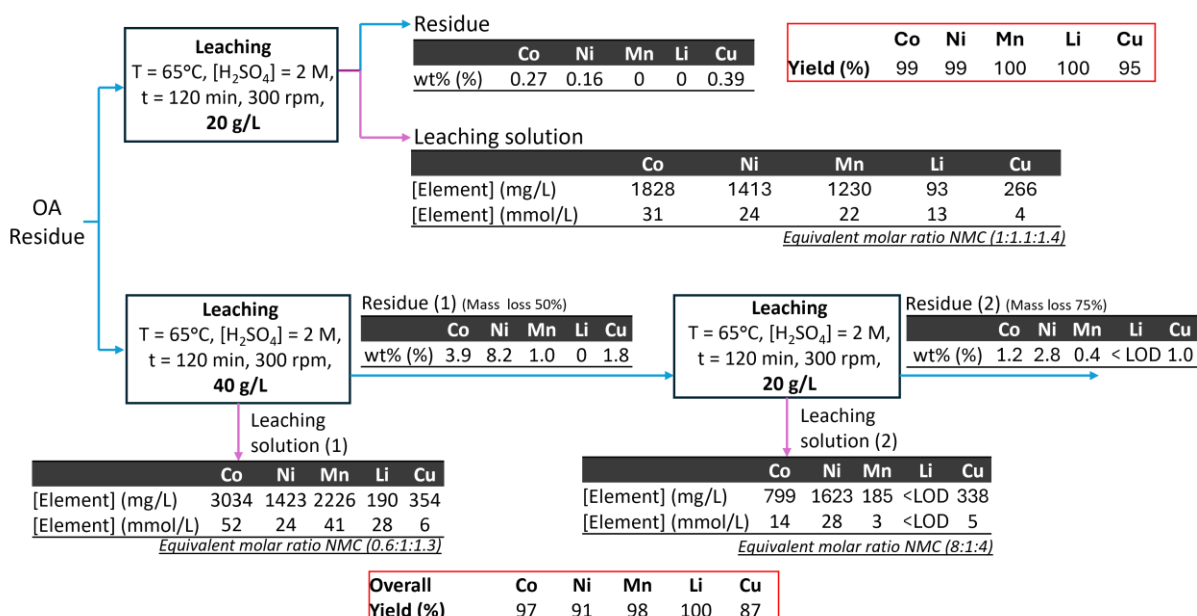


Figure 27: Potential leaching routes: one-stage leaching (high recovery and towards NMC 111 production) or two stage leaching (40 g/L and 20 g/L).

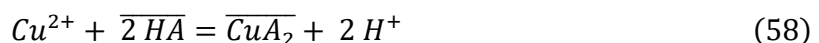
5.3.3 Purification leaching solution 2 -Towards the production of CAM precursors

The results presented here are based on Manuscript V.

Impurity concern – Removal of Cu

As the background section (page 10) explains, Cu exhibits toxic effects on regenerated CAM. It is the one remaining impurity element at this stage of the process present in the solution at ca. 300 mg/L (Figure 27). Thus, it must be removed and left at a trace level. The limit of acceptance would vary depending on the desired performance. In this thesis, it was set at 5 mg/L [91]. Precipitation techniques were judged unsuitable for this separation, as seen in Figure 19, no recovery can be expected by adjusting the pH. Minimizing of co-precipitation of valuable elements (losses) is crucial in the process, hence another separation technique must be considered to remove the Cu from the solution.

Solvent extraction was selected as the preferred method. It allows a selective and effective metal recovery from an aqueous solution, even at trace levels. Cu extraction has been well-documented over the years. However, its extraction from a sulfuric aqueous matrix accompanied by residual oxalic acid is still undone. Oxalic acid still has a complexing ability and could form some soluble anionic Cu oxalate form, which could resist the extraction system. The selected extractant is the Acorga M5640, a hydroxy oxime-type organic acid extractant widely used in the industry because of its high selectivity for Cu [150]. It is an acidic extractant expected to follow Equation 58 (\overline{HA} is the protonated form of the extractant). Hence, Cu extraction efficiency is significantly impacted by the pH. For instance, optimal extraction conditions for Acorga M5640 were found at an equilibrium pH of 2.5, where nearly 92% of Cu was extracted [150,151]. Other authors demonstrate that about 85% extraction could be achieved from a feed containing Cu and Zn in perchloric acid at an initial pH of 1 [152].



It is worth noting that Li in very low quantities in the leaching solution which should not affect the NMC synthesis [94,95].

pH control

To optimize Cu extraction, equilibrium pH control (e.g., adding a base to neutralize the leachate solution, such as NaOH) would be recommended.

The pH of the solution was adjusted to see if it would change the metal speciation while removing acidity; precipitation tests were performed on the leachate solution (S/L = 20 g/L). The neutralization was done by slowly adding small drops of NaOH 10 M under constant agitation, and the pH was measured continuously. The variation of concentration is depicted in Figure 28. It shows that the elements are unstable in the solution; after a couple of hours, the metal concentration is decreased by half, and white powder is visible at the bottom of the reactor. The XRD pattern (Figure 28d) obtained after pH 2 and 4 precipitation reveals that oxalates are formed.

This precipitate is again a solid solution with the general formula $(\text{Co}, \text{Ni}, \text{Mn})\text{C}_2\text{O}_4 \cdot 2\text{H}_2\text{O}$ phase (no peak splitting observed), meaning that all elements co-precipitate together.

This is problematic for Cu removal as the equilibrium pH cannot be controlled during the solvent extraction because of the 3rd phase which would be formed. The leaching solution pH was adjusted at 0.4 to keep all metals in solution and continue the process without precipitation.

Despite the complication this might cause for Cu separation, it gives a strong chance to recover the other transition elements as oxalate and synthesize cathode material from oxalate. Metal oxalates are already known to have substantial potential as precursors for CAM or as energy materials in some storage devices [153–156]. Additionally, if metal oxalate precipitates, the sulfuric acid solution could be regenerated and reused in the process.

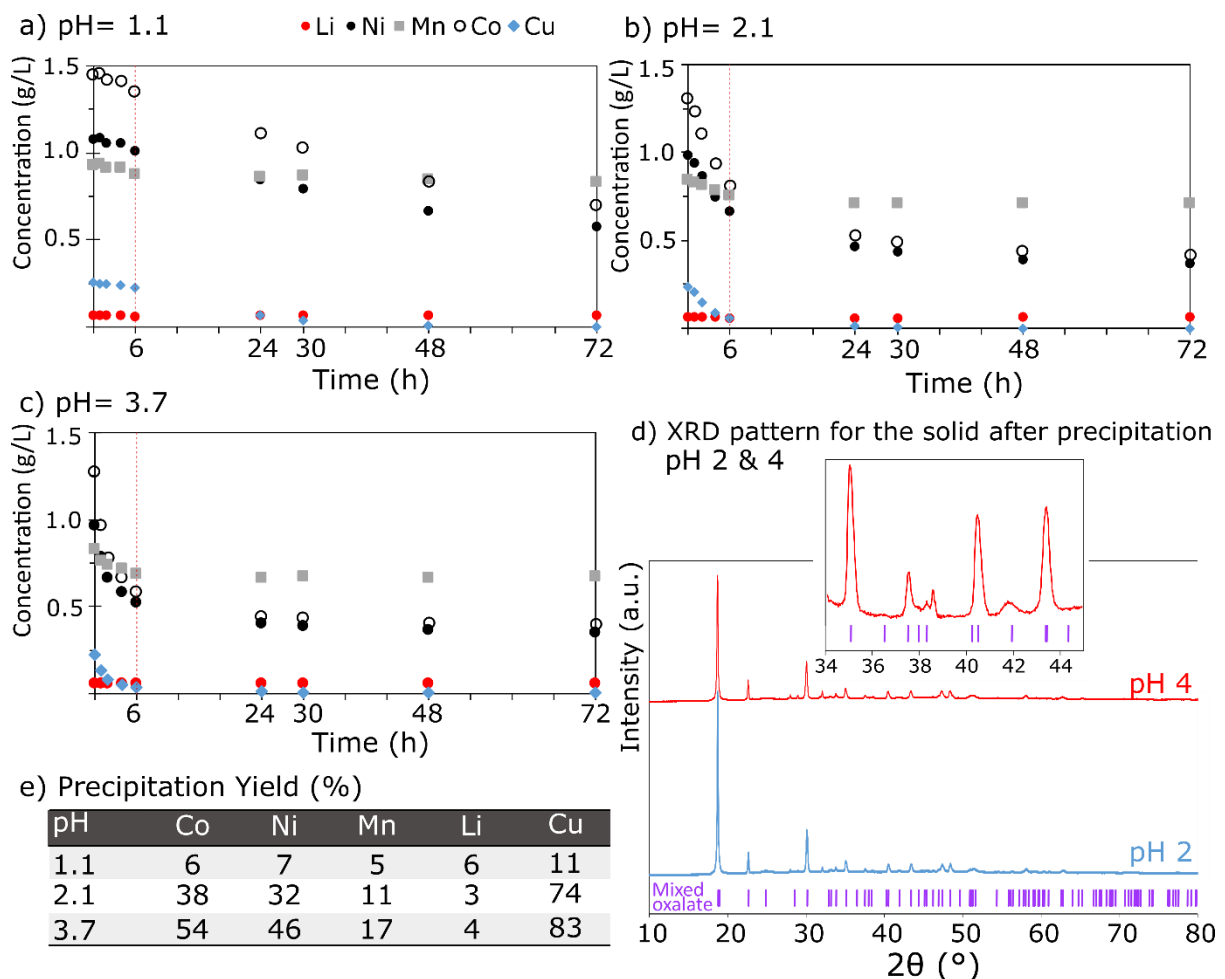


Figure 28: Evolution of the metal concentration in the leaching solution 2 (20 g/L, 2 M, 65°C, 120 min) after adjusting the pH a) 1.1, b) 2.1, c) 3.7, d) XRD pattern of the obtained crystals and, e) Precipitation yields for every element after 6 h, the red line marks the end of agitation.

Solvent extraction of the Cu

As demonstrated above, equilibrium pH control is not an option in this process as precipitation occurs, impacting the solvent extraction even more, with a potential 3rd phase formation [126]. Different leaching strategies have been emphasized above; for the solvent extraction study, the leaching solution at 80 g/L is used as it presents the highest concentration of Cu. At low feed pH, the extraction is more sensitive to variations in the feed Cu concentration [150,157]. Thus, all leachate solutions will be tested under optimum conditions. Before solvent extraction, all solutions had their pH adjusted to 0.4 ± 0.1.

The extraction yield and D-value of Cu, Mn, Co, and Ni are shown in Figure 29 under different set of conditions, and the selectivity of Acorga M5640 for Cu is demonstrated; for all graphs shown, the co-extraction of the other TM is under 0.5%. For all tests, the phase separation is easily achieved (natural gravity), and the organic phase changes from transparent to golden yellow once Cu is loaded.

Equilibrium is reached after 15 min (Figure 29a), and 35% of Cu is extracted. The very low co-extraction of the other valuable metals is a key factor in the operation- No scrubbing will be considered which would have complicated the purification process and increase operational costs. A time of 30 min is selected for further investigations. Temperature slightly impacts the extraction yield; it increases from 35% at 25°C to 49% at 60°C (Figure 29b). This slight increase is not surprising as the extraction mechanism with Acorga M5640 is an endothermic reaction [150,152]. The temperature also affects the physical properties of the organic phase, such as viscosity and density, which are not limiting in this case. Hence, experiments were performed at 25°C, as this decreases the need for energy and the complexity of the process. The parameter that most impacts Cu recovery is the concentration in Acorga M5640 (given in volume percentage in ESCAID). For 5% v/v Acorga M5640, the extraction is at 21%, while it is about 50% for a concentration of 30% v/v. Co, Mn, and Ni co-extraction is not strongly affected and keeps an average value of about 2% (Figure 29c). An extraction of 50% is low, considering the applied condition, but not surprising considering the very low concentration of the element in the solution. As mentioned above, the pH is extremely low, which can affect the extraction mechanism, i.e., it can lead to the extractant protonation and affect the equilibrium.

In the same way of the Acorga M5640 concentration, increasing θ largely favours the extraction (Figure 29e). Extraction capacities are identical depending on the leachate solution used as feed (Figure 24d), which was essential in the development process. All experiments are batch experiments, and multistage operations will be needed to achieve a satisfying separation of Cu (under 5 mg/L, so above 99% efficiency percentage). Kremser equations, 34 and 35 (Page 22), are used to determine the theoretical number of stages (*n*) needed. Data obtained for the batch experiments (D-values) were computed to obtain the theoretical number of stages needed to achieve the 99% required extraction; results are reported in Figure 29f. Cross-current extraction would require fewer stages, but it consumes a large volume of organic material as fresh organic solution is distributed at each stage. Counter-current extraction would need more stages and a minimum θ of 2 for effective extraction and is industrially preferred. With this prediction, we would still recommend its usage as less volume is spent. Experimental validation would be needed to validate this theoretical number.

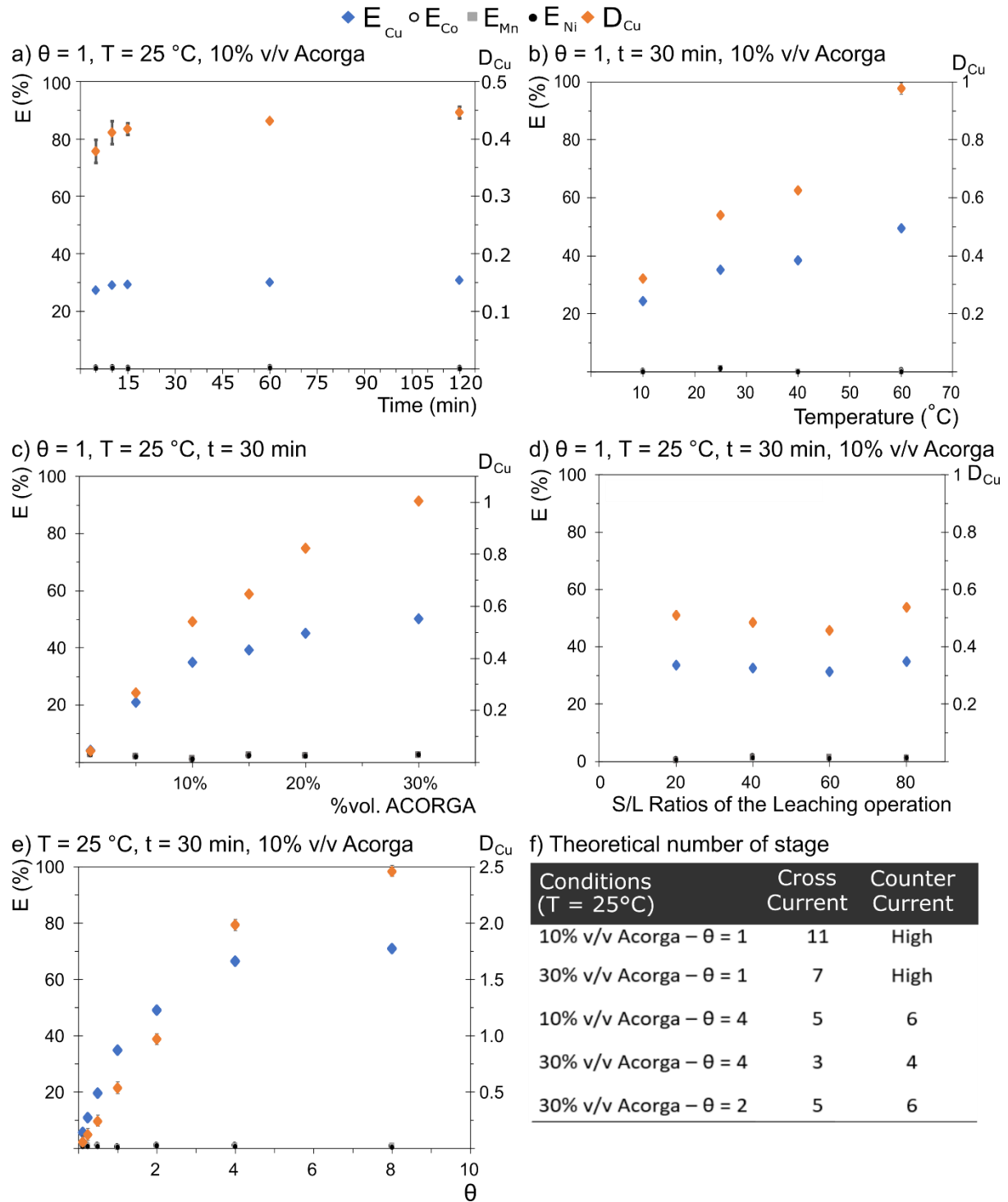


Figure 29: SX test towards Cu removal – a) Kinetics of extraction (Fixed $\theta = 1$, $25^\circ C$, 10 vol% Acorga M540), b) Influence of temperature (Fixed $\theta = 1$, 30 min, 10 vol% Acorga M540), c) Concentration of Acorga (Fixed $\theta = 1$, $25^\circ C$, 30min), d) different leaching solution – influence of the feed variation (Fixed $\theta = 1$, $25^\circ C$, 30min, 10 vol% Acorga M540), e) Phase ratios influence (Fixed $25^\circ C$, 30 min, 10 vol% Acorga M540), and f) Calculation of theoretical number of stage to achieve $\%E = 0.99$ (Equation 34 and 35).

Additionally, some stripping experiments were performed to investigate the unloading of Cu. They were performed with 2 M H_2SO_4 at $25^\circ C$ and θ at 0.5. 100% of the Cu could be stripped for all organics solutions tested.

5.3.4 Conclusions and perspectives on Strategy 2

The second strategy is very promising; it is an innovative option for recycling LiBs. In the first leaching 1, with an oxalic concentration of 0.6 M, a S/L ratio of 60 g/L, a temperature of 60°C for 60 min, about 90% of the Li can be recovered (along with 100% of Al). The mechanism was investigated, and this work allowed a precise description of the mechanism driving the operation. It was shown that the solid residue 1 is composed of a mixture of solid solution (a disordered phase of TM oxalate) and graphite. This solid enters a second leaching 2, with two primary objectives: 1/ to separate the valuable elements from the graphite and 2/ to start thinking about the re-synthesis of CAM. At this research stage, the best option is 2 M sulfuric acid leaching with an S/L ratio of 20 g/L, at 65°C for 2 hours. Over 95% of the TM were recovered and present as sulphate in the solution. The instability of Ni in the solution was demonstrated as it easily re-precipitates as oxalate in the bulk, forming a new phase in the leaching residue.

The next stage was to start considering the production of CAM, and for this purpose, impurity removal was necessary. It was proven that the metal oxalate readily precipitates when the pH is increased. A pH as low as 1 leads to high oxalate precipitation. No more investigations were pursued for this, as it directly correlates with the synthesis of the CAM precursor.

Due to this instability, solvent extraction with Acorga M5640 was performed to remove Cu. High selectivity towards Cu was shown. Despite the impossibility of controlling the equilibrium pH, it was demonstrated that 99% could be removed by applying 3 stages cross-current extraction with an Acorga M5640 concentration of 30 vol% and a θ of 4, at room temperature.

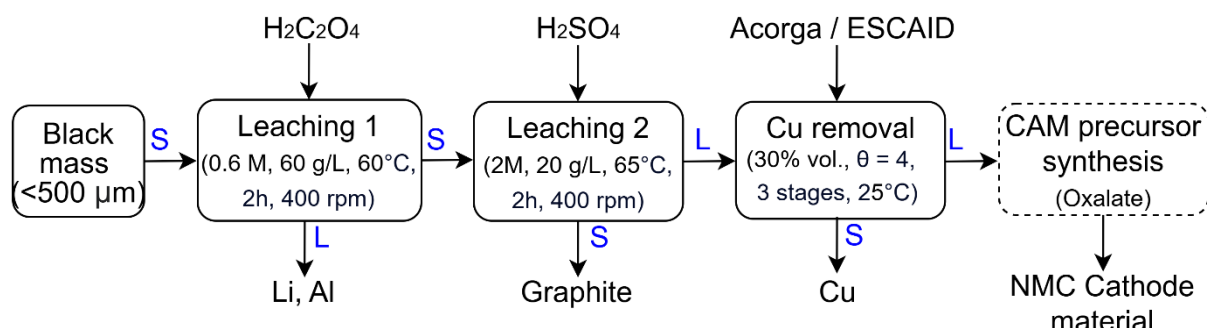


Figure 30: Summary of the developed route based on oxalic acid with the identified optimal conditions: 1) $H_2C_2O_4$ Leaching 1; 2) H_2SO_4 Leaching 2 for the TM; 3) Cu removal.

6 CONCLUSION

This thesis compares two unique LiB recycling strategies, both based on early Li recovery, which could be of high interest in the future.

First, the pyrolysis and black mass followed by the water leaching has shown limited recovery in Li, with a maximum of 70% that could be recovered (70°C, 20 g/L, and 60 min). Despite this limited recovery, the process is highly likely to be applied in industry. First, because of its maturity, processes based on sulfuric acid have been widely investigated, and some are even already applied in the world. This pyrolysis step as a pre-treatment would offer a new and advantageous way to 1/ concentrate the BM, which could then be transported elsewhere for its wet processing, 2/ increase the Li overall recovery, and finally 3/ have strong potential to re-synthesize the CAM material. Aside from the industrial aspects, this work has succeeded in detailing the mechanism of reduction of the NMC material, showing the various species in which Li can be found. The limited recovery of Li is attributed to the insolubility of the by-products formed (LiF, Li₃PO₄, and LiAlO₂). Moreover, due to high fluorine content, special attention has been given to fluorine. Currently, fluorine will combine with Li and form LiF during the production of Li products. This remains a significant drawback and a challenge to solve. Finally, the pyrolysis enabled the recovery of all metals, as more than 95% could be recovered without the use of a reducing agent which would reduce the chemical need for this operation.

The process based on the use of oxalic acid is very innovative; so far, no strong interest has been given to this candidate in developing the whole process. The first leaching (oxalic acid) led to the recovery of about 90% of Li and 100% of Al (oxalic acid 0.6M, 60°C, 50 g/L, and 60 min). The thesis gave a strong importance to defining the dissolution mechanism, defining that the operation is chemically controlled but can turn into a more diffusion-controlled mechanism at higher temperatures. This nature of operation shows how vital acid concentration is for the dissolution, but also, as shown in this work, needs to be well tuned to avoid the excess of acid reacting with the TM oxalate complexes, forming soluble oxalate complexes. Some Li recovery limitations were observed, mainly attributed to forming a product layer around unreacted core particles (revealed during Leaching 2). This phenomenon is complex to avoid and constitutes a big drawback for the rest of the process. However, some more research during the industrialization phase could be carried out to find a solution; some leaching equipment is made to tackle these issues. Then the rest of the process was investigated to evaluate how the residue could be processed to end in the re-synthesis of the CAM. Rapidly, it was decided to aim towards oxalate precursors, which have great potential as a CAM precursor. In this work, sulfuric acid leaching separates the TM from the graphite: more than 95% of Ni, Mn, and Co could be recovered (sulfuric acid 2M, 65°C, 20 g/L, and 120 min). Then Cu was removed with SX with Acorga M5640 despite the impossibility of adjusting the equilibrium pH. More than 99% of Cu could be removed from the solution, after 3 stages cross-current extraction with an Acorga M5640 concentration of 30 vol% and a θ of 4, at room temperature. The resulting solution has a strong potential to produce oxalate precursor.

FUTURE WORK

At this research stage, a definitive comparison of the two proposed routes remains challenging due to their respective advantages and drawbacks. Future work will involve a comprehensive life cycle assessment (LCA) and economic feasibility evaluations to provide a more robust analysis. Both will be planned once the entire process is finalized. The LCA is a crucial tool for quantifying environmental impact, which is more relevant at the end of the research, as the assumptions made at the early stage can potentially lead to inaccurate conclusions as the process matures. Similarly, a thorough economic evaluation is planned later. This assessment will be pivotal in determining the industrial viability of each route, it involves more refined cost estimations based on experimental data and preliminary process flow diagrams. It helps identify key cost drivers and areas for potential economic optimization. Currently, this evaluation is premature, as key process parameters are yet to be fully investigated and optimized on the lab scale. One relevant example is the regeneration of oxalic acid, which is pointed out by the literature as crucial when developing a process based on organic acid.

Given the innovative nature and higher uncertainty associated with the oxalic acid route, our future efforts will primarily focus on its optimization. Specifically, the lithium-loaded leaching solution (Leaching Solution 1) necessitates purification. Based on the solution specifications, we strongly recommend initially exploring ion exchange or adsorption to remove TM impurities. This is followed by a second ion exchange step to exchange lithium ions with protons. This strategy could significantly enhance the subsequent regeneration of oxalic acid.

Furthermore, we propose investigating alternative leaching agents to ascertain if sulfuric acid is the most effective option. Regarding Cu removal, we suggest exploring two other approaches: 1) evaluating alternative extractants with lower pH sensitivity or equilibrium pH, such as LIX reagents known for Cu selectivity, or 2) investigating cementation as a method to precipitate Cu as a metallic compound, potentially utilizing another transition metal present in the CAM to avoid introducing additional impurities.

Finally, the re-synthesis of the CAM will be undertaken to complete the process development. As stated in the introduction, this work has not been the target, but this research relevance is strongly connected with the success of the last operation.

ACKNOWLEDGEMENTS

I wish to express my deepest gratitude to those who have supported me throughout this doctoral journey. First and foremost, I extend my sincere appreciation to my supervisor, Dr. Martina Petranikova, for trusting me with this position and being supportive in every project I pursued, from the supervision of various students, the international conferences, or my trip to Brazil, where I could experience another academic set-up. Her expertise and mentorship have been invaluable in shaping this research. I am also profoundly grateful to my co-supervisors, Dr. Nathalia Vieceli, for her dedicated support and constructive criticism, who provided me with an excellent example of a dedicated worker, and Dr. Burcak Ebin, for all the fruitful discussions. Their contributions significantly enhanced the quality of this work. I would also like to thank Dr. Laura Altenschmidt, a dedicated member of this research project, for her valuable scientific insights and excellent collaboration in pursuit of our common goal, but also for the completion of this thesis.

I also sincerely thank Prof. Teodora Retegan Vollmer, my examiner, for her careful review and thoughtful insights. Our discussions about research or career paths have always been instructive. Additionally, I would like to acknowledge Prof. Christian Ekberg, the Head of the Department, for his support and for providing a stimulating academic environment. I have enjoyed being his student and appreciated all the pleasant fika discussions.

To my colleagues and friends within the department, particularly Thomas, Luis, Andrea, Nils, and Dogac, I extend my heartfelt thanks for their camaraderie, intellectual discussions, and unwavering support. Their collaboration and shared experiences have made this process both enriching and enjoyable. Additionally, I cannot pass without thanking more of my colleagues who made the experience in Gothenburg outside the lab more enjoyable: Thea, Anna, Yigit, Martin, Ilyes, Arushi, and Ioanna. During this journey, I met temporary workers who truly made a difference: Franco, Matea, Camille, and Jerney. Your time with us was significant.

Beyond the academic sphere, I am immensely grateful to the friends I met here outside of work, especially Jana, Clément, Romain, Nils, Svenja, and Felix, for their reliable friendship. Their presence provided a much-needed balance and source of strength throughout these years; leaving far from home can be challenging, but I have felt at home thanks to you. This was well complemented by my older friends, who gave me much love and support to accomplish this challenge: Albane, Julia, Justine, Thomas, Anouk, and Manon.

Finally, I wish to express my deepest love and appreciation to my parents, my brother, Marie, and Manon. Their unconditional love and encouragement have been the cornerstone of my success. I am eternally grateful for their unwavering support and understanding. Merci de m'inspirer et de me donner de la force chaque jour. Je vous aime.

My final words are for you, Alejandro. This thesis would have been a totally different experience without your support, love, and patience. I cherish all the moments from the crazy dances, restless climbing sessions, cooking experiences, games, and long walks, which helped me stay balanced and happy at all times. I te quiaime.

REFERENCES

1. Intergovernmental Panel on Climate Change - Contribution of Working Groups I, II. and III. *Climate Change 2023 - Synthesis Report*; Geneva, Switzerland, 2023;
2. Asiva Noor Rachmayani *Electrification Accelerating the Energy Transition*; Pami Aalto, Faculty of Management, Business and Politics Unit, Tampere University, Tampere, F., Ed.; Elsevier.; Tampere, Finland, 2015; ISBN 978-0-12-822143-3.
3. International Energy Agency (IEA) *Recycling of Critical Minerals - Strategies to Scale up Recycling and Urban Mining*; Paris, 2024;
4. International Energy Agency (IEA) Electric Vehicles - Technology Deep Dive - Tracking Report Available online: <https://www.iea.org/reports/electric-vehicle> (accessed on 10 May 2025).
5. Dewulf, J.; Van der Vorst, G.; Denturck, K.; Van Langenhove, H.; Ghysel, W.; Tytgat, J.; Vandepitte, K. Recycling Rechargeable Lithium-Ion Batteries: Critical Analysis of Natural Resource Savings. *Resour Conserv Recycl* **2010**, *54*, 229–234, doi:10.1016/j.resconrec.2009.08.004.
6. International Energy Agency (IEA) The Role of Critical Minerals in Clean Energy Transitions. *IEA Publications 2021*.
7. Harper, G.; Anderson, P.A.; Kendrick, E.; Mrozik, W.; Christensen, P.; Lambert, S.; Greenwood, D.; Das, P.K.; Ahmeid, M.; Milojevic, Z.; et al. Roadmap for a Sustainable Circular Economy in Lithium-Ion and Future Battery Technologies. *Journal of Physics: Energy* **2023**, *5*, doi:10.1088/2515-7655/acaa57.
8. European Commission Critical Raw Material (CRM) Available online: https://single-market-economy.ec.europa.eu/sectors/raw-materials/areas-specific-interest/critical-raw-materials_en (accessed on 12 May 2025).
9. Chen, Q.; Lai, X.; Gu, H.; Tang, X.; Gao, F.; Han, X.; Zheng, Y. Investigating Carbon Footprint and Carbon Reduction Potential Using a Cradle-to-Cradle LCA Approach on Lithium-Ion Batteries for Electric Vehicles in China. *J Clean Prod* **2022**, *369*, doi:10.1016/j.jclepro.2022.133342.
10. Yoo, E.; Lee, U.; Kelly, J.C.; Wang, M. Life-Cycle Analysis of Battery Metal Recycling with Lithium Recovery from a Spent Lithium-Ion Battery. *Resour Conserv Recycl* **2023**, *196*, 9, doi:10.1016/j.resconrec.2023.107040.
11. Rinne, M.; Elomaa, H.; Porvali, A.; Lundström, M. Simulation-Based Life Cycle Assessment for Hydrometallurgical Recycling of Mixed LIB and NiMH Waste. *Resour Conserv Recycl* **2021**, *170*, doi:10.1016/j.resconrec.2021.105586.

12. Meng, F.; McNeice, J.; Zadeh, S.S.; Ghahreman, A. Review of Lithium Production and Recovery from Minerals, Brines, and Lithium-Ion Batteries. *Mineral Processing and Extractive Metallurgy Review* **2021**, *42*, 123–141, doi:10.1080/08827508.2019.1668387.
13. Qing, J.; Zhang, G.; Zeng, L.; Guan, W.; Cao, Z.; Li, Q.; Wang, M.; Chen, Y.; Wu, S. Deep Fluoride Removal from the Sulfate Leaching Solution of Spent LIBs by Complexation Extraction with Al³⁺ Loaded Solvent. *Sep Purif Technol* **2023**, *305*, 122343, doi:10.1016/j.seppur.2022.122343.
14. Gutsch, M.; Leker, J. Costs, Carbon Footprint, and Environmental Impacts of Lithium-Ion Batteries – From Cathode Active Material Synthesis to Cell Manufacturing and Recycling. *Appl Energy* **2024**, *353*, 122132, doi:10.1016/j.apenergy.2023.122132.
15. Binnemans, K.; Tom, P. The Twelve Principles of Circular Hydrometallurgy. *Journal of Sustainable Metallurgy* **2023**, *9*, 1–25, doi:10.1007/s40831-022-00636-3.
16. European Parliament and the Council of the European Union *Regulation (EU) 2023/1542 - Batteries and Waste Batteries, Amending Directive 2008/98/EC and Regulation (EU) 2019/1020 and Repealing Directive 2006/66/EC*; 2023; Vol. 66;.
17. Neumann, J.; Petranikova, M.; Meeus, M.; Gamarra, J.D.; Younesi, R.; Winter, M.; Nowak, S. Recycling of Lithium-Ion Batteries—Current State of the Art, Circular Economy, and Next Generation Recycling. *Adv Energy Mater* **2022**, 1–26, doi:10.1002/aenm.202102917.
18. International Energy Agency (IEA) *Global EV Outlook 2022 Securing Supplies for an Electric Future*; Paris, 2022;
19. Hayagan, N.; Aymonier, C.; Croguennec, L.; Philippot, G. A Holistic Review on the Direct Recycling of Lithium- Ion Batteries from Electrolytes to Electrodes. *J Mater Chem A Mater* **2024**, 31685–31716, doi:10.1039/D4TA04976D.
20. AUDI AG. - Electric has gone Audi E-Tron Battery Available online: <https://electrichasgoneaudi.net/models/e-tron/drivetrain/battery/> (accessed on 10 May 2025).
21. Heelan, J.; Gratz, E.; Zheng, Z.; Wang, Q.; Chen, M.; Apelian, D.; Wang, Y.A.N. Current and Prospective Li-Ion Battery Recycling and Recovery Processes. *The Minerals, Metals & Materials Society Current* **2016**, *68*, 2632–2638, doi:10.1007/s11837-016-1994-y.
22. Jung, J.; Sui, P.-C.; Zhang, J. *Hydrometallurgical Recycling of Lithium-Ion Battery Materials*; Taylo & Fr.; 2023; ISBN 9781032216027.
23. Shi, G.; Cheng, J.; Wang, J.; Zhang, S.; Shao, X.; Chen, X.; Li, X.; Xin, B. A Comprehensive Review of Full Recycling and Utilization of Cathode and Anode as Well as Electrolyte from Spent Lithium-Ion Batteries. *J Energy Storage* **2023**, *72*, doi:10.1016/j.est.2023.108486.

24. Latini, D.; Vaccari, M.; Lagnoni, M.; Orefice, M.; Mathieu, F.; Huisman, J.; Tognotti, L.; Bertei, A. A Comprehensive Review and Classification of Unit Operations with Assessment of Outputs Quality in Lithium-Ion Battery Recycling. *J Power Sources* **2022**, *546*, doi:10.1016/j.jpowsour.2022.231979.
25. Nunes-Pereira, J.; Costa, C.M.; Lanceros-Méndez, S. Polymer Composites and Blends for Battery Separators: State of the Art, Challenges and Future Trends. *J Power Sources* **2015**, *281*, 378–398, doi:10.1016/j.jpowsour.2015.02.010.
26. Winslow, K.M.; Laux, S.J.; Townsend, T.G. A Review on the Growing Concern and Potential Management Strategies of Waste Lithium-Ion Batteries. *Resour Conserv Recycl* **2018**, *129*, 263–277, doi:10.1016/j.resconrec.2017.11.001.
27. Siqi Zhao, W.H. and G.L. *Recycling of Spent Lithium-Ion Batteries - Processing Methods and Environmental Impacts*; Liang An, D. of M.E., Ed.; Hong King, China, 2019; ISBN 978-3-030-31833-8.
28. Ding, H.; Yuan, S.; Lei, S.; Wang, W.; Wen, G.; Dong, Z. Technology and Principle on Preferentially Selective Lithium Extraction for Spent Ternary Lithium Batteries: A Review. *Sep Purif Technol* **2024**, *355*, 129691, doi:10.1016/j.seppur.2024.129691.
29. Christian Julien, Alain Mauger, Ashok Vijh, K.Z. *Lithium Batteries - Science and Technology*; Springer International Publishing Switzerland: Geneva, Switzerland, 2016; ISBN 9783319191072.
30. Gerold, E.; Schinnerl, C.; Antrekowitsch, H. Critical Evaluation of the Potential of Organic Acids for the Environmentally Friendly Recycling of Spent Lithium-Ion Batteries. *Recycling* **2022**, *7*, 16, doi:10.3390/recycling7010004.
31. Lombardo, G. Comparison of Incineration and Pyrolysis of NMC-Lithium-Ion Batteries – Determination of the Effects on the Chemical Composition , and Potential Formation of Hazardous by-Products . PhD Thesis, Chalmers University of Technology, 2020.
32. Malik, M.; Ho, K.; Azimi, G. Review on the Synthesis of LiNixMnyCo1-xYO_2 (NMC) Cathodes for Lithium-Ion Batteries. *Materials Today Energy journal* **2022**, *28*, doi:10.1016/j.mtener.2022.101066.
33. Pimenta, V.; Sathiya, M.; Batuk, D.; Abakumov, A.M.; Giaume, D. Synthesis of Li-Rich NMC: A Comprehensive Study. *Chemistry of Material* **2017**, *29*, 9923–9936, doi:10.1021/acs.chemmater.7b03230.
34. Le Thi, T.; Phan Van, T.; Nguyen Van, B.; To Van, N.; Nguyen Van, T.; Doan, T.P.; Ngo, T.L.; Vu, N.H.; Nguyen, T.T.; Nguyen, H.N.; et al. Modified Coprecipitation Synthesis of Nickel-Rich NMC ($\text{Li1.0Ni0.6Mn0.2Co0.2O}_2$) for Lithium-Ion Batteries: A Simple, Cost-Effective, Environmentally Friendly Method. *ACS Omega* **2023**, *8*, 45414–45427, doi:10.1021/acsomega.3c04717.

35. Yao, X.; Xu, Z.; Yao, Z.; Cheng, W.; Gao, H.; Zhao, Q.; Li, J.; Zhou, A. Oxalate Co-Precipitation Synthesis of LiNi_{0.6}Co_{0.2}Mn_{0.2}O₂ for Low-Cost and High-Energy Lithium-Ion Batteries. *Mater Today Commun* **2019**, *19*, 262–270, doi:10.1016/j.mtcomm.2019.02.001.
36. Lu, H.; Zhou, H.; Svensson, A.M.; Fossdal, A.; Sheridan, E.; Lu, S.; Vullum-Bruer, F. High Capacity Li[Ni_{0.8}Co_{0.1}Mn_{0.1}]O₂ Synthesized by Sol-Gel and Co-Precipitation Methods as Cathode Materials for Lithium-Ion Batteries. *Solid State Ion* **2013**, *249–250*, 105–111, doi:10.1016/j.ssi.2013.07.023.
37. European commission (EU) *Critical Raw Materials Resilience: Charting a Path towards Greater Security and Sustainability*; Brussel, 2020;
38. Yu, W.; Guo, Y.; Xu, S.; Yang, Y.; Zhao, Y.; Zhang, J. Comprehensive Recycling of Lithium-Ion Batteries: Fundamentals, Pretreatment, and Perspectives. *Energy Storage Mater* **2023**, *54*, 172–220, doi:10.1016/j.ensm.2022.10.033.
39. Dessim, A.; Pritam, S.; Wensheng, Z.; Aleksandar, N.N. A Review of Pretreatment Methods for Spent Lithium-Ion Batteries to Produce Black Mass—Comparison of Processes of Asia Pacific Recyclers. *Mineral Processing and Extractive Metallurgy Review* **2024**, *1–18*, doi:10.1080/08827508.2024.2367420.
40. Parashar, M.; Titirici, M.; Johansson, P.; Ribadeneyra, M.C.; Au, H. 2024 Roadmap for Sustainable Batteries. *Journal of Physics : Energy* **2024**, *6*, 1–72, doi:10.1088/2515-7655/ad6bc0.
41. Hampel, C. Battery Reuse & Recycling Expand to Scale in China Available online: <https://www.electrive.com/2022/01/29/battery-reuse-recycling-expands-to-scale-in-china/> (accessed on 10 May 2025).
42. Harper, G.; Sommerville, R.; Kendrick, E.; Driscoll, L.; Slater, P.; Stolkin, R.; Walton, A.; Christensen, P.; Heidrich, O.; Lambert, S.; et al. Recycling Lithium-Ion Batteries from Electric Vehicles. *Nature* **2019**, *575*, 75–86, doi:10.1038/s41586-019-1682-5.
43. Sommerville, R.; Shaw-Stewart, J.; Goodship, V.; Rowson, N.; Kendrick, E. A Review of Physical Processes Used in the Safe Recycling of Lithium Ion Batteries. *Sustainable Materials and Technologies* **2020**, *25*, 1–10, doi:10.1016/j.susmat.2020.e00197.
44. Lim, P. ‘Black Mass’ Needs Common Global Specs to Commoditize Recycled Battery Raw Materials Available online: <https://www.fastmarkets.com/insights/black-mass-needs-common-global-specs-to-commoditize-recycled-battery-raw-materials> (accessed on 12 May 2025).
45. Zheng, X.; Zhu, Z.; Lin, X.; Zhang, Y.; He, Y.; Cao, H.; Sun, Z. A Mini-Review on Metal Recycling from Spent Lithium Ion Batteries. *Engineering* **2018**, *4*, 361–370, doi:10.1016/j.eng.2018.05.018.

46. Zachmann, N.; Fox, R. V.; Petranikova, M.; Ebin, B. Implementation of a Sub-and Supercritical Carbon Dioxide Process for the Selective Recycling of the Electrolyte from Spent Li-Ion Battery. *Journal of CO₂ Utilization* **2024**, *81*, 19–22, doi:10.1016/j.jcou.2024.102703.
47. Marie Salces, A.; Bremerstein, I.; Rudolph, M.; Vanderbruggen, A. Joint Recovery of Graphite and Lithium Metal Oxides from Spent Lithium-Ion Batteries Using Froth Flotation and Investigation on Process Water Re-Use. *Miner Eng* **2022**, *184*, doi:10.1016/j.mineng.2022.107670.
48. Contestabile, M.; Panero, S.; Scrosati, B. Laboratory-Scale Lithium-Ion Battery Recycling Process. *J Power Sources* **2001**, *92*, 65–69, doi:10.1016/S0378-7753(00)00523-1.
49. Wang, H.; Friedrich, B. Development of a Highly Efficient Hydrometallurgical Recycling Process for Automotive Li-Ion Batteries. *Journal of Sustainable Metallurgy* **2015**, *1*, 168–178, doi:10.1007/s40831-015-0016-6.
50. Ferreira, D.A.; Prados, L.M.Z.; Majuste, D.; Mansur, M.B. Hydrometallurgical Separation of Aluminium, Cobalt, Copper and Lithium from Spent Li-Ion Batteries. *J Power Sources* **2009**, *187*, 238–246, doi:10.1016/j.jpowsour.2008.10.077.
51. Dahllöf, L.; Romare, M.; Wu, A. *Mapping of Lithium-Ion Batteries for Vehicles - A Study of Their Fate in the Nordic Countries*; Springer: Copenhangen, Danmark, 2016; ISBN 9783319191072.
52. Guo, Y.; Li, Y.; Lou, X.; Guan, J.; Li, Y.; Mai, X.; Liu, H.; Zhao, C.X.; Wang, N.; Yan, C.; et al. Improved Extraction of Cobalt and Lithium by Reductive Acid from Spent Lithium-Ion Batteries via Mechanical Activation Process. *J Mater Sci* **2018**, *53*, 13790–13800, doi:10.1007/s10853-018-2229-0.
53. Wang, M.; Liu, K.; Yu, J.; Zhang, C.C.; Zhang, Z.; Tan, Q. Recycling Spent Lithium-Ion Batteries Using a Mechanochemical Approach. *Circular Economy* **2022**, *1*, 100012, doi:10.1016/j.cec.2022.100012.
54. Wu, J.; Xiao, L.; Liu, P.; Zhu, Y.; Li, J. Direct Regeneration and Upcycling of Cathode Material from Spent Lithium-Ion Batteries: Recent Advances and Perspectives. *Sep Purif Technol* **2025**, *355*, 1–23, doi:10.1016/j.seppur.2024.129574.
55. Barbosa de Mattos, D.F.; Duda, S.; Petranikova, M. Recycling of Lithium Iron Phosphate (LiFePO₄) Batteries from the End Product Quality Perspective. *Batteries* **2025**, *11*, doi:10.3390/batteries11010033.
56. Umicore Battery Recycling Solutions - Our Recycling Process Available online: <https://csm.umincore.com/en/battery-recycling/our-recycling-process/> (accessed on 10 May 2025).

57. Armand, M.; Axmann, P.; Bresser, D.; Copley, M.; Edstr, K.; Ekberg, C.; Guyomard, D.; Lestriez, B.; Nov, P.; Petranikova, M.; et al. Lithium-Ion Batteries – Current State of the Art and Anticipated Developments. *Power sources* **2020**, *479*, 26, doi:10.1016/j.jpowsour.2020.228708.
58. Mao, J.K.; Li, J.; Xu, Z. Coupling Reactions and Collapsing Model in the Roasting Process of Recycling Metals from LiCoO₂ Batteries. *J Clean Prod* **2018**, *205*, 923–929, doi:10.1016/j.jclepro.2018.09.098.
59. Li, J.; Wang, G.; Xu, Z. Environmentally-Friendly Oxygen-Free Roasting/Wet Magnetic Separation Technology for in Situ Recycling Cobalt, Lithium Carbonate and Graphite from Spent LiCoO₂/Graphite Lithium Batteries. *J Hazard Mater* **2016**, *302*, 97–104, doi:10.1016/j.jhazmat.2015.09.050.
60. Zhang, Y.; Wang, W.; Fang, Q.; Xu, S. Improved Recovery of Valuable Metals from Spent Lithium-Ion Batteries by Efficient Reduction Roasting and Facile Acid Leaching. *Waste Management* **2020**, *102*, 847–855, doi:10.1016/j.wasman.2019.11.045.
61. Liu, P.; Xiao, L.; Tang, Y.; Chen, Y.; Ye, L.; Zhu, Y. Study on the Reduction Roasting of Spent LiNi_xCo_yMn_zO₂ Lithium-Ion Battery Cathode Materials. *J Therm Anal Calorim* **2019**, *136*, 1323–1332, doi:10.1007/s10973-018-7732-7.
62. Xu, P.; Liu, C.; Zhang, X.; Zheng, X.; Lv, W.; Rao, F.; Yao, P.; Wang, J.; Sun, Z. Synergic Mechanisms on Carbon and Sulfur during the Selective Recovery of Valuable Metals from Spent Lithium-Ion Batteries. *ACS Sustain Chem Eng* **2021**, *9*, 2271–2279, doi:10.1021/acssuschemeng.0c08213.
63. Makuzza, B.; Tian, Q.; Guo, X.; Chattopadhyay, K.; Dawei, Y. Pyrometallurgical Options for Recycling Spent Lithium-Ion Batteries_A Comprehensive Review. *Power sources* **2021**, *491*, 1–21, doi:10.1016/j.jpowsour.2021.229622.
64. Zhang, J. Chapter 10 - Application of Hydrometallurgy in Spent Lithium-Ion Battery Recycling. In *Nano Technology for Battery Recycling, Remanufacturing, and Reusing*; Elsevier Inc., 2022; pp. 183–216 ISBN 9780323911344.
65. Joulié, M.; Laucournet, R.; Billy, E. Hydrometallurgical Process for the Recovery of High Value Metals from Spent Lithium Nickel Cobalt Aluminum Oxide Based Lithium-Ion Batteries. *J Power Sources* **2014**, *247*, 551–555, doi:10.1016/j.jpowsour.2013.08.128.
66. Shuva, Md.A.H.; Kurny, A. Hydrometallurgical Recovery of Value Metals from Spent Lithium Ion Batteries. *American Journal of Materials Engineering and Technology* **2013**, *1*, 8–12, doi:10.12691/materials-1-1-2.
67. Partinen, J.; Halli, P.; Varonen, A.; Wilson, B.P.; Lundström, M. Investigating Battery Black Mass Leaching Performance as a Function of Process Parameters by Combining Leaching

Experiments and Regression Modeling. *Miner Eng* **2024**, *215*, 1–10, doi:10.1016/j.mineng.2024.108828.

68. Porvali, A.; Chernyaev, A.; Shukla, S.; Lundström, M. Lithium Ion Battery Active Material Dissolution Kinetics in Fe(II)/Fe(III) Catalyzed Cu-H₂SO₄ Leaching System. *Sep Purif Technol* **2020**, *236*, 116305, doi:10.1016/j.seppur.2019.116305.
69. Joulié, M.; Laucournet, R.; Billy, E. Hydrometallurgical Process for the Recovery of High Value Metals from Spent Lithium Nickel Cobalt Aluminum Oxide Based Lithium-Ion Batteries. *J Power Sources* **2014**, *247*, 551–555, doi:10.1016/j.jpowsour.2013.08.128.
70. Larouche, F.; Tedjar, F.; Amouzegar, K.; Houlachi, G.; Bouchard, P.; Demopoulos, G.P.; Zaghib, K. Progress and Status of Hydrometallurgical and Direct Recycling of Li-Ion Batteries and Beyond. *Materials* **2020**, *13*, doi:10.3390/ma13030801.
71. Verma, A.; Corbin, D.R.; Shiflett, M.B. Lithium and Cobalt Recovery for Lithium-Ion Battery Recycle Using an Improved Oxalate Process with Hydrogen Peroxide. *Hydrometallurgy* **2021**, *203*, doi:10.1016/j.hydromet.2021.105694.
72. Golmohammazadeh, R.; Faraji, F.; Rashchi, F. Recovery of Lithium and Cobalt from Spent Lithium Ion Batteries (LIBs) Using Organic Acids as Leaching Reagents : A Review. *Resour Conserv Recycl* **2018**, *136*, 418–435, doi:10.1016/j.resconrec.2018.04.024.
73. Ekberg, C.; Petranikova, M. Chap 7: Lithium Batteries Recycling. In *Lithium Process Chemistry: Resources, Extraction, Batteries, and Recycling*; Elsevier Inc., 2015; pp. 233–267 ISBN 9780128014172.
74. Chen, X.; Xu, B.; Zhou, T.; Liu, D.; Hu, H.; Fan, S. Separation and Recovery of Metal Values from Leaching Liquor of Mixed-Type of Spent Lithium-Ion Batteries. *Sep Purif Technol* **2015**, *144*, 197–205, doi:10.1016/j.seppur.2015.02.006.
75. Chernyaev, A.; Wilson, B.P.; Lundström, M. Study on Valuable Metal Incorporation in the Fe–Al Precipitate during Neutralization of LIB Leach Solution. *Nature Scientific Reports* **2021**, *11*, doi:10.1038/s41598-021-02019-2.
76. Chernyaev, A.; Zhang, J.; Seisko, S.; Louhi-Kultanen, M.; Lundström, M. Fe³⁺ and Al³⁺ Removal by Phosphate and Hydroxide Precipitation from Synthetic NMC Li-Ion Battery Leach Solution. *Nature Scientific Reports* **2023**, *13*, 1–12, doi:10.1038/s41598-023-48247-6.
77. Alemrajabi, M.; Karlsson, I.; Sjödhäls, R.; Nehrenrheim, E.; Petranikova, M.; Tunsu, C. Process for the Recovery of Cathode Materials in the Recycling of Batteries 2020.
78. Swain, B. Recovery and Recycling of Lithium: A Review. *Sep Purif Technol* **2017**, *172*, 388–403, doi:10.1016/j.seppur.2016.08.031.

79. Stallmeister, C.; Schwich, L.; Friedrich, B. *Early Stage Li-Removal – Avoidance of Lithium Losses During the Thermal and Chemical Recycling Routes of Batteries*; 2017;
80. Raiguel, S.; Avdibegović, D.; Binnemans, K. Removal of Lithium from Aqueous Solutions by Precipitation with Sodium and Choline Alkanoate Soaps. *Green Chemistry* **2024**, *27*, doi:10.1039/d4gc05586a.
81. Salces, A.M.; Kelly, N.; Streblow, G.J.; Temel, E.T.; Rudolph, M.; Chagnes, A.; Vanderbruggen, A. A Contribution to Understanding Ion-Exchange Mechanisms for Lithium Recovery from Industrial Effluents of Lithium-Ion Battery Recycling Operations. *J Environ Chem Eng* **2024**, *12*, 112951, doi:10.1016/j.jece.2024.112951.
82. Li, X.; Li, X.; Chen, G.; Li, H.; Duan, Y.; Sun, Y.; Tiraferri, A.; Liu, B. Efficient Recovery of Lithium from Spent Lithium-Ion Battery Raffinate by Mn and Al-Based Adsorbents: Pretreatment, Adsorption Mechanism, and Performance Comparison. *Sep Purif Technol* **2025**, *354*, 128652, doi:10.1016/j.seppur.2024.128652.
83. Zhao, R.; Sun, H.; Liu, L.; Wei, Q.; Ren, X.; Ying, Z. A New Solvent Extraction Technology and Mechanism for the Separation and Recovery of Li⁺ Using Benzene Sulfonamide Acid Substance. *Sep Purif Technol* **2025**, *356*, doi:10.1016/j.seppur.2024.129913.
84. Wesselborg, T.; Virolainen, S.; Sainio, T. Recovery of Lithium from Leach Solutions of Battery Waste Using Direct Solvent Extraction with TBP and FeCl₃. *Hydrometallurgy* **2021**, *202*, 105593, doi:10.1016/j.hydromet.2021.105593.
85. Krüger, S.; Hanisch, C.; Kwade, A.; Winter, M.; Nowak, S. Effect of Impurities Caused by a Recycling Process on the Electrochemical Performance of Li[Ni0.33Co0.33Mn0.33]O₂. *Journal of Electroanalytical Chemistry* **2014**, *726*, 91–96, doi:10.1016/j.jelechem.2014.05.017.
86. Sa, Q.; Gratz, E.; He, M.; Lu, W.; Apelian, D.; Wang, Y. Synthesis of High Performance LiNi_{1/3}Mn_{1/3}Co_{1/3}O₂ from Lithium Ion Battery Recovery Stream. *J Power Sources* **2015**, *282*, 140–145, doi:10.1016/j.jpowsour.2015.02.046.
87. Yang, L.; Xi, G.; Xi, Y. Recovery of Co, Mn, Ni, and Li from Spent Lithium Ion Batteries for the Preparation of Li_xNi_yCoyMnzO₂ Cathode Materials. *Ceram Int* **2015**, *41*, 11498–11503, doi:10.1016/j.ceramint.2015.05.115.
88. Azmi, M.U.; Hapid, A.; Fatahillah, H.E.H.; Kawigraha, A.; Abidin, F.; Novitasari, Y. Precipitation of Nickel-Manganese-Cobalt Sulphate From. *5th International Seminar on Metallurgy and Materials (ISMM2022)* **2024**, *3003*, doi:doi.org/10.1063/5.0186127.
89. Zheng, Y.; Liu, Y.; Hou, J.; Meng, Z.; Zhou, X.; Yang, Z. Unraveling the Nature of Sulfide Ions in Hydrometallurgical Recycling of NCM622 Cathode Material. *Energy Storage Mater* **2024**, *65*, doi:10.1016/j.ensm.2023.103128.

90. Paulino, J.; Sastre, P.; Saleem, U.; Prasetyo, E.; Bandyopadhyay, S. Resynthesis of Cathode Active Material from Heterogenous Leachate Composition Produced by Electric Vehicle (EV) Battery Recycling Stream. *J Clean Prod* **2023**, *429*, doi:10.1016/j.jclepro.2023.139343.
91. Nasser, O.A.; Petranikova, M. Review of Achieved Purities after Li-Ion Batteries Hydrometallurgical Treatment and Impurities Effects on the Cathode Performance. *Batteries* **2021**, *7*, doi:10.3390/batteries7030060.
92. Wu, Z.J.; Wang, D.; Gao, Z.F.; Yue, H.F.; Liu, W.M. Effect of Cu Substitution on Structures and Electrochemical Properties of $\text{Li}[\text{NiCo}_{1-X}\text{Cu}_X\text{Mn}]_{1/3}\text{O}_2$ as Cathode Materials for Lithium Ion Batteries. *Dalton Transactions* **2015**, *44*, 18624–18631, doi:10.1039/c5dt02552d.
93. Zhang, R.; Meng, Z.; Ma, X.; Chen, M.; Chen, B.; Zheng, Y.; Yao, Z.; Vanaphuti, P.; Bong, S.; Yang, Z.; et al. Understanding Fundamental Effects of Cu Impurity in Different Forms for Recovered $\text{LiNi}_{0.6}\text{Co}_{0.2}\text{Mn}_{0.2}\text{O}_2$ Cathode Materials. *Nano Energy* **2020**, *78*, 105214, doi:10.1016/j.nanoen.2020.105214.
94. Beak, M.; Park, J.; Park, S.; Jeong, S.; Kang, J.; Choi, W.; Yoon, W.S.; Kwon, K. Understanding the Effect of Nonmetallic Impurities in Regenerated Cathode Materials for Lithium-Ion Battery Recycling by Tracking down Impurity Elements. *J Hazard Mater* **2022**, *425*, 1–9, doi:10.1016/j.jhazmat.2021.127907.
95. Wang, Q.; Fox, R. V.; Shi, M.; Snyder, S.W.; Ilevbare, G.O.; Ginosar, D.M. Electrodialysis: An Effective Methodology to Purify the Leachate of Spent Li-Ion Batteries. *Sep Purif Technol* **2025**, *359*, doi:10.1016/j.seppur.2024.130430.
96. Jandová, J.; Dvořák, P.; Kondás, J.; Havlák, L. Recovery of Lithium from Waste Materials. *Ceramics - Silikaty* **2011**, *56*, 50–54.
97. Xiao, J.; Li, J.; Xu, Z. Novel Approach for in Situ Recovery of Lithium Carbonate from Spent Lithium Ion Batteries Using Vacuum Metallurgy. *Environ Sci Technol* **2017**, *51*, 11960–11966, doi:10.1021/acs.est.7b02561.
98. Maroufi, S.; Assefi, M.; Khayyam Nekouei, R.; Sahajwalla, V. Recovery of Lithium and Cobalt from Waste Lithium-Ion Batteries through a Selective Isolation-Suspension Approach. *Sustainable Materials and Technologies* **2020**, *23*, 2–6, doi:10.1016/j.susmat.2019.e00139.
99. Balachandran, S.; Forsberg, K.; Lemaître, T.; Lombardo, G.; Petranikova, M. Comparative Study for Selective Lithium Recovery via Chemical Transformations during Incineration and Dynamic Pyrolysis on EV Li-Ion Batteries. *Metals (Basel)* **2021**, *11*, 1–16, doi:10.3390/met11081240.
100. Krishnamurty, K. V.; Harris, G.M.; Sastri, V.S. The Chemistry of the Metal Oxalato Complexes. *Chem Rev* **1960**, *70*, 213–240, doi:10.1021/cr60264a001.

101. Sohn, J.S.; Shin, S.M.; Yang, D.H.; Kim, S.K.; Lee, C.K. Comparison of Two Acidic Leaching Processes for Selecting the Effective Recycle Process of Spent Lithium Ion Battery. *Geosystem Engineering* **2006**, *9*, 1–6, doi:10.1080/12269328.2006.10541246.
102. Zeng, X.; Li, J.; Shen, B. Novel Approach to Recover Cobalt and Lithium from Spent Lithium-Ion Battery Using Oxalic Acid. *J Hazard Mater* **2015**, *295*, 112–118, doi:10.1016/j.jhazmat.2015.02.064.
103. Zhang, X.; Bian, Y.; Xu, S.; Fan, E.; Xue, Q.; Guan, Y.; Wu, F.; Li, L.; Chen, R. Innovative Application of Acid Leaching to Regenerate Li(Ni_{1/3}Co_{1/3}Mn_{1/3})O₂ Cathodes from Spent Lithium-Ion Batteries. *ACS Sustain Chem Eng* **2018**, *6*, 5959–5968, doi:10.1021/acssuschemeng.7b04373.
104. Li, Q.; Fung, K.Y.; Xu, L.; Wibowo, C.; Ng, K.M. Process Synthesis: Selective Recovery of Lithium from Lithium-Ion Battery Cathode Materials. *Ind Eng Chem Res* **2019**, *58*, 3118–3130, doi:10.1021/acs.iecr.8b04899.
105. Lv, W.; Wang, Z.; Cao, H.; Sun, Y.; Zhang, Y.; Sun, Z. A Critical Review and Analysis on the Recycling of Spent Lithium-Ion Batteries. *ACS Sustain Chem Eng* **2018**, *6*, 1504–1521, doi:10.1021/acssuschemeng.7b03811.
106. Zou, Y.; Chernyaev, A.; Ossama, M.; Seisko, S.; Lundström, M. Leaching of NMC Industrial Black Mass in the Presence of LFP. *Nature Scientific Reports* **2024**, *14*, 1–14, doi:10.1038/s41598-024-61569-3.
107. Lombardo, G.; Ebin, B.; Mark, M.R.; Steenari, B.M.; Petranikova, M. Incineration of EV Lithium-Ion Batteries as a Pretreatment for Recycling – Determination of the Potential Formation of Hazardous by-Products and Effects on Metal Compounds. *J Hazard Mater* **2020**, *393*, 122372, doi:10.1016/j.jhazmat.2020.122372.
108. Vignes, A. *Extractive Metallurgy 2 - Metallurgical Reaction Processes*; John Wiley and Sons, 2011; ISBN 978-1-84821-287-9.
109. Kwon, O. sung; Sohn, I. Fundamental Thermokinetic Study of a Sustainable Lithium-Ion Battery Pyrometallurgical Recycling Process. *Resour Conserv Recycl* **2020**, *158*, 104809, doi:10.1016/j.resconrec.2020.104809.
110. Lombardo, G.; Ebin, B.; Steenari, B.M.; Alemrajabi, M.; Karlsson, I.; Petranikova, M. Comparison of the Effects of Incineration, Vacuum Pyrolysis and Dynamic Pyrolysis on the Composition of NMC-Lithium Battery Cathode-Material Production Scraps and Separation of the Current Collector. *Resour Conserv Recycl* **2021**, *164*, 105142, doi:10.1016/j.resconrec.2020.105142.
111. Lombardo, G.; Ebin, B.; St Foreman, M.R.J.; Steenari, B.M.; Petranikova, M. Chemical Transformations in Li-Ion Battery Electrode Materials by Carbothermic Reduction. *ACS Sustain Chem Eng* **2019**, *7*, 13668–13679, doi:10.1021/acssuschemeng.8b06540.

112. Christmann, P.; Gloaguen, E.; Labb  , J.F.; Melleton, J.; Piantone, P. Chap1 : Global Lithium Resources and Sustainability Issues. In *Lithium Process Chemistry: Resources, Extraction, Batteries, and Recycling*; Elsevier Inc., 2015; pp. 1–40 ISBN 9780128014172.
113. Petranikova, M.; Naharro, P.L.; Vieceli, N.; Lombardo, G.; Ebin, B. Recovery of Critical Metals from EV Batteries via Thermal Treatment and Leaching with Sulphuric Acid at Ambient Temperature. *Waste Management* **2022**, *140*, 164–172, doi:10.1016/j.wasman.2021.11.030.
114. Hirschler, M.M. Effect of Oxygen on the Thermal Decomposition of Poly(Vinylidene Fluoride). *Eur Polym J* **1982**, *18*, 463–467, doi:10.1016/0014-3057(82)90184-7.
115. Nicol, M.; Welham, N.; Senanayake, G. *Hydrometallurgy - Theory*; Candice Janco, 2019; Vol. 1; ISBN 9788578110796.
116. Free, M.L. *Hydrometallurgy - Fundamentals and Applications*; John Wiley & Sons, 2013; Vol. 1; ISBN 9788578110796.
117. Habashi, F. *Textbook of Hydrometallurgy*; Sainte-Foy, Qu  bec, 1993; ISBN 2980324701.
118. Weller Mark, Overton Tina, Rourke Jonathan, A.F. *Inorganic Chemistry*; 7th ed.; Oxford University Press: Oxford, 2018; ISBN 978-0-19-876812-8.
119. Xue, X.; Wang, W.; Fan, H.; Xu, Z.; Pedruzzi, I.; Li, P.; Yu, J. Adsorption Behavior of Oxalic Acid at Water–Feldspar Interface: Experiments and Molecular Simulation. *Adsorption* **2019**, *25*, 1191–1204, doi:10.1007/s10450-019-00111-8.
120. Rosenqvist, T. Chapter 5 Reaction Kinetics. In *Principles of Extractive Metallurgy*; Clark, B.J., Ed.; 1974; pp. 114–145 ISBN 0-07-053847-6.
121. Faraji, F.; Alizadeh, A.; Rashchi, F.; Mostoufi, N. Kinetics of Leaching: A Review. *Reviews in Chemical Engineering* **2022**, *38*, 113–148, doi:10.1515/revce-2019-0073.
122. Schorr, M.; Yahalom, J. Kinetics and Structure Aspects of the Dissolution of Metals in Acids. *ECS Trans* **2008**, *13*, 143–150, doi:10.1149/ma2008-01/15/612.
123. Schwich, L.; Schubert, T.; Friedrich, B. Early-Stage Recovery of Lithium from Tailored Thermal Conditioned Black Mass Part I: Mobilizing Lithium via Supercritical CO₂ - Carbonation. *Metals (Basel)* **2020**, *11*, 177, doi:10.3390/met11020177.
124. David R. Lide *Handbook in Chemistry and Physics*; Standard R.; CRC Press Inc., 2004;
125. Sun, L.; Qiu, K. Organic Oxalate as Leachant and Precipitant for the Recovery of Valuable Metals from Spent Lithium-Ion Batteries. *Waste Management* **2012**, *32*, 1575–1582, doi:10.1016/j.wasman.2012.03.027.

126. Ritcey G.M. and Ashbrook A.W. *Solvent Extraction - Principles and Applications to Process Metallurgy*; Elsevier Science Publisher, 1984; ISBN 0-444-41751-2.
127. Zanoletti, A.; Carena, E.; Ferrara, C.; Elza, B. A Review of Lithium-Ion Battery Recycling : Technologies, Sustainability, and Open Issues. *Batteries* **2024**, *10*, doi:10.3390/batteries10010038.
128. Lei, S.; Sun, W.; Yang, Y. Solvent Extraction for Recycling of Spent Lithium-Ion Batteries. *J Hazard Mater* **2022**, *424*, doi:10.1016/j.jhazmat.2021.127654.
129. Gerlach, R.W.; Dobb, D.E.; Raab, G.A.; Nocerino, J.M. Gy Sampling Theory in Environmental Studies. 1. Assessing Soil Splitting Protocols. *J Chemom* **2002**, *16*, 321–328, doi:10.1002/cem.705.
130. Puigdomenech, I. HYDRA (Hydrochemical Equilibrium Constant Database) and MEDUSA (Make Equilibrium Diagrams Using Sophisticated Algorithms) 2020.
131. Douglas C. Montgomery *Design and Analysis of Experiments*; John Wiley & Sons, Ed.; 2009; ISBN 978-0-470-39882-1.
132. Mousa, E.; Hu, X.; Ånnhagen, L.; Ye, G.; Cornelio, A.; Fahimi, A.; Bontempi, E.; Frontera, P.; Badenhorst, C.; Santos, A.C.; et al. Characterization and Thermal Treatment of the Black Mass from Spent Lithium-Ion Batteries. *Sustainability (Switzerland)* **2023**, *15*, doi:10.3390/su15010015.
133. Rouquette, L.M.J.; Lemaître, T.; Vieceli, N.; Petranikova, M. Intensification of Lithium Carbonation in the Thermal Treatment of Spent EV Li-Ion Batteries via Waste Utilization and Selective Recovery by Water Leaching. *Resources, Conservation and Recycling Advances* **2023**, *17*, 0–8, doi:10.1016/j.rcradv.2022.200125.
134. Petranikova, M.; Rouquette, L.M.J.; Locati, A.; Ebin, B. Advances in Hydrometallurgical Processing of Black Mass from EV Li-Ion Batteries. In Proceedings of the 14th International Conference on Process Hydrometallurgy; 2023; pp. 1–8.
135. Sun, L.; Qiu, K. Vacuum Pyrolysis and Hydrometallurgical Process for the Recovery of Valuable Metals from Spent Lithium-Ion Batteries. *J Hazard Mater* **2011**, *194*, 378–384, doi:10.1016/j.jhazmat.2011.07.114.
136. Maryadele J. O'Neil *The Merck Index - An Encyclopedia of Chemicals, Drugs, and Biologicals*. *13th Edition.*; Co., M. and, Ed.; Whitehouse Station, 2001;
137. Kuzuhara, S.; Ota, M.; Tsugita, F.; Kasuya, R. Recovering Lithium from the Cathode Active Material in Lithium-Ion Batteries via Thermal Decomposition. *Metals (Basel)* **2020**, *10*, 433, doi:10.3390/met10040433.
138. Babanejab, S. *Eco-Friendly Recovery and Alloying of Metals from Spent Lithium-Ion Batteries*; Luleå University of Technology: Luleå, 2025; ISBN 978-91-8048-710-8.

139. ChemicalBook - Available online:
https://www.chemicalbook.com/ChemicalProductProperty_EN_CB2105321.htm
(accessed on 23 April 2025).
140. Babanejad, S.; Ahmed, H.; Andersson, C.; Samuelsson, C.; Lennartsson, A.; Hall, B.; Arnerlöf, L. High-Temperature Behavior of Spent Li-Ion Battery Black Mass in Inert Atmosphere. *Journal of Sustainable Metallurgy* **2022**, *8*, 566–581, doi:10.1007/s40831-022-00514-y.
141. Rouquette, L.M.J.; Vieceli, N.; Petranikova, M. Complete and Selective Recovery of Lithium from EV Lithium-Ion Batteries: Modeling and Optimization Using Oxalic Acid as a Leaching Agent. *Sep Purif Technol* **2023**, *320*, doi:10.1016/j.seppur.2023.124143.
142. Guimarães, L.F.; Botelho Junior, A.B.; Espinosa, D.C.R. Sulfuric Acid Leaching of Metals from Waste Li-Ion Batteries without Using Reducing Agent. *Miner Eng* **2022**, *183*, doi:10.1016/j.mineng.2022.107597.
143. Tembo, P.M.; Werner, R.N.; Subramanian, V. Application of a Simple Organic Acid as a Green Alternative for the Recovery of Cathode Metals from Lithium-Ion Battery Cathode Materials. *Green Technologies and Sustainability* **2024**, *3*, 100135, doi:10.1016/j.grets.2024.100135.
144. He, H.; Feng, J.; Gao, X.; Fei, X. Selective Separation and Recovery of Lithium, Nickel, MnO₂, and Co₂O₃ from LiNi0.5Mn0.3Co0.2O₂ in Spent Battery. *Chemosphere* **2022**, *286*, doi:10.1016/j.chemosphere.2021.131897.
145. Wang, L.; Zhang, R.; Jiang, Y.; Tian, H.; Tan, Y.; Zhu, K.; Yu, Z.; Li, W. Interfacial Synthesis of Micro-Cuboid Ni0.55Co0.45C2O4 Solid Solution with Enhanced Electrochemical Performance for Hybrid Supercapacitors. *Nanoscale* **2019**, *11*, 13894–13902, doi:10.1039/c9nr03790j.
146. Puzan, A.N.; Baumer, V.N.; Lisovytskiy, D. V.; Mateychenko, P. V. Structure Disorder and Thermal Decomposition of Manganese Oxalate Dihydrate, MnC₂O₄·2H₂O. *J Solid State Chem* **2018**, *260*, 87–94, doi:10.1016/j.jssc.2018.01.022.
147. Puzan, A.N.; Baumer, V.N.; Lisovytskiy, D. V.; Mateychenko, P. V. Structure Transformations in Nickel Oxalate Dihydrate NiC₂O₄·2H₂O and Nickel Formate Dihydrate Ni(HCO₂)₂·2H₂O during Thermal Decomposition. *J Solid State Chem* **2018**, *266*, 133–142, doi:10.1016/j.jssc.2018.07.005.
148. Vinayan, B.P.; Zhao-Karger, Z.; Diemant, T.; Chakravadhanula, V.S.K.; Schwarzburger, N.I.; Cambaz, M.A.; Behm, R.J.; Kübel, C.; Fichtner, M. Performance Study of Magnesium-Sulfur Battery Using a Graphene Based Sulfur Composite Cathode Electrode and a Non-Nucleophilic Mg Electrolyte. *Nanoscale* **2016**, *8*, 3296–3306, doi:10.1039/c5nr04383b.

149. National Institute of Advanced Industrial Science and Technology (AIST) Spectral Database for Organic Compounds SDBS Available online: <https://sdbbs.db.aist.go.jp/SearchInformation.aspx> (accessed on 16 May 2025).
150. Nozari, I.; Azizi, A. An Investigation into the Extraction Behavior of Copper from Sulfate Leach Liquor Using Acorga M5640 Extractant: Mechanism, Equilibrium, and Thermodynamics. *Min Metall Explor* **2020**, *37*, 1673–1680, doi:10.1007/s42461-020-00280-z.
151. Nobahar, A.; Melka, A.B.; Pusta, A.; Paulo, J.; Carlier, J.D.; Costa, M.C. A New Application of Solvent Extraction to Separate Copper from Extreme Acid Mine Drainage Producing Solutions for Electrochemical and Biological Recovery Processes. *Mine Water Environ* **2022**, *41*, 387–401, doi:10.1007/s10230-022-00858-7.
152. Deep, A.; Kumar, P.; Carvalho, J.M.R. Recovery of Copper from Zinc Leaching Liquor Using ACORGA M5640. *Sep Purif Technol* **2010**, *76*, 21–25, doi:10.1016/j.seppur.2010.09.015.
153. Choi, J.W.; Kim, J.; Kim, S.K.; Yun, Y.S. Simple, Green Organic Acid-Based Hydrometallurgy for Waste-to-Energy Storage Devices: Recovery of NiMnCoC₂O₄ as an Electrode Material for Pseudocapacitor from Spent LiNiMnCoO₂ Batteries. *J Hazard Mater* **2022**, *424*, 127481, doi:10.1016/j.jhazmat.2021.127481.
154. Wang L, Zhang R, Jiang Y, Tian H, Tan Y, Zhu K, Yu Z, L.W. Interfacial Synthesis of Micro-Cuboid Ni_{0.55}Co_{0.45}C₂O₄ Solid Solution with Enhanced Electrochemical Performance for Hybrid Supercapacitors. *Nanoscale* **2019**, doi:10.1039/c9nr03790j.
155. Ang, W.A.E.; Cheah, Y.L.; Wong, C.L.; Hng, H.H.; Madhavi, S. One-Pot Solvothermal Synthesis of Co_{1-X}Mn_XC₂O₄ and Their Application as Anode Materials for Lithium-Ion Batteries. *J Alloys Compd* **2015**, *638*, 324–333, doi:10.1016/j.jallcom.2015.02.203.
156. Ghosh, S.; Jana, R.; Ganguli, S.; Inta, H.R.; Tudu, G.; Koppisetti, H.V.S.R.M.; Datta, A.; Mahalingam, V. Nickel–Cobalt Oxalate as an Efficient Non-Precious Electrocatalyst for an Improved Alkaline Oxygen Evolution Reaction. *Nanoscale Adv* **2021**, *3*, 3770–3779, doi:10.1039/d1na00034a.
157. Hosseinzadeh, M.; Petersen, J.; Azizi, A. Solvent Extraction Studies of Copper from a Heap Leach Liquor Using Mextral 5640H. *Minerals* **2022**, *12*, 1–14, doi:10.3390/min12101322.

APPENDIX

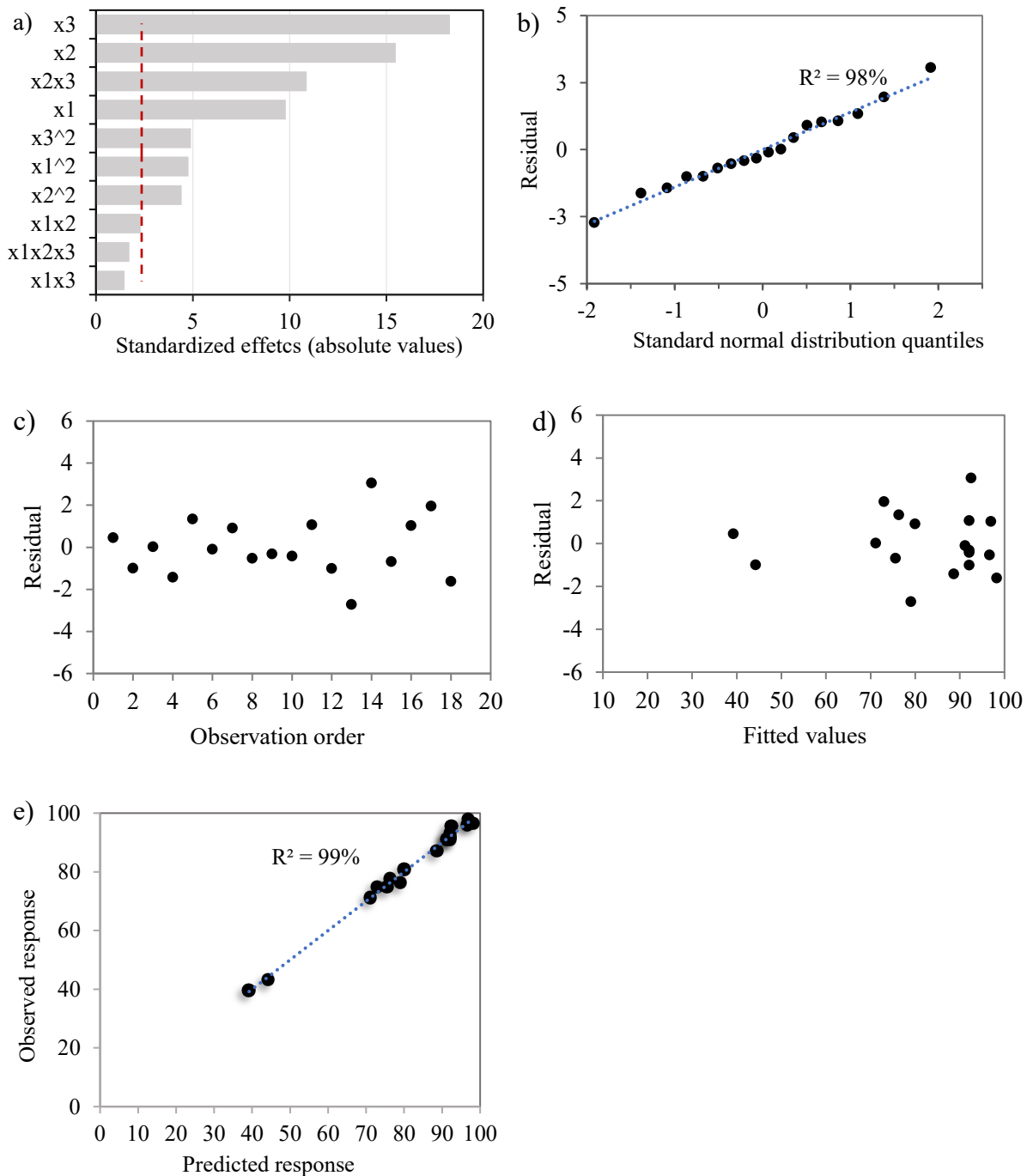
Appendix 1: Results of the analysis of variance of the fitted model for all the elements

Element	Source	Degrees of freedom	Sum of Square SS	Mean Square MS	F-value	p-value
Lithium	Total	17	4922.4	289.6	-	-
	Regression	10	4889.1	488.9	102.8	0.000001
	Residual	7	33.3	4.8	-	-
	Lack of Fit	4	31.0	7.7	10.0	0.0441
	Pure error	3	2.3	0.8	-	-
Aluminium	Total	17	6758.1	397.5	-	-
	Regression	10	6247.1	624.7	8.6	0.0047
	Residual	7	511.0	73.0	-	-
	Lack of Fit	-	-	-	-	-
	Pure error	-	-	-	-	-
Manganese	Total	17	25.2	1.5	-	-
	Regression	10	22.2	2.2	5.1	0.0206
	Residual	7	3.0	0.4	-	-
	Lack of Fit	4	3.0	0.8	75.2	0.0024
	Pure error	3	0.0	0.0	-	-
Cobalt	Total	17	5.3	289.6	-	-
	Regression	10	5.1	0.5	15.3	0.0008
	Residual	7	0.2	0.0	-	-
	Lack of Fit	4	0.2	0.1	16.8	0.0216
	Pure error	3	0.0	0.0	-	-
Nickel	Total	17	30.5	1.8	-	-
	Regression	10	29.4	2.9	18.5	0.0004
	Residual	7	1.1	0.2	-	-
	Lack of Fit	4	1.1	0.3	20.1	0.0167
	Pure error	3	0.0	0.0	-	-
Copper	Total	17	77.7	4.6	-	-
	Regression	10	65.8	6.6	3.9	0.0424
	Residual	7	11.9	1.7	-	-
	Lack of Fit	4	11.8	3.0	888.6	0.0001
	Pure error	3	0.0	0.0	-	-

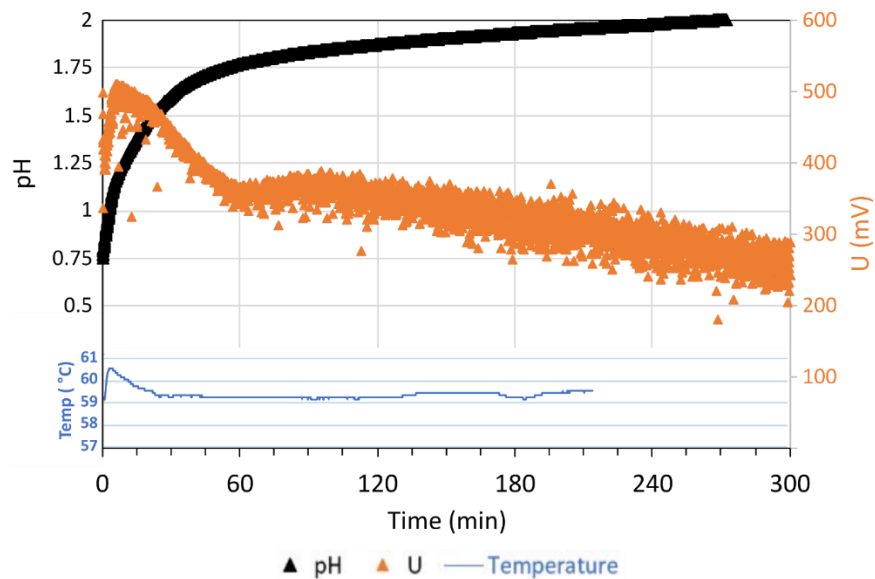
Appendix 2: Sum-up of the significant parameters obtain for the regression models for every element

Element	Effect	Coefficient	Standard error	t Stat	p-value
Lithium	Intercept	92.09	0.86	107.32	1.61E-12
	OA Concentration	6.76	0.69	9.80	2.45E-05
	Time	10.68	0.69	15.49	1.13E-06
	Temperature	12.61	0.69	18.28	3.63E-07
	Time*Temperature	-8.40	0.77	-10.89	1.22E-05
	OA Conc. * OA Conc.	-6.33	1.32	-4.78	2.01E-03
	Time * Time	-5.85	1.32	-4.42	3.09E-03
	Temperature*Temperature	-6.50	1.32	-4.90	1.75E-03
Aluminium	Intercept	94.43	3.36	28.09	1.86E-08
	Time	16.24	2.70	6.01	5.36E-04
	Temperature	13.58	2.70	5.03	1.52E-03
	Time*Temperature	-8.60	3.02	-2.85	2.48E-02
Manganese	Intercept	2.64	0.26	10.18	1.90E-05
	Time	-0.55	0.21	-2.64	3.34E-02
	OA Conc. * OA Conc.	1.22	0.40	3.04	1.90E-02
Cobalt	Intercept	0.48	0.07	6.70	2.78E-04
	OA Concentration	-0.48	0.06	-8.28	7.33E-05
	OA Conc. * Temperature	-0.29	0.06	-4.49	2.83E-03
	OA Conc.* Time * Temperature	0.16	0.06	2.55	3.83E-02
	OA Conc. * OA Conc.	0.63	0.11	5.64	7.86E-04
Nickel	Intercept	0.40	0.16	2.53	3.90E-02
	OA Concentration	-1.01	0.13	-8.04	8.80E-05
	Time	-0.70	0.13	-5.56	8.47E-04
	Temperature	-0.41	0.13	-3.27	1.37E-02
	OA Conc. * Temperature	-0.37	0.14	-2.63	3.41E-02
	OA Conc.* Time * Temperature	0.52	0.14	3.67	7.92E-03
	OA Conc. * OA Conc.	1.41	0.24	5.82	6.53E-04
Copper	Intercept	1.32	0.51	2.57	3.69E-02
	OA Concentration	-1.66	0.41	-4.04	4.96E-03
	OA Conc. * OA Conc.	2.28	0.79	2.88	2.36E-02

Appendix 3: Pareto chart of the standardized effects of the factors (x_1 : acid concentration, x_2 : time and x_3 : temperature) for the regression model of Lithium (a) and Analysis of residuals: standard normal distribution of the residuals (b); residual versus observation order (c); residuals versus fitted values (d) and Response predicted by the model versus experimentally observed response (e)



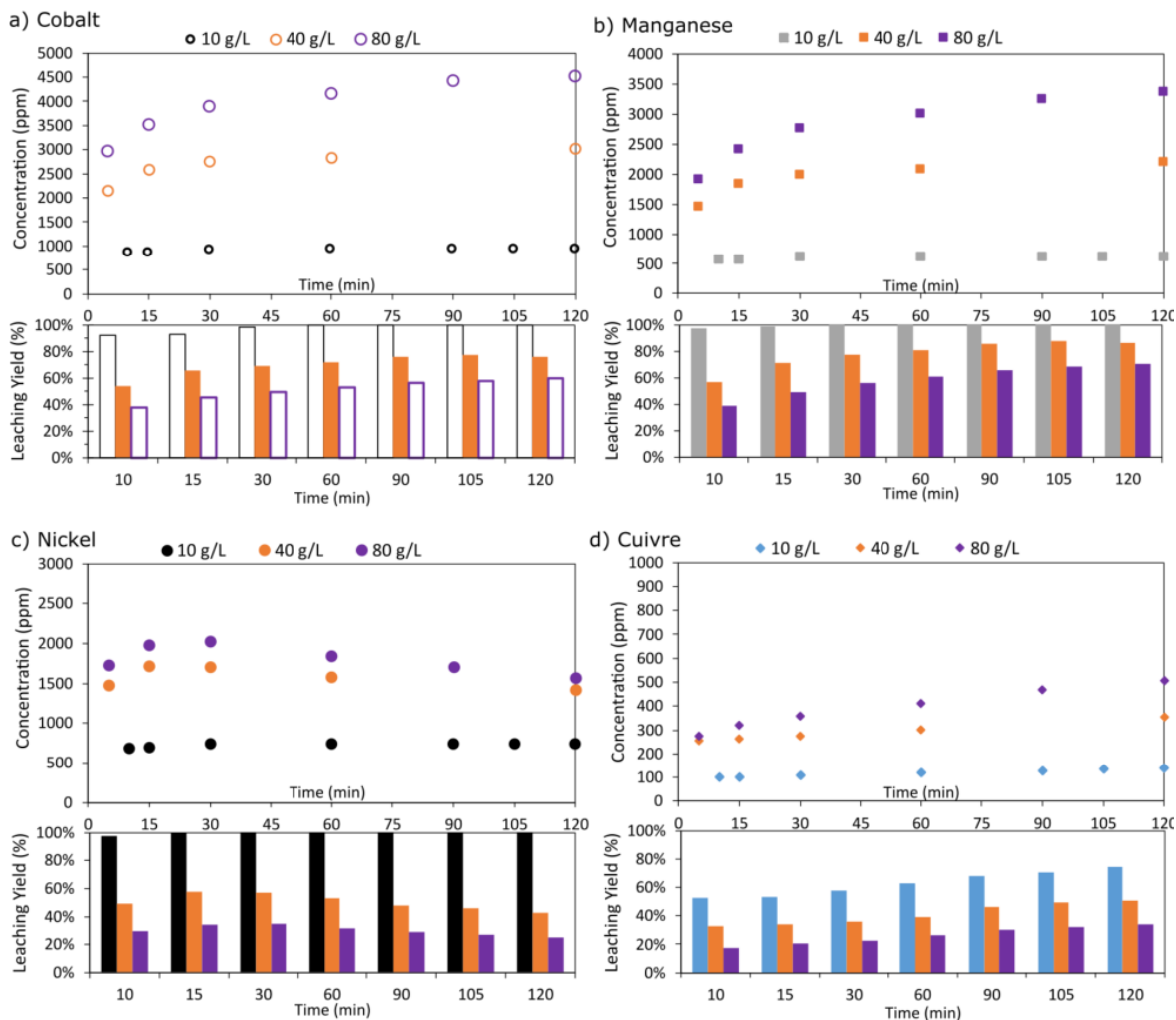
Appendix 4: Oxalic acid leaching of the Black mass – Evolution of E (orange), pH (black), and temperature (blue) during the operation.



Appendix 5: Composition of the residue wt% (%) after the oxalic acid leaching (420 min, 400 rpm, 0.6 M oxalic acid) at different temperatures (obtained after aqua regia digestion + ICP measurement)

T (°C) / Black mass wt% (%)	Co	Ni	Mn	Fe	Cu	Al	Li
80	10.8	8.7	8.0	0.1	4.3	1.1	3.3
70	9.31	6.66	5.92	<LOD	1.32	<LOD	0.53
60	9.50	6.77	6.05	<LOD	1.56	<LOD	0.58
50	9.09	6.50	5.82	<LOD	1.64	<LOD	0.51
40	8.74	6.22	5.63	<LOD	1.55	<LOD	0.50
30	9.08	6.46	5.83	<LOD	1.67	<LOD	0.57
	9.41	6.68	5.93	<LOD	1.98	<LOD	0.64

Appendix 6: Evolution of the leaching yield and concentration during the leaching operation under $T = 65^\circ\text{C}$, $[\text{H}_2\text{SO}_4] = 2 \text{ M}$, 300 rpm agitation and different S/L ratios, 10, 40, and 80°C for Co a), Mn b), Ni c), and Cu d)



Appendix 7: FT-IR spectra of the leaching residue 2 ($T = 65^\circ\text{C}$, $[\text{H}_2\text{SO}_4] = 2 \text{ M}$, $t = 120 \text{ min}$, 300 rpm agitation) at different S/L ratios

